Hadron Structure in Deep Inelastic Scattering

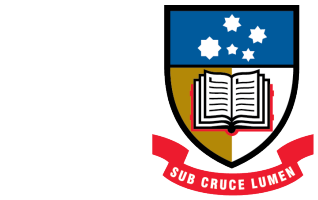

THE UNIVERSITY of ADELAIDE

Andrew Casey

School of Chemistry & Physics

University of Adelaide

A thesis submitted as a portfolio of publications for the degree of

Doctor of Philosophy

August 2013

Contents

I would like to dedicate this thesis to my loving wife, Andrea, and
my precious daughter, Georgina ...

Abstract

Deep inelastic scattering (DIS) is an experimental process used to probe a wide variety of properties of hadronic matter. It is a process in which leptons collide with hadrons at high energies, resulting in the hadron being broken into a large number of other particles. Information obtained from this process is combined with what is known from studies of the strong force in Quantum Chromodynamics (QCD), to extract details of the hadronic structure. In this thesis, functions that can be extracted from DIS cross sections are discussed including structure functions, parton distribution functions, and fragmentation functions for single hadron and dihadron cases.

This thesis is presented as a portfolio of publications that investigate some of the previously mentioned functions that can be extracted from DIS processes, which includes semi-inclusive deep inelastic scattering (SIDIS). The first paper describes our method for generating the dihadron fragmentation functions (DFFs) within the Nambu–Jona-Lasinio-jet model. These functions describe the probability of detecting two hadrons with particular light-cone momentum fractions. The DFFs for combinations of pions and kaons calculated in the first paper are obtained at the model momentum scale of $Q_0^2 = 0.2$ GeV^2. Several properties of these functions are explored, including how they change if strange quarks are included.

In the second paper, the appropriate evolution equations are applied to the NJL-jet model calculated DFFs to determine the DFFs at a typical experimental scale of $Q^2 = 4$ GeV^2 for combinations of pions and kaons. A comparison with the results of another model at $Q^2 = 109$ GeV^2 are also presented in this paper, with compelling results.

The final paper departs from the DFFs and instead investigates the gluon spin contribution to the spin of the proton, which is extracted from the spin dependent structure function g_1 using renormalization group techniques. An upper bound is suggested at leading order for the value of this contribution, with an estimate of the error calculated as well.

Statement of Originality

This work contains no material which has been accepted for the award of any other degree or diploma in any university or other tertiary institution to Andrew Casey and, to the best of my knowledge and belief, contains no material previously published or written by another person, except where due reference has been made in the text.

I give consent to this copy of my thesis when deposited in the University Library, being made available for loan and photocopying, subject to the provisions of the Copyright Act 1968.

The author acknowledges that copyright of published works contained within this thesis (as listed below) resides with the copyright holder(s) of those works.

I also give permission for the digital version of my thesis to be made available on the web, via the Universitys digital research repository, the Library catalogue, and also through web search engines, unless permission has been granted by the University to restrict access for a period of time.

Publications for the Portfolio

Calculating Dihadron Fragmentation Functions in the NJL-jet model

Andrew Casey, Hrayr H. Matevosyan, and Anthony W. Thomas,
Physical Review D, 85,114049, 2012.

Cited as Ref. [1]

Dihadron Fragmentation Functions from the NJL-jet model and their QCD Evolution

Andrew Casey, Ian C. Cloët, Hrayr H. Matevosyan, and Anthony W. Thomas,
Physical Review D, 86, 11401885, 2012.

Cited as Ref. [2]

Gluon Polarization in the Proton

Steven D. Bass, Andrew Casey, and Anthony W. Thomas,
Physical Review C, 83, 038202, 2011.

Cited as Ref. [3]

Signed:

Andrew Casey

Acknowledgements

I would first like to thank my supervisors, Anthony W. Thomas and Hrayr H. Matevosyan, who have guided me through the research that constitutes this thesis. In addition to the help they provided to the research, I wish to extend my gratitude for their aid while I was hospitalized, during which time they handled the various loose ends that I was incapable of dealing with. Thanks also to Rodney J. Crewther and Derek B. Leinweber, who supervised me during the first year of my PhD candidature. Many thanks to my other co-authors, Steven D. Bass and Ian C. Cloët, for their discussions on several aspects of the research.

I thank the University of Adelaide, for awarding me the scholarship and providing the resources I required that allowed me to conduct this research. To the staff who aided me throughout my time here, particularly the CSSM administrative staff, Silvana Santucci, Bronwyn Gibson and Sharon Johnson.

To the many friends I have made throughout my time at the University. In particular those who I studied physics with including Felix Jorkowski, Cael Hasse, Lewis Tunstall, Dale Roberts, Ben Menadue and Ka Wu.

Thanks to my parents also, without whom I wouldn't have made it this far. Their support and patience throughout my life has been much appreciated.

Finally, I thank my wife, Andrea, who I met early on in the candidature and who has supported me throughout. She has been exceptionally strong, having given birth to our daughter, Georgina, and supporting me during my time in hospital when I was struck with Guillain-Barré syndrome, as well as throughout my recovery afterwards.

List of Figures

Chapter 1

Contextual Statement

1.1 Contextual Statement

This thesis is presented as a portfolio of three publications on the topic of hadronic structure in deep inelastic scattering. In Chapter 2 we introduce the field of knowledge, which includes such topics as Quantum Chromodynamics, DIS processes and DGLAP evolution equations. A brief review of the NJL model is presented in Chapter 3, where the Lepage-Brodsky invariant mass regularization scheme is described for the determination of the distribution and fragmentation functions. Only the papers in Sections 1.1.1 and 1.1.2 are related to the NJL-jet model described in Chapter 3, with the paper in Section 1.1.3 describing a separate calculation in the understanding of the hadronic structure. We now present the information for the published papers and the aims of these papers.

1.1.1 Calculating Dihadron Fragmentation Function in the NJL-jet model

Authors: Andrew Casey, Hrayr H. Matevosyan and Anthony W. Thomas
Journal: Physical Review D 85, 114049 (2012)
URL: http://link.aps.org/doi/10.1103/PhysRevD.85.114049
Aims: In this paper we employ the NJL-jet model to determine the dihadron fragmentation functions for select combinations of pions and kaons at the model momentum scale $Q_0^2 = 0.2$ GeV^2. The aims of this paper are to study various

properties of the DFFs at the model scale also serves the purpose of presenting the DFFs that will be used in the paper that follows which focuses on evolving the DFFs to a higher momentum scale.

1.1.2 Dihadron Fragmentation Functions from the NJL-jet model and their QCD Evolution

Authors: Andrew Casey, Ian C. Cloët Hrayr H. Matevosyan and Anthony W. Thomas
Journal: Physical Review D 86, 114018 (2012)
URL: http://link.aps.org/doi/10.1103/PhysRevD.86.114018
Aims: To enable us to compare the NJL-jet model results for the DFFs to those of other models or experimental data, we first require the DFFs to be evolved to a typical experimental scale of $Q^2 = 4$ GeV^2. This is achieved by employing the DGLAP evolution equations for the DFFs we obtained in the previous paper. In this paper we also present a comparison with the DFFs of another model to assess the validity of our results and the implementation of the evolution equations.

1.1.3 Gluon Polarization in the Proton

Authors: Steven D. Bass, Andrew Casey and Anthony W. Thomas
Journal: Physical Review C 83, 038202 (2011)
URL: http://link.aps.org/doi/10.1103/PhysRevC.83.038202
Aims: When it was discovered that the quarks contributed much less of the spin of the proton than initially assumed, the search for other sizeable contributions began. Other than the quark spin, three other quantities are identified as sources of proton spin, namely the quark orbital angular momentum, the gluon orbital angular momentum and the gluon polarization. The focus of this paper is to study the gluon polarization Δg in the proton using renormalization group arguments.

Chapter 2

QCD and the Parton Model

2.1 History

Experimental particle physicists studying cosmic rays in the 1950's observed a large number of particles which at the time were assumed to be elementary. These included the "mesons" (such as the pions, kaons and etas), which had masses between that of the electron and proton, and the "baryons" (such as the protons, lambdas and sigmas) which were significantly heavier than the mesons. With so many new particles being discovered, it was suggested that they couldn't all be elementary particles, and so there must be some deeper structure to these particles that we can use to describe them. This led to many attempts to order the mesons and baryons into groups based on their properties, such as charge, isospin, strangeness and mass. In the mid-60's, a classification scheme known as the eightfold way [4–6] emerged which organized the mesons and baryons into octets. It was later realized that the eightfold pattern could be explained in terms of elementary particles known as *quarks*. The quarks were at this time, theoretical constructs with no experimental observation of their existence. The mesons and baryons would eventually be collectively referred to as hadrons. Hadrons are composite particles of quarks bound together by the strong force, with mesons containing valence pairs of quarks and antiquarks, and baryons containing three valence quarks.

Following the deep-inelastic scattering experiments of electrons off of a proton

target at SLAC in 1968 [7], evidence for the existence of point-like objects contained within the proton was observed. These point-like objects found in hadrons where initially termed "partons" in the parton model by Feynman [8]. Feynman's parton model described hadrons in a reference frame in which the momentum was infinite. An important feature of this frame is that during the time in which the photon interacts with the parton, there are no parton-parton interactions and we can ignore the final state interactions.

Bjorken and Paschos [9] applied the parton model to electron-proton deep-inelastic scattering with the assumption that in the limit of the square of the momentum transfer of the exchanged photon (Q^2) going to infinity, the structure functions (explained in later subsection) display a scaling behavior, being dependent only on the Bjorken scaling variable x. The deep-inelastic scattering experiments at SLAC displayed this scaling behavior approximately [10]. The scaling behavior was approximate because infinite momentum is not possible in reality, and thus we can only consider increasingly large values of Q^2. Terms that violated the scaling behavior would have a large cumulative effect in perturbation theory. An asymptotically free quantum field theory that contained couplings that approach zero as the scale increases, would result in the scaling violation being much less severe. The combination of this idea of asymptotic freedom with the parton model proposed by Feynman and the quark model, led to the formulation of Quantum Chromodynamics (QCD). QCD is a non-abelian gauge field theory that describes the strong interactions between the fundamental particles known as quarks and gluons that carry "color" charge. The term "parton" now refers to quarks and gluons, and is mostly used when referring to high energy collisions, while quarks and gluons are the preferred terms when discussing QCD.

2.2 Quantum Chromodynamics

Quantum chromodynamics is the theory which describes the strong interactions between quarks and gluons. It is an SU(3) non-abelian gauge theory in which the interactions are mediated by gluons. Quarks and gluons both carry a type of charge called "color charge" which is analogous to the electromagnetic charge in

quantum electrodynamics (QED). Color charge was introduced in order to solve, for example, how three up quarks could exist in a Δ^{++} particle with their spin axis pointing in the same direction. Without color, this particle would violate Pauli's exclusion principle which states that no two identical fermions may occupy the same state. While the electromagnetic charge of a particle takes the form of a positive or negative value, the color charge of quark (anti-quark) takes the form of one of three values: blue (anti-blue), green (anti-green) or red (anti-red). Gluon color combinations are described in the $SU(3)$ adjoint representation by eight independent generators (Gell-Mann matrices, $\lambda_{i=1,...,8}$). In experimental tests of QCD we observe a phenomenon known as (color) confinement, which results in an inability to observe free quarks or gluons as particles are confined to color neutral states. Color neutrality can be attained by combining a particle of one color with another particle with the anti-color of the first, or by combining three particles with one of each of the colors. Hadrons, being particles composed of quarks and gluons, must therefore be color neutral.

Confinement is just one interesting property of QCD, with asymptotic freedom being another. Asymptotic freedom [11, 12], the discovery of which earned Gross, Politzer and Wilczek the 2004 Nobel Prize in Physics, causes the coupling strength between the quarks and gluons to become asymptotically weaker as the energy of the interactions increases, resulting in much fewer interactions at very high energies. It is this weakening of the interactions at high energies that allows perturbative calculations to be performed. To show this we will first discuss the QCD Lagrangian, followed by a discussion of the running of the strong coupling constant. The description of QCD presented here is based on that of Ref. [13], which we use as a resource for several other sections throughout this review of background material.

2.2.1 QCD Lagrangian

The free field and interaction dynamics of a quantum field theory are described by its Lagrangian density. To obtain the Lagrangian density for QCD we first consider the interactions involving quarks. The quark fields as a function of space

are written as

$$\psi(x) = \begin{pmatrix} \psi_r \\ \psi_g \\ \psi_b \end{pmatrix} \tag{2.1}$$

for each active flavor of the quarks. The quarks have a corresponding mass matrix $M = diag(m_u, m_d, ...)$. The terms in the Lagrangian must be invariant under local gauge transformations. The generators of the unitary gauge transformations U are the Gell-Mann matrices λ_a, where $a = 1, ..., 8$. The transformations themselves are written in the form

$$U = e^{-i\frac{\lambda_a \theta_a}{2}} \tag{2.2}$$

where θ_a represent eight real parameters. The Gell-Mann matrices, which are presented in Appendix .1, are traceless ($Tr(\lambda_a) = 0$) and satisfy the Lie algebra $[\lambda_a, \lambda_b] = 2if_{abc}\lambda_c$, where f_{abc} are structure functions that are antisymmetric in color. They also have the trace property $Tr(\lambda_a\lambda_b) = 2\delta_{ab}$. The quark fields transform under the gauge transformation as

$$\psi \to \psi' = U\psi \tag{2.3}$$

We require the Lagrangian density to be invariant under transformation of color at each point in space so that we have local gauge invariance. For QCD, this requires a covariant derivative D_μ (instead of just ∂_μ) for the interaction term between quarks and the gluons, which we define so that $D_\mu\psi$ transforms in the same way as ψ under gauge transformations. The gluon fields are represented as G^a_μ, such that $G_\mu \equiv \sum_a t_a G^a_\mu$ where $t_a \equiv \lambda_a/2$. The covariant derivative is then expressed as

$$D_\mu\psi = (\partial_\mu - igG_\mu)\psi, \tag{2.4}$$

where g is the coupling for the quark-gluon interactions. $D_\mu\psi$ must then transform as

$$D_\mu\psi \to (D_\mu\psi)' \equiv \partial_\mu\psi' - igG'_\mu\psi' \tag{2.5}$$

$$= U(D_\mu\psi). \tag{2.6}$$

To remain gauge invariant, we must determine how G_μ transforms, which we can find by the rearrangement of Eq. (2.5)

$$\partial_\mu \psi' - igG'_\mu U\psi = U(D_\mu \psi\ ) \tag{2.7}$$

$$\partial_\mu U\psi - igG'_\mu U\psi = U(\partial_\mu - igG_\mu)\psi \tag{2.8}$$

$$(\partial_\mu U)\psi + U\partial_\mu \psi - igG'_\mu U\psi = U(\partial_\mu - igG_\mu)\psi, \tag{2.9}$$

which gives $G'_\mu U = UG_\mu - \frac{i}{g}\partial_\mu U$, and therefore, using the unitarity property of the transformation ($UU^{-1} = I$, where I is the identity matrix),

$$G'_\mu = UG_\mu U^{-1} - \frac{i}{g}(\partial_\mu U)U^{-1}. \tag{2.10}$$

For small values of θ_a we can calculate infinitesimal gauge transformations, since $U = e^{-i\frac{\lambda_a \theta_a}{2}} \approx 1 - it_a\theta_a$, to first order in θ_a. This results in the gluon field transformation, to the same order, of

$$G^{a\prime}_\mu = G^a_\mu - \frac{1}{g}(\partial_\mu \theta^a) + f_{abc}\theta^b G^c_\mu, \tag{2.11}$$

where the last term, which involves the f_{abc} factor, arises from the non-commuting generators, a feature we obtain in a non-abelian theory, but not an abelian one such as QED.

In an abelian theory such as electromagnetism, the field strength tensor $F_{\mu\nu}$ can be expressed as

$$F_{\mu\nu} = \frac{i}{e}[D_\mu, D_\nu] = \frac{i}{e}(\partial_\mu A_\nu - \partial_\nu A_\mu) \tag{2.12}$$

where e is the coupling constant, A_μ is the photon field and, just for this equation, the covariant derivative is $D_\mu = \partial_\mu - ieA_\mu$. However, in QCD, the generators t_a do not commute, resulting in an extra term in the field strength tensor for the gluon such that

$$G^a_{\mu\nu} = \frac{i}{g}[D_\mu, D_\nu] = \partial_\mu G^a_\nu - \partial_\nu G^a_\mu + gf^{abc}G^b_\mu G^c_\nu \tag{2.13}$$

where g is the coupling constant. Multiplying $G^a_{\mu\nu}$ with $G^{\mu\nu}_a$, allows us to write

the kinetic term for the gluons in the Lagrangian density. The extra term in the gluon field strength tensor due to the non-commuting generators, results in self interactions between the gluon fields which is something that does not occur between the gauge fields in QED. The gluons can self-interact through a three-gluon vertex or a four-gluon vertex. The resulting gauge invariant Lagrangian density for QCD is of the form

$$\mathcal{L}_{QCD} = \bar{\psi}(i\not{D} - M)\psi - \frac{1}{4}G^a_{\mu\nu}G^{\mu\nu}_a. \tag{2.14}$$

Feynman rules can be calculated to describe the interactions, though we do not go in to the details here, and the Feynman diagrams for these interactions involve loops. In this thesis we consider diagrams up to one-loop order in perturbation theory as the calculations are simpler, with higher loop calculations being an interesting topic for future work. Calculations involving these loops result in divergent integrals, which are dealt with by a combination of regularization and renormalization. An important feature of renormalization is that we must choose a renormalization scale μ, which we use to add counterterms to the Lagrangian so that the infinities caused by loop divergences are shifted to something more manageable. Depending on the choice of renormalization scale, the Feynman diagram for a particular process may be well approximated by a simple tree-level diagram, while at a different renormalization scale, it may become much more complicated and several loops may need to be included.

The physical values we wish to extract, however, must be independent of the renormalization scale, as it is not a physical quantity itself. Since we do not calculate to all orders of the loops in the theory, a dependence on the renormalization scale arises. The variation of the coupling constant with respect to the renormalization scale can be described by beta-functions, which we will discuss in Section 2.2.2.

2.2.2 Running of α_s and Asymptotic Freedom

In QED, the charge of the electron is screened by a cloud of virtual e^+e^- pairs that are created from the vacuum and then annihilate each other. This screening results in the charge of the electron appearing lower the further away from the

electron we probe (low energy). Quarks in QCD also experience a screening effect of their color charge as a result of $q\bar{q}$ pairs from the vacuum. The quarks, however, also experience antiscreening due to gluon self interactions. This antiscreening results in the coupling strength increasing for large distances. Therefore, at small probing energies, the coupling is strong, which results in an inability to describe the physics at this energy scale using perturbative methods, but does however display the color confinement of QCD.

For large energy scales, or small distances, the coupling strength is very small, asymptoting in the high energy probe region, resulting in the quarks behaving almost as free particles. This is the property referred to as asymptotic freedom, and it is very important in perturbative calculations of QCD. In this high energy regime , we can expand the coupling perturbatively. It is convenient to write the strong coupling constant as

$$\alpha_s(\mu^2) = \frac{g^2(\mu)}{4\pi}. \tag{2.15}$$

The dependence of α_s on the renormalization scale (μ) is logarithmic due to the loop diagrams. We can describe the strong coupling constant's dependence on $\ln \mu^2$ using the QCD beta function

$$\beta(\alpha_s) = \frac{\partial \alpha_s(\mu^2)}{\partial \ln \mu^2} = -\left(\frac{\beta_0}{2\pi}\alpha_s^2 + \frac{\beta_1}{(2\pi)^2}\alpha_s^3 + ...\right), \tag{2.16}$$

where β_{n-1} are the n-loop calculated beta function coefficients. The one-loop and two-loop calculated beta function coefficients are

$$\beta_0 = \frac{33 - 2n_f}{3} \tag{2.17}$$

$$\beta_1 = \frac{153 - 19n_f}{3}, \tag{2.18}$$

where n_f is the number of flavors considered, and at most we have $n_f = 6$, which results in both these quantities being positive for $n_f \leq 6$. The strong coupling constant is also always positive as it is related to the square of $g(\mu)$. Therefore, the beta function in Eq. (2.16) is negative and α_s decreases with increasing scale as a result of the minus sign on the right-hand side of Eq. (2.16). This decrease

of the coupling with increasing scale is where asymptotic freedom originates. While the two-loop calculated beta function coefficient was shown above, all the calculations in the chapters that follow are calculated to one-loop order. The solution of the one-loop calculation for α_s is

$$\alpha_s(\mu^2) = \frac{\alpha_s(\mu_0^2)}{1 + \beta_0 \alpha_s(\mu_0^2) \ln \frac{\mu^2}{\mu_0^2}}, \tag{2.19}$$

where μ_0 is some scale at which we start our calculation. We define the mass scale Λ so that $1 = \beta_0 \alpha_s(\mu_0^2) \ln \frac{\mu_0^2}{\Lambda^2}$, which we then insert into Eq. (2.19) to obtain $\Lambda = \mu_0 exp(-2\pi/(\beta_0 \alpha_s(\mu_0^2)))$. This allows us to write α_s at leading order as

$$\alpha_s(Q^2) = \frac{4\pi}{\beta_0 \ln \frac{Q^2}{\Lambda^2}}, \tag{2.20}$$

where we have set $\mu = Q$ and there is no dependence on the scale μ_0.

2.3 Experimental Processes

2.3.1 Overview

Our theoretical understanding of the structure of the nucleon has progressed greatly in recent decades due in no small part to the advances of experimental processes including deep-inelastic scattering (DIS) and semi-inclusive deep-inelastic scattering (SIDIS). In this section we introduce these two processes as examples of scattering processes from which we can extract functions, such as parton distribution functions (PDFs) and fragmentation functions (FFs), that encode the deep nucleon structure. This section uses Ref. [13] as its primary resource for the description of these processes.

2.3.2 QCD Factorization Theorem

The QCD factorization theorem is a very important tool in the description of the experimental cross sections, and we will use it frequently in this section as well as Section 2.4.3 where we describe the Dokshitzer-Gribov-Lipatov-Altarelli-

Parisi (DGLAP) evolution equations [14–16]. In simple terms, QCD factorization theorem states that the cross section for scattering processes can be written as a convolution of short and long distance functions [17]. This allows us to separate out the perturbatively calculable parts, such as the partonic cross sections, and the non-perturbative, process independent functions, such as PDFs and/or FFs. To achieve this we introduce a factorization scale which we denote as μ. Above the factorization scale is the perturbative region, while below the factorization scale is the non-perturbative region.

A simple example of this is the cross section for a process such as

$$l + N \to l' + X, \tag{2.21}$$

where l and l' are the incoming and outgoing leptons, N is the struck hadron and X is the remnants of the collision. Employing factorization theorem allows us to write the hadronic cross sections as [18]

$$\sigma_N = \sum_q \sigma_q \otimes f_q^N, \tag{2.22}$$

where σ_N and σ_p are the hadronic and partonic cross sections, respectively, and f_q^N is the parton distribution function for the parton q in the hadron N. This is also shown diagrammatically [19] in Fig. 2.1. The notation used for the convolution is

$$f(x) \otimes g(x) \equiv \int_x^1 \frac{dy}{y} f\left(\frac{x}{y}\right) g(y), \tag{2.23}$$

for arbitrary functions f and g.

The factorization scale is interesting in that it is an unphysical quantity, but because the calculations are limited to a certain order in perturbation theory, physical quantities such as σ_N, which can't be μ-dependent, are expressed as the convolution of quantities that have some μ-dependence. This property plays an important role in our explanation of the DGLAP evolution equations, which are presented in Section 2.4.3.

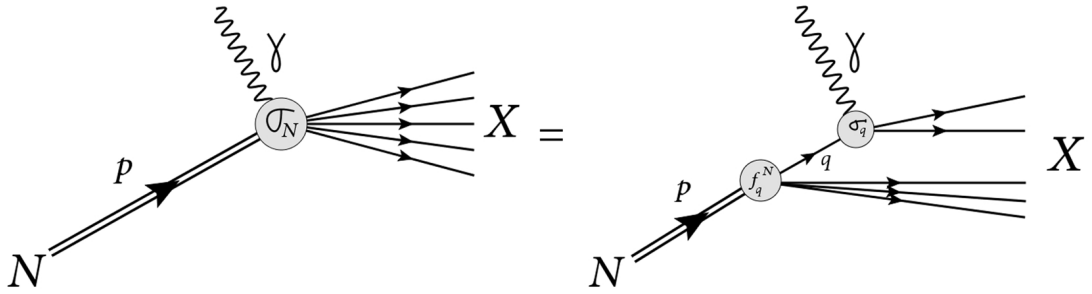

Figure 2.1: Diagrammatic representation of QCD factorization theorem

2.3.3 Deep Inelastic Scattering

Deep-inelastic scattering is a process in which the small-distance structure of hadrons is probed by a high energy lepton. We consider the inclusive process of the form

$$l(k) + N(p) \to l'(k') + X(p'), \tag{2.24}$$

shown diagrammatically in Fig. 2.2, where $l(k)$ is the incoming lepton with 4-momentum $k^\mu = (E, \vec{k})$, l' is the scattered lepton with 4-momentum $k'^\mu = (E', \vec{k'})$, $N(p)$ is the hadron with 4-momentum $p^\mu = (\sqrt{m_N^2 + \vec{p}^2}, \vec{p})$ being probed and $X(p')$ is all the remnants from the scattering process. The scattered lepton is the final particle that is detected in this process, with the observed quantities being the angle at which the lepton scatters and the momentum of the lepton.

During the scattering process, in the one-photon exchange approximation, the lepton emits a virtual photon that transfers momentum to the hadron. The 4-momentum that is transferred is written in terms of the initial and final lepton energy and momenta as

$$q^\mu = (E - E', \vec{k} - \vec{k'}). \tag{2.25}$$

The transfer of momentum is generally discussed in terms of the square of the momentum transfer, $Q^2 = -q^2$, where Q^2 is usually referred to as the virtuality of the photon. The energy transfer between the leptons is denoted as $\nu = E - E'$.

The mass squared, W^2, of the scattered remnants, also known as the invariant mass squared, is equal to the square of the sum of p and q. In the laboratory

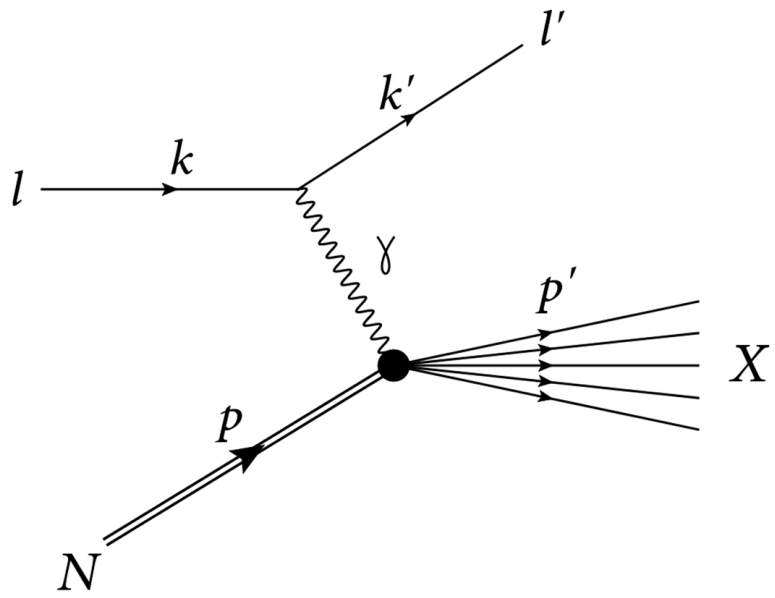

Figure 2.2: Deep inelastic scattering process

frame with $p^\mu = (m_N, \vec{0})$, we obtain

$$\begin{aligned} W^2 &= (p+q)^2 \\ &= p^2 + 2p\cdot q + q^2 \\ &= m_N^2 + 2p\cdot q - Q^2 \\ &= m_N^2 + Q^2(\frac{2p\cdot q}{Q^2} - 1) \\ &= m_N^2 + Q^2(\frac{2p\cdot q}{Q^2})(1 - \frac{Q^2}{2p\cdot q}) \\ &= m_N^2 + \frac{Q^2}{x_{Bj}}(1 - x_{Bj}), \end{aligned} \tag{2.26}$$

where x_{Bj}, which is the Bjorken scaling variable, is defined as

$$x_{Bj} \equiv \frac{Q^2}{2p\cdot q}. \tag{2.27}$$

The differential cross section for the DIS process can be written as

$$\frac{d\sigma}{d\Omega dE'} = \frac{\alpha^2}{Q^4}\frac{E'}{E}L^{\mu\nu}W_{\mu\nu}, \tag{2.28}$$

where α is the fine structure constant ($= e^2/4\pi$), $d\Omega$ is the solid angle that the lepton is scattered into, $L^{\mu\nu}$ is the leptonic tensor and $W_{\mu\nu}$ is the hadronic tensor.

The leptonic and hadronic tensors are factorized out separately since leptonic and hadronic currents interact only through the transfer of a virtual photon. We write the leptonic tensor [13] as

$$\begin{aligned} L^{\mu\nu}(k,k') &= \sum_{s'} \bar{u}_s(k)\gamma^\mu u_{s'}(k')\bar{u}_{s'}(k')\gamma^\nu u_s(k) \\ &= 2(k^\mu k'^\nu - k\cdot k' g^{\mu\nu} + k^\nu k'^\mu - i\epsilon^{\mu\nu\alpha\beta}s_\alpha q_\beta), \end{aligned} \tag{2.29}$$

where s_α is the lepton spin vector, u_s is leptons Dirac spinor, γ^μ are the Dirac matrices, $g^{\mu\nu}$ is the Minkowski space metric tensor, $\epsilon^{\mu\nu\alpha\beta}$ is the four-dimensional Levi-Civita symbol with $\epsilon^{0123} = +1$ and the small lepton mass has been neglected. The generalized hadronic tensor can be written in the following way, using Lorentz invariance, gauge invariance ($q^\mu W_{\mu\nu} = q^\nu W_{\mu\nu} = 0$) and parity conservation.

$$\begin{aligned} W_{\mu\nu}(p,p') &= \frac{1}{2m_h}\sum_X \langle h_s(p)|J_\mu(0)|X(p')\rangle\langle X(p')|J_\nu(0)|h_s(p)\rangle \\ &= \left(\frac{q_\mu q_\nu}{q^2} - g_{\mu\nu}\right)W_1(\nu,Q^2) \\ &\quad + \left(p_\mu - \frac{p\cdot q}{q^2}q_\mu\right)\left(p_\nu - \frac{p\cdot q}{q^2}q_\nu\right)\frac{W_2(\nu,Q^2)}{m_N^2} \\ &\quad + i\epsilon_{\mu\nu\alpha\beta}q^\alpha\left[S^\beta G_1(\nu,Q^2) + \frac{S^\beta p\cdot q - p^\beta S\cdot q}{m_N^2}G_2(\nu,Q^2)\right] \end{aligned} \tag{2.30}$$

where $W_1(\nu,Q^2)$, $W_2(\nu,Q^2)$, $G_1(\nu,Q^2)$ and $G_2(\nu,Q^2)$ are structure functions and S_β is the hadron spin vector. $W_1(\nu,Q^2)$ and $W_2(\nu,Q^2)$ are observed in scattering of unpolarized particles, whereas $G_1(\nu,Q^2)$ and $G_2(\nu,Q^2)$ are observed in the scattering of polarized leptons and hadrons. These functions are generally replaced by the structure functions $F_1(x,Q^2) = m_N W_1(\nu,Q^2)$, $F_2(x,Q^2) = \nu W_2(\nu,Q^2)$, $g_1(x,Q^2) = m_N\nu G_1(\nu,Q^2)$ and $g_2(x,Q^2) = \nu^2 G_2(\nu,Q^2)$, to investigate scaling

behavior in the asymptotic limit. In the naïve parton model, these structure functions can be written in terms of unpolarized ($q_i(x)$) and helicity ($\Delta q_i(x)$) distribution functions such that,

$$F_1(x, Q^2) = \frac{1}{2} \sum_i e_i^2 q_i(x) \tag{2.31}$$

$$F_2(x, Q^2) = x \sum_i e_i^2 q_i(x) \tag{2.32}$$

$$g_1(x, Q^2) = \frac{1}{2} \sum_i e_i^2 \Delta q_i(x) \tag{2.33}$$

$$g_2(x, Q^2) = 0, \tag{2.34}$$

where i is a sum over the active quark flavors and e_i is the charge of the quarks of flavor i in terms of the elementary charge e. The light-cone momentum fraction $x \equiv p_{i-}/p_-$ of the struck parton (with momentum p_i) that we have used here is related to the Bjorken scaling variable x_{Bj} in the frame where the proton has very high energy (the infinite momentum frame as is used in the parton model is discussed in Section 2.4.1). In Ref. [20] (from which we reproduce this calculation using our notation for the relevant momenta), a brief derivation is presented in the photon-nucleon centre of mass frame to show the relationship between x and x_{Bj}. The on-shell condition for a struck parton is given by

$$(p_f)^2 = 2p_i \cdot q + q^2 = \hat{s} + \hat{t} + \hat{u} = 0, \tag{2.35}$$

where p_f is the momentum of the parton after it is struck, and $\hat{s} = (k + p_i)^2$, $\hat{t} = (k - k')^2$ and $\hat{u} = (p_i - k')^2$ are elementary Mandelstam variables. After cancellation of the appropriate terms, this expression is written as

$$\hat{s} + \hat{t} + \hat{u} = -(p_{i\perp})^2 \frac{x_{Bj}}{x} + Q^2 \frac{x}{x_{Bj}} - Q^2 = 0, \tag{2.36}$$

where $p_{i\perp} = |\boldsymbol{p_{i\perp}}|$ is the transverse momentum of the struck parton. Using the

quadratic formula and the bounds $x \in [0, 1]$ to write x as

$$x = \frac{x_{Bj}}{2}\left(1 + \sqrt{1 + \frac{4(p_{i\perp})^2}{Q^2}}\right). \tag{2.37}$$

In the limit of very large Q^2, the second term in the square root approaches zero, resulting in $x = x_{Bj}$. In this thesis, the light-cone momentum fraction x is the preferred notation when discussing structure functions and parton distribution functions, however, in Section 2.4.2 we use x_{Bj} to enforce the fact that we are discussing Bjorken scaling.

Unpolarized parton distribution functions describe the probability to detect a parton i with light-cone momentum fraction x inside the target, and extractions of these quantities are obtained through fits to unpolarized DIS cross sections [21]. The helicity parton distribution functions measures the density of partons with spin parallel minus the density of partons with spin anti-parallel, with momentum fraction x of the longitudinally polarized target. The helicity distributions are extracted from the cross sections of polarized DIS experiments. The measurements obtained from DIS experiments are unable to distinguish contributions from particular flavors of quark, or between quarks and antiquarks, and so SIDIS cross section asymmetries [22], which are sensitive to the individual quark and antiquark flavors, become very important tools in the determination of the parton distribution functions.

2.3.4 Semi-Inclusive Deep-Inelastic Scattering

In DIS, the information we extract is the energy and angle of the scattered lepton. SIDIS experiments detect not only the information about the final lepton, but also information about one final emitted hadron. This provides us with a greater ability to probe the quark flavor structure of the nucleon. We consider the SIDIS process, which is shown diagrammatically in Fig. 2.3 of the form

$$l(k) + N(p) \to l'(k') + h_1(p_1) + X(p'), \tag{2.38}$$

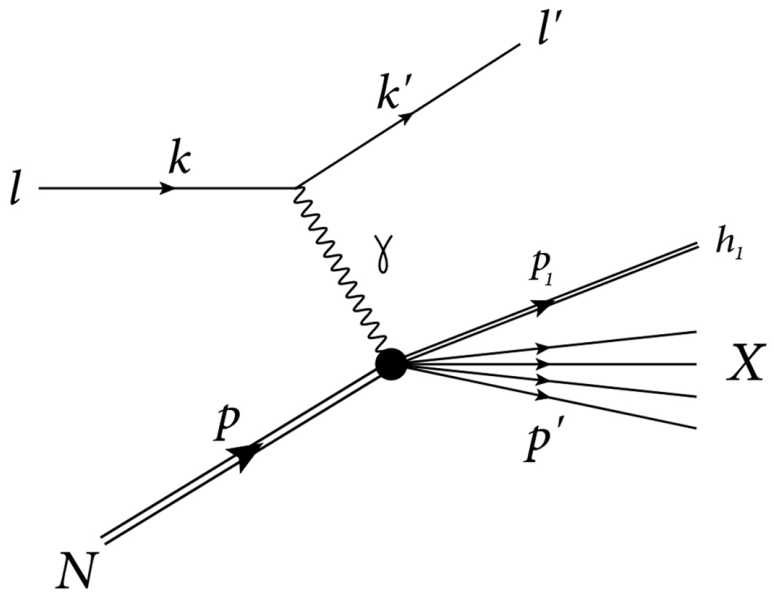

Figure 2.3: Semi-inclusive deep inelastic scattering process

where we now have a detected hadron h_1 with momenta p_1 and therefore a slightly different collection of remnant hadronic matter as there is one less hadron included in X. Using the so-called factorization theorem, the cross section for this process, with unpolarized initial and final state particles, can be written in terms of the convolution [18]

$$d\sigma^h = \sum_q f_{q/N}(x, Q^2) \otimes d\sigma^q \otimes D_q^{h_1}(z, Q^2), \tag{2.39}$$

where $f_{q/N}(x, Q^2)$ are the parton distributions of quarks q in hadron N, $d\sigma^q$ is the partonic cross section and $D_q^{h_1}(z, Q^2)$ are the fragmentation functions. The fragmentation functions represent the probability for a quark or gluon to fragment in to hadron h_1 with light-cone (LC) momentum fraction z of the fragmenting quark. SIDIS processes allow extraction of the third leading twist distribution functions, known as transversity distribution functions ($\Delta_T q_i(x)$) [23], which describe transversely polarized quarks within transversely polarized nucleon and appear in SIDIS asymmetries with the Collins fragmentation functions [24–26]. Dihadron fragmentation functions, which appear in two hadron inclusive DIS,

are also of interest in the extraction of transversity [27, 28], with comparable results [29] to those obtained in Refs [24–26].

In the next chapter we will present a brief review of the Nambu–Jona-Lasinio (NJL) model, which has previously been employed to calculate distribution and fragmentation functions [30–33]. Dihadron fragmentation functions arise in processes in which there are two detected hadrons rather than one. The work presented in Ref. [1] discusses the extension of this model to include calculations of the dihadron fragmentation functions for pions and kaons. To be able to compare the NJL-jet model results with other models or experimental data, we require the DGLAP evolution equations for both the single hadron and dihadron fragmentation functions, which we obtain in Section 2.4.3. These equations allow us to determine these functions for a range of Q^2 values, but before we get to them, we first describe where they arise.

2.4 Parton Model

In the parton model, we assume that hadrons are constituted by a number of pointlike, loosely bound particles called partons [8]. This is a reasonable assumption as long as the energy scales considered are much larger than the mass of the hadron, and thus the mass of the partons too, so that these masses can be neglected. Colliding hadrons at high energies produces a plethora of particles. This is an indicator that hadrons have a deeper structure that we can investigate. Since the particles are travelling at high speeds in these kinds of scattering processes, it is convenient to work in the infinite momentum frame, wherein the hadrons are assumed to have infinite momentum in the direction of the particle beam (usually labelled the z direction). We again use Ref. [13] here as a guide for the description of the parton.

2.4.1 Infinite Momentum Frame

The infinite momentum frame in which the parton model is described has a couple of interesting features. Since the momentum is so large, any particles produced in interactions tend to be collinear with the colliding beam. In this

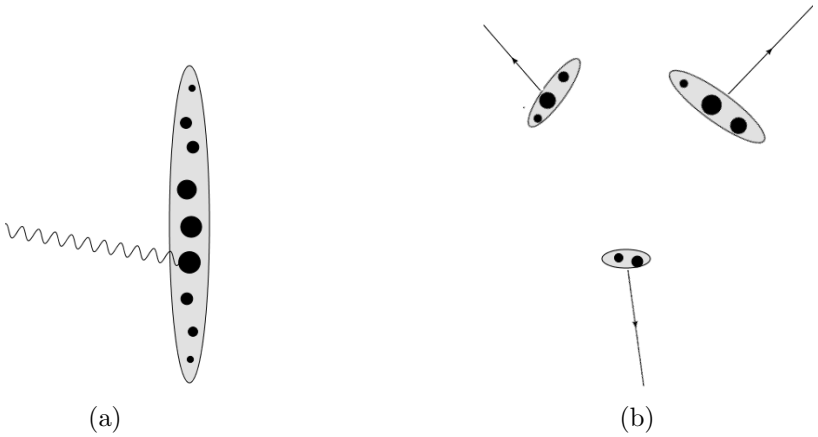

Figure 2.4: Parton picture of scattering with a photon probing a hadron (a) before the virtual photon has an affect and (b) after the virtual photon collides, resulting in multiple smaller combinations of partons

thesis we consider cross sections in which the transverse momentum has been integrated over. In the infinite momentum frame we encounter the relativistic effects Lorentz contraction and time dilation, and these effects are presented in this picture of the scattering interactions. Lorentz contraction in the infinite momentum frame results in the distribution of the partons being spread out into a long disc shape [34], as shown in Fig 2.4. The partons in this frame are considered to be spread far enough apart that the probability of interactions between the partons, after the transfer of the virtual photon, is very small. Time dilation also limits the likelihood of parton-parton interactions occurring in this frame. The hadron would be moving so fast that the duration of any interaction would be very long inside the hadron, such that the partons would appear to be almost frozen in place within the hadron. From the laboratory frame this could be alternatively viewed as the interaction involving the virtual photon occurring very quickly, while the parton-parton interactions would take too long to occur.

For these reasons, the interactions between partons can be ignored, and the partons considered as 'free' so that the scattering we observe can occur. We note, however, that we know from QCD that the partons, which we identify with quarks and gluons, are 'free' as a result of asymptotic freedom, rather than due to the relativistic effects that we mentioned that produce the desired effect within

the infinite momentum frame of the parton model.

2.4.2 Bjorken Scaling

One of the main concepts that the parton model entails is that any object with a finite size must have a form factor to help describe its internal structure. In elastic collisions, the form factors depend only on the momentum transfer $Q^2 = 2M\nu$, where ν is the virtual photons energy and M is the hadronic mass. Inelastic collisions, however, depend on two variables, the momentum transfer Q^2 and the Bjorken scaling variable $x_{Bj} = Q^2/(2M\nu)$, and as result we replace the form factors of the form $F_i(Q^2)$ with structure functions of the form $F_i(x_{Bj}, Q^2)$.

Back in the late 1960's, Bjorken derived a scaling behavior for the structure functions that arise in the hadronic tensor of electron-nucleon DIS processes [35]. This scaling behavior, which was derived from current algebra techniques, predicted that in the asymptotic or high-Q^2 (and high-ν so that ν/Q^2 is fixed) limit, the structure functions would depend only on the Bjorken scaling variable x_{Bj}, and not on the scale Q^2. The Bjorken scaling behavior was later observed in DIS experiments at SLAC [10], though it was only approximately true. Scaling violations are observed for the structure functions in perturbative calculations at each order. These violations would be quite severe if it weren't for asymptotic freedom. Since the coupling becomes small at large Q^2, the effect of the scaling violations, which are a result of mass singularities, have a much smaller effect. The corrections to the scaling violations have a logarithmic dependence on the momentum scale, which can be described by a set of equations which determine the change of functions, such as PDFs, with respect to $\ln Q^2$. While these equations go by a variety of names, we refer to them here as the Dokshitzer-Gribov-Lipatov-Altarelli-Parisi (DGLAP) evolution equations [14–16], which we now discuss.

2.4.3 DGLAP Evolution Equations

The DGLAP evolution equations are named after multiple authors who derived them around the same time. The authors were, in the order that their initials appear in the acronym, Yu. L. Dokshitzer [14], V.N. Gribov and L.N. Lipatov [15],

and G.Altarelli and G. Parisi [16]. These equations allow us to calculate corrections to non-perturbative functions that arise due to scaling violations that are associated with the radiative gluons that are produced at high energies. While perturbative QCD cannot be used to determine parton distribution functions or fragmentation functions, due to their non-perturbative characteristics that depend on momentum fractions, it can be used to determine their dependence on momentum scale as this is perturbative. We employ DGLAP evolution equations for this purpose on numerous occasions in this thesis. We limit ourselves to leading order evolution equations and note that evolution to low Q^2, such that we approach the hadronic or partonic masses, become less accurate as the non-perturbative effects become more significant in this region. At that point, higher order perturbation theory is required to obtain more accurate results.

In the literature there are typically two extremes when DGLAP evolution equations are being discussed. Authors generally will sometimes simply write down the evolution equations without showing much, if any, description of how they arise. Other times, however, there will be a detailed derivation taking in to account a variety of aspects including model-scheme dependent terms. Rather than derive the evolution equations using renormalization group equations or by considering Mellin moments, the derivation we present here will focus on a simplistic interpretation in which we use the convolution properties of the cross sections and their appropriate factorizations. While this won't be rigorous enough to describe model-scheme dependence, which typically don't survive the derivations to the evolution equations anyway, it will introduce the main features of the evolution equations, such as the logarithmic dependence on scale and the relevant splitting functions.

We note that the use of the DGLAP evolution equations for the single hadron and dihadron fragmentation functions is a focus of the work we presented in Ref. [2]. In that work, we obtain results for the single hadron and dihadron fragmentation functions evolved to a typical experimental scale of 4 GeV^2, as well as a comparison with the results obtained by Majumder et. al. in their work [36].

2.4.3.1 Parton Distribution Function Evolution Equations

We consider a simple process $e^- + h \to \gamma(Q) \to (e^-)' + X$, where h is a hadron, e^- is an electron which emits a virtual photon γ with momenta Q, such that it recoils as $(e^-)'$, and X is the remnants of the process. The hadronic cross section is an observable quantity and must therefore be independent of any logarithmic dependency on the factorization scale μ^2, which implies

$$\frac{d}{d\ln\mu^2}\left(\frac{d\sigma_h}{dx}\right) = 0. \tag{2.40}$$

For this process we have a hadronic cross section that factorizes as [17, 18, 21]

$$\frac{d\sigma_h}{dx} = \sum_i \sigma_i \otimes f_i^h, \tag{2.41}$$

where σ_i is the cross section for a parton i and f_i^h is the parton distribution function for a parton i in hadron h. Applying Eq. (2.40) to Eq. (2.41) gives us

$$\begin{aligned} \sum_i \frac{d}{d\ln\mu^2}(\sigma_i \otimes f_i^h) &= 0 \\ \sum_i \frac{d}{d\ln\mu^2}(\sigma_i) \otimes f_i^h + \sum_i \sigma_i \otimes \frac{d}{d\ln\mu^2}(f_i^h) &= 0 \end{aligned} \tag{2.42}$$

If we were able to calculate the partonic cross section and parton distribution functions to all orders in perturbation theory, they would also be independent of the factorization scale, but since we are limited in the order at which we calculate, they both acquire a factorization scale dependence.

We interpret increasing Q^2 as increasing the resolution with which we are probing the hadron, allowing us to consider there to be a probability that a parton will be resolved as splitting in to two other partons. At leading order, we consider only one splitting being resolved, such that the evolution is affected by a factor of $\alpha_s(Q^2)\ln(Q^2/\mu^2)$. Higher orders result in multiple splitting and terms up to $(\alpha_s(Q^2)\ln(Q^2/\mu^2))^n$ would have to be considered, where $n = 1$ for leading order (LO), $n = 2$ for next-to-leading order (NLO), and so forth. The probability of splittings is described by the four LO splitting functions shown in

Fig. 2.5. For each of the splittings, there are three partons, with the incoming parton being labelled as i and the two outgoing partons labelled as j and k. The parton j receives a fraction η of the incoming parton's momentum, while the parton k receives a fraction $1-\eta$ of the incoming parton's momentum. Both $P_{qq}(\eta)$ and $P_{gq}(\eta)$ are splitting processes described as gluon radiation, with the primary difference being which of the two partons, that the quark splits into, takes the momentum fraction η. $P_{qg}(\eta)$ is the quark pair production splitting function, while $P_{gg}(\eta)$ is the splitting function for gluon splitting into two gluons.

The partonic cross section is therefore of the form

$$\sigma_i = \sum_j (\alpha_s \ln(Q^2/\mu^2)) P_{ji}(\eta) \otimes \sigma_j, \tag{2.43}$$

which when we take the derivative with respect to $\ln \mu^2$ gives

$$\frac{d\sigma_i}{d\ln\mu^2} = -\sum_j \alpha_s P_{ji}(\eta) \otimes \sigma_j, \tag{2.44}$$

and thus from Eq. (2.42) we obtain

$$\begin{aligned} -\sum_{i,j} \alpha_s P_{ji}(\eta) \otimes \sigma_j \otimes f_i^h + \sum_i \sigma_i \otimes \frac{d}{d\ln\mu^2}(f_i^h) &= 0 \\ \sum_{i,j} \sigma_i \otimes (-\alpha_s P_{ij}(\eta) \otimes f_j^h) + \sum_i \sigma_i \otimes \left(\frac{d}{d\ln\mu^2}(f_i^h)\right) &= 0, \end{aligned} \tag{2.45}$$

where we relabelled the indices in the first term, set the factorization scale to $\mu = Q$ and equated the bracketed terms to obtain the DGLAP evolution equations for the PDFs

$$\frac{d}{d\ln Q^2}\left(f_i^h\right) = \sum_j \alpha_s P_{ij}(\eta) \otimes f_j^h. \tag{2.46}$$

The splitting functions are known up to NNLO, however we only require the LO

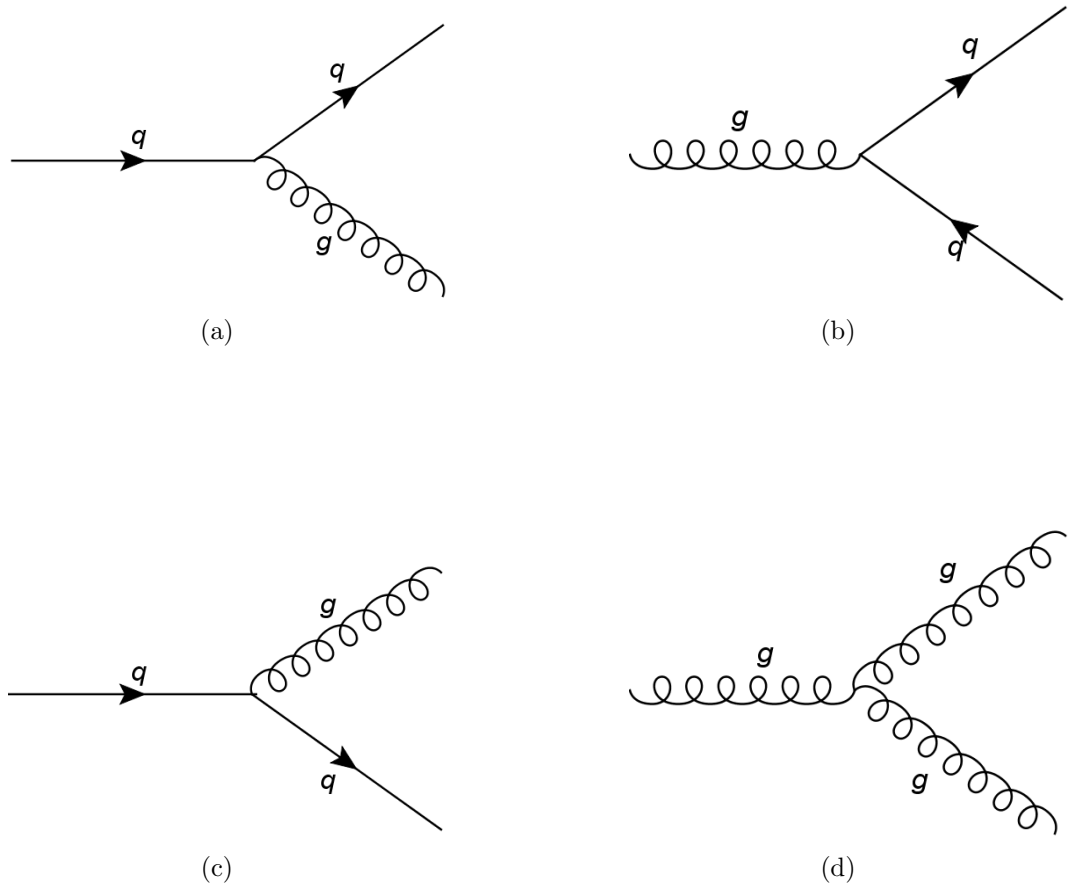

Figure 2.5: Processes of the LO splittings involved in DGLAP evolution equations. Diagram for (a) $P_{qq}(\eta)$, (b) $P_{qg}(\eta)$, (c) $P_{gq}(\eta)$ and (d) $P_{gg}(\eta)$. The incoming parton has a momentum fraction of 1, the parton at the top has a momentum fraction of η and thus the parton at the bottom has momentum fraction of $1-\eta$.

splitting functions (obtained from [37]) which are given by

$$P_{q_j q_i}(\eta) = \delta_{ij} C_F \left[\frac{1+y^2}{(1-y)_+} + \frac{3}{2}\delta(1-y) \right] \tag{2.47}$$

$$P_{qg}(\eta) = T_R \left[y^2 + (1-y)^2 \right] \tag{2.48}$$

$$P_{gq}(\eta) = C_F \left[\frac{1+(1-y)^2}{y} \right] \tag{2.49}$$

$$P_{gg}(\eta) = 2C_G \left[\frac{y}{(1-y)_+} + \frac{1-y}{y} + y(1-y) + \left(\frac{11}{12} - \frac{1}{3}\frac{n_f T_R}{C_G} \right) \delta(1-u) \right], \tag{2.50}$$

where $C_G = N_c = 3$, $C_F = \frac{N_c^2-1}{2N_c} = \frac{4}{3}$, $T_R = \frac{1}{2}$, N_c is the number of colors and n_f is the number of flavors. The '+' prescription used is defined for an arbitrary function $a(x)$ by

$$\int_0^1 dx' \frac{a(x')}{(1-x')_+} = \int_0^1 dx' \frac{a(x') - a(1)}{(1-x')}, \tag{2.51}$$

which can be written as

$$\int_x^1 dx' \frac{a(x')}{(1-x')_+} = \int_x^1 dx' \frac{a(x') - a(1)}{(1-x')} + a(1)\ln(1-x). \tag{2.52}$$

2.4.3.2 Single Hadron Fragmentation Function Evolution Equations

To obtain the DGLAP evolution equations for the fragmentation functions we perform a similar combination of steps in which we consider the process $e^+ + e^- \to \gamma(Q) \to h(p) + X$ where γ is a virtual photon with momenta Q, h is hadron with momenta p and X is the remnant matter from the collision [38]. Using the factorization theorem, the cross section for this process can be written as the convolution of the partonic cross section σ^i, which is perturbatively calculable, and the fragmentation function $D_i^h(z)$, which is non-perturbative, in the following form [38]

$$\frac{d\sigma^h}{dz} = \sum_i \sigma^i \otimes D_i^h. \tag{2.53}$$

The hadronic cross section, however, is a physical quantity and therefore must be independent of the scale of factorization, μ, such that

$$\frac{\partial \frac{d\sigma^h}{dz}}{\partial \ln \mu^2} = 0. \tag{2.54}$$

Since the partonic cross section and the fragmentation function pick up a dependence on the scale as result of factorization, this dependence must cancel out so that the hadronic cross section remains independent of the scale. For this to be

true, the following must hold

$$\begin{aligned}\frac{\partial \frac{d\sigma^h}{dz}}{\partial \ln \mu^2} &= \frac{\partial(\sum_i \sigma^i \otimes D_i^h)}{\partial \ln \mu^2} \\ &= \sum_j \frac{\partial \sigma^j}{\partial \ln \mu^2} \otimes D_j^h + \sum_i \sigma^i \otimes \frac{\partial D_i^h}{\partial \ln \mu^2} \\ &= 0. \end{aligned} \tag{2.55}$$

The derivatives of the partonic cross sections and fragmentation functions must be related to the partonic cross sections and fragmentation functions, respectively, convoluted with a function that is common to both, which we denote as $\frac{\alpha_s(Q^2)}{2\pi} P_{ji}$, of the form

$$\frac{\partial \sigma^j}{\partial \ln \mu^2} = -\sum_i \sigma^i \otimes \frac{\alpha_s(Q^2)}{2\pi} P_{ji} \tag{2.56}$$

$$\frac{\partial D_i^h}{\partial \ln \mu^2} = \sum_j D_j^h \otimes \frac{\alpha_s(Q^2)}{2\pi} P_{ji}, \tag{2.57}$$

so that

$$\begin{aligned}\sum_j \frac{\partial \sigma^j}{\partial \ln \mu^2} \otimes D_j^h &= -\sum_i \sigma^i \otimes \frac{\partial D_i^h}{\partial \ln \mu^2} \\ -\frac{\alpha_s(Q^2)}{2\pi} \sum_{i,j} \sigma^i \otimes P_{ji} \otimes D_j^h &= -\frac{\alpha_s(Q^2)}{2\pi} \sum_{i,j} \sigma^i \otimes D_j^h \otimes P_{ji}. \end{aligned} \tag{2.58}$$

We could relabel the indices in Eq. (2.56) to compare it with Eq. (2.44) and notice that the indices on the splitting functions are switched. This is a result of the splitting occurring after the interaction of the virtual photon, rather than before it. This is also why the evolution equations for the parton distribution functions (Eq. (2.46)) and the fragmentation functions (Eq. (2.57)) have splitting functions with switched indices, as the parton distribution functions are functions of the initial state, while the fragmentation functions are final state functions. Expanding out the convolution of Eq. (2.57) we can write the corresponding

evolution equation for the SFFs in the more familiar form

$$\frac{\partial}{\partial \ln Q^2} D_i^h(z, Q^2) = \frac{\alpha_s(Q^2)}{2\pi} \sum_j \int_z^1 \frac{dy}{y} P_{ji}(y) D_j^h \left(\frac{z}{y}, Q^2 \right), \tag{2.59}$$

where we have set $\mu = Q$.

2.4.3.3 Dihadron Fragmentation Function Evolution Equations

The QCD evolution equations for DFFs are derived from factorization of the cross-section for the production of two hadrons in $e^+e^- \to \gamma(Q) \to h_1(z_1) + h_2(z_2) + X$ [38], in much the same way as the PDFs and FFs were. More care is required there because there are two processes in which two hadrons can fragment from a parton. The first process considered is when both hadrons are fragmented in the same decay chain from the same parton. The parton from which the two hadrons are originate has momentum fraction u, since the hadrons are not necessarily produced at the first emission step. This momentum fraction must lie between $z_1 + z_2$ and one, since the parton must have enough momentum to provide the momentum fractions z_1 and z_2 to the emitted two hadrons, and the most momentum fraction it can carry is one. The second process considers the possibility of the hadrons being fragmented from separate partons, which are decaying along the same direction so that they are part of the same jet. For this process, we assume that the parton that produces h_1 carries momentum fraction u, while the parton the emits h_2 must then carry momentum fraction $1-u$, where the initial parton carries a momentum fraction of one.

QCD factorization theorem allows the cross section for the production of two hadron's in e^+e^- annihilation to be written as [38]

$$\frac{d\sigma^{h_1 h_2}}{dz_1 dz_2} = \sum_i \sigma^i \otimes D_i^{h_1 h_2} + \sum_{i,j} \sigma^{ij} \otimes D_i^{h_1} \otimes D_j^{h_2}, \tag{2.60}$$

where σ^i is the cross section for parton i and σ^{ij} is the partonic cross section for production of partons i and j. The notation used for the convolutions, where we use f and g as arbitrary functions, is the same as in Eq. (2.23). We now apply the same procedure on Eq. (2.60) as was applied to Eq. (2.53). Taking the derivative

with respect to $\ln \mu^2$, we obtain

$$\begin{aligned}\frac{d(\frac{d\sigma^{h_1 h_2}}{dz_1 dz_2})}{d\ln\mu^2} =& \sum_i \frac{d(\sigma^i)}{d\ln\mu^2} \otimes D_i^{h_1 h_2} + \sum_i \sigma^i \otimes \frac{d(D_i^{h_1 h_2})}{d\ln\mu^2} + \sum_{i,j} \frac{d(\sigma^{ij})}{d\ln\mu^2} \otimes D_i^{h_1} \otimes D_j^{h_2} \\ &+ \sum_{i,j} \sigma^{ij} \otimes \frac{d(D_i^{h_1})}{d\ln\mu^2} \otimes D_j^{h_2} + \sum_{i,j} \sigma^{ij} \otimes D_i^{h_1} \otimes \frac{d(D_j^{h_2})}{d\ln\mu^2} \\ =& 0, \end{aligned} \tag{2.61}$$

Using Eqs. (2.56) and (2.57), we can rewrite almost all of these terms except for the derivatives of the DFF and σ^{ij}. The derivative of σ^{ij} receives contributions from three possible processes. The first is the process in which a parton k splits to produce partons i and j, where parton k had a cross-section of σ^k and a splitting function of $\hat{P}_{ji}^k$. The splitting functions $\hat{P}_{ji}^k$ are the same as the splitting functions of the form P_{ik} (making sure the indices are consistent), except we drop the delta functions as there are no virtual contributions. The second process involves the two partons b and j (σ_{bj}), where b splits in to a parton i, resulting in partons i and j. The third process is similar to the second, with the parton j being produced as a result of a splitting from a parton a instead of i from b. This results in the derivative of the form

$$\frac{d(\sigma^{ij})}{d\ln\mu^2} = -\frac{\alpha_s(Q^2)}{2\pi} \sum_k \sigma^k \otimes \hat{P}_{ji}^k - \frac{\alpha_s(Q^2)}{2\pi} \sum_b \sigma^{bj} \otimes P_{ib} - \frac{\alpha_s(Q^2)}{2\pi} \sum_a \sigma^{ia} \otimes P_{aj}, \tag{2.62}$$

which we can then insert into Eq. (2.61), resulting in

$$
\begin{aligned}
&-\frac{\alpha_s(Q^2)}{2\pi}\sum_{i,j}\sigma^j\otimes P_{ij}\otimes D_i^{h_1h_2}+\sum_i\sigma^i\otimes\frac{d(D_i^{h_1h_2})}{d\ln\mu^2}\\
&\qquad-\frac{\alpha_s(Q^2)}{2\pi}\sum_{i,j,k}\sigma^k\otimes\hat{P}_{ji}^k\otimes D_i^{h_1}\otimes D_j^{h_2}\\
&-\frac{\alpha_s(Q^2)}{2\pi}\sum_{b,i,j}\sigma^{bj}\otimes P_{ib}\otimes D_i^{h_1}\otimes D_j^{h_2}-\frac{\alpha_s(Q^2)}{2\pi}\sum_{a,i,j}\sigma^{ia}\otimes P_{aj}\otimes D_i^{h_1}\otimes D_j^{h_2}\\
&+\frac{\alpha_s(Q^2)}{2\pi}\sum_{b,i,j}\sigma^{ij}\otimes P_{bi}\otimes D_b^{h_1}\otimes D_j^{h_2}+\frac{\alpha_s(Q^2)}{2\pi}\sum_{a,i,j}\sigma^{ij}\otimes P_{aj}\otimes D_i^{h_1}\otimes D_a^{h_2}=0,
\end{aligned}
\tag{2.63}
$$

where the third and fourth lines cancel each other, after a relabeling of indices. Further relabeling of indices on the remaining terms leads to

$$
\begin{aligned}
\sum_i\sigma^i\otimes\frac{d(D_i^{h_1h_2})}{d\ln\mu^2}=&\frac{\alpha_s(Q^2)}{2\pi}\sum_{i,j}\sigma^i\otimes P_{ji}\otimes D_j^{h_1h_2}\\
&+\frac{\alpha_s(Q^2)}{2\pi}\sum_{i,j,k}\sigma^i\otimes\hat{P}_{kj}^i\otimes D_j^{h_1}\otimes D_k^{h_2}.
\end{aligned}
\tag{2.64}
$$

Using the convolution in Eq.(2.23) and setting $\mu=Q$, we obtain the corresponding DGLAP evolution equations used to describe the Q^2-dependence of the DFFs in the form

$$
\begin{aligned}
\frac{d}{d\ln Q^2}D_i^{h_1h_2}(z_1,z_2,Q^2)=&\sum_j\frac{\alpha_s(Q^2)}{2\pi}\int_{z_1+z_2}^1\frac{du}{u^2}\;D_j^{h_1h_2}\left(\frac{z_1}{u},\frac{z_2}{u},Q^2\right)P_{ji}(u)\\
&+\sum_{j,k}\frac{\alpha_s(Q^2)}{2\pi}\int_{z_1}^{1-z_2}\frac{du}{u(1-u)}\,D_j^{h_1}\left(\frac{z_1}{u},Q^2\right)D_k^{h_2}\left(\frac{z_2}{1-u},Q^2\right)\hat{P}_{kj}^i(u),
\end{aligned}
\tag{2.65}
$$

where the sums are over $u,\ d,\ s,\ \bar{u},\ \bar{d},\ \bar{s}$ and g for $N_f=3$ (number of flavors). We restrict ourselves to the up, down and strange quarks and antiquarks as the heavy quark fragmentations would be very small. Their inclusion is left for future extensions of this line of research.

2.5 Proton Spin Crisis

In Section 2.3.3 we introduced the nucleon structure functions $F_1,\ F_2,\ g_1$ and g_2, which in the Bjorken limit were independent of Q^2 and thus only depended on the scaling variable x. The spin dependent structure function g_1 for the proton provides us with a starting point for determining the contributions to the spin of the proton. The proton is a subatomic particle that is comprised of three valence quarks bound together by gluons, with a spin of $\frac{1}{2}$. It was initially believed that the protons spin could be calculated by summing the spins of the quarks that it is composed of. Through experiments in the late 1980's by the European Muon Collaboration (EMC) [39], it was shown that the quarks contribute only a small portion of the protons spin. It was this result that led to what is referred to as the "Proton Spin Crisis", which led to a search for how much other components may contribute to the spin of the proton.

In fact, the spin of the quarks, written as $\Delta\Sigma$, contributes approximately a third of the spin to the proton. This leaves about two thirds of the spin unaccounted for. There are three candidates that are considered to contribute to the proton's spin. The first of these is the orbital angular momentum of the quarks which is represented by the symbol L_q. Two others are the gluon spin, ΔG, and the orbital angular momentum of the gluons, L_g. We write the spin of the proton in terms of these quantities as

$$\frac{1}{2} = \Delta\Sigma + L_q + \Delta G + L_g, \tag{2.66}$$

which can also be written as $\frac{1}{2} = J_q + J_g$ where J_q and J_g are the total angular momenta of the quarks and gluons, respectively, and each are the sum of their respective spin and orbital angular momentum components.

When the EMC determined that the quark spin contribution was smaller than expected, they did so through measuring the spin asymmetry in DIS of longitudinally polarized muons by longitudinally polarized protons over a large range of x. This allowed them to determine the spin dependent structure function of the proton, $g_1^p(x)$, and its integral over x. The result obtained by the EMC

was

$$\Delta\Sigma = \Delta u + \Delta d + \Delta s \approx (14 \pm 9 \text{ [statistical]} \pm 21 \text{ [systematic]})\%, \tag{2.67}$$

where Δu, Δd and Δs are the up, down and strange quark contributions to the spin of the proton, where [40]

$$\Delta q = \int_0^1 \Delta q(x) dx, \tag{2.68}$$

with helicity distribution functions $\Delta q(x)$ for each quark flavor. The EMC result (Eq. 2.67) allowed for a quark spin contribution consistent with zero, which could have meant that the proton contained a large amount of polarized gluons. Polarized gluons can contribute to $g_1^p(x)$ through the $U(1)$ axial anomaly [41–46]. In that case, the axial anomaly can be accounted for by writing the quark spin contribution as

$$\Delta\Sigma = \Delta\Sigma_{quark} - \frac{N_f \alpha_s(Q^2)}{2\pi} \Delta G(Q^2), \tag{2.69}$$

where $\Delta\Sigma_{quark}$ is the prediction from the quark model.

However, $\Delta\Sigma$ has been more precisely calculated to now be about a third, $\Delta\Sigma \approx (33 \pm 3 \pm 5)\%$ [47–49]. Myhrer and Thomas [50] showed that using $\Delta\Sigma_{quark} \approx 67\%$, calculated from the naive bag model, and $\alpha_s(Q^2) \approx 0.3$, $\Delta G(Q^2)$ would have to be approximately 2.4. Experimental data indicates that $\Delta G(Q^2)$ is much smaller than this. Through the combination of one-gluon exchange and pion-cloud corrections [50], Myhrer and Thomas were able to obtain a model calculation for $\Delta\Sigma_{quark}$ between 0.35 and 0.4, which would allow for values of $\Delta G(Q^2)$ consistent with experimental data [51].

2.5.1 Polarization of the Gluon in the Proton

The spin structure function is related to the quark spin contribution through [52]

$$\int_0^1 dx g_1^p(x, Q^2) = \left(\frac{1}{12} g_A^{(3)} + \frac{1}{36} g_A^{(8)} \right) c_{NS}(Q^2) + \frac{1}{9} c_S(Q^2) g_A^{(0)}|_{inv}, \tag{2.70}$$

where $g_A^{(3)}$ (Eq. (2.71)) and $g_A^{(8)}$ (Eq. (2.72)) are the isovector and octet axial charges, respectively, and $c_{NS}(Q^2)$ and $c_S(Q^2)$ are the non-singlet and singlet Wilson coefficients, respectively. The scale-invariant flavor singlet axial charge is equivalent to $g_A^{(0)}(Q^2)$ evaluated in the limit $Q^2 \to \infty$, such that $g_A^{(0)}|_{inv} = g_A^{(0)}(\infty)$. The axial charges can be written, in the $N_f = 3$ flavor theory, in terms of Δq as

$$g_A^{(3)} = \Delta u - \Delta d \tag{2.71}$$

$$g_A^{(8)} = \Delta u + \Delta d - 2\Delta s \tag{2.72}$$

$$g_A^{(0)}|_{inv}/E_{N_f}(\alpha_s) \equiv g_A^{(0)} = \Delta u + \Delta d + \Delta s. \tag{2.73}$$

where Δq refers to the expectation value

$$2M_p s_\mu \Delta q = \langle p, s|\bar{q}\gamma_\mu\gamma_5 q|p, s\rangle. \tag{2.74}$$

Here M_p and s_μ are the mass and spin of the proton, respectively. $E_{N_f}(\alpha_s)$ is a renormalization group factor in the N_f flavor theory written as

$$E_{N_f}(\alpha_s) = exp \int_0^{\alpha_s} d\tilde{\alpha_s}\gamma_{N_f}(\tilde{\alpha_s})/\beta_{N_f}(\tilde{\alpha_s}), \tag{2.75}$$

where $\gamma_{N_f}(\tilde{\alpha_s})$ is the anomalous dimension and $\beta(\tilde{\alpha_s})$ is the QCD beta function. The singlet axial-vector current $J_{\mu 5} = \sum_{q=u,d,s} \bar{q}\gamma_\mu\gamma_5 q$ has a non-zero anomalous dimension (at two loops) [53] $\gamma_{N_f}(\alpha_s)$, and so $E_{N_f}(\alpha_s)$ is used to correct this. To evaluate the expression for $E_f(\alpha_s)$ in Eq. (2.75), we use the perturbative QCD expressions for $\gamma_{N_f}(\alpha_s)$ and $\beta_{N_f}(\alpha_s)$:

$$\gamma_{N_f}(\alpha_s) = N_f \left(\frac{\alpha_s}{\pi}\right)^2 + ... \tag{2.76}$$

and

$$\beta_{N_f}(\alpha_s) = -\left(11 - \frac{2}{3}N_f\right)\frac{\alpha_s^2}{2\pi} + ... \tag{2.77}$$

to first order in α_s, where $C_F = \frac{4}{3}$ and $C_A = 3$.

The scale-invariant flavor singlet axial charge is equivalent to $g_A^{(0)}(Q^2)$ evaluated in the limit $Q^2 \to \infty$, such that $g_A^{(0)}|_{inv} = g_A^{(0)}(\infty)$. Using Eq. (2.73) we can

relate these to $E_{N_f}(\alpha_s)$ in the following way:

$$g_A^{(0)}|_{inv} = g_A^{(0)}(\infty) = E_{N_f}(\alpha_s) g_A^{(0)}(Q^2) \tag{2.78}$$

In Eq. (2.69), the quark spin was related to contribution from the gluon spin. This can be written in terms of $g_A^{(0)}(Q^2)$ such that

$$g_A^{(0)} = \left(\sum_q \Delta q - N_f \frac{\alpha_s}{2\pi} \Delta g \right)_{\text{partons}} + \mathcal{C}_\infty, \tag{2.79}$$

where $\mathcal{C}_\infty$ denotes a potential non-perturbative gluon topological contribution. The singlet axial charge measured by polarized DIS equals $g_A^{(0)} - \mathcal{C}_\infty$.

In Eq. (2.79), the $\Delta q_{partons}$ and $\mathcal{C}_\infty$ terms are renormalization group invariant, so the difference between $g_A^{(0)}|_\infty$ and $g_A^{(0)}|_{Q^2}$ is related only to the difference between terms involving the gluonic contribution in the following way:

$$g_A^{(0)}|_{inv} - g_A^{(0)}|_{Q^2} = -N_f \left((\frac{\alpha_s}{2\pi} \Delta g)|_\infty - (\frac{\alpha_s}{2\pi} \Delta g)|_{Q^2} \right). \tag{2.80}$$

Using Eq. (2.78), and rearranging to obtain $(\frac{\alpha_s}{2\pi} \Delta g)|_{Q^2}$, this can be written as

$$\left(\frac{\alpha_s}{2\pi} \Delta g \right)|_{Q^2} = \left(\frac{\alpha_s}{2\pi} \Delta g \right)|_\infty - \frac{1}{N_f} g_A^{(0)}|_{inv} \left(\frac{1}{E_{(N_f)}(\alpha_s)} - 1 \right), \tag{2.81}$$

In the limit where $Q^2 \to \infty$, $E_{N_f}(\alpha_s)$ goes to a value of one. This implies that

$$\alpha_s(Q^2) \Delta g(Q^2) \to \text{constant}, \quad Q^2 \to \infty. \tag{2.82}$$

By considering the 4-flavor theory and employing Eqs. (2.79) and (2.81), we can investigate the gluon polarization Δg and even suggest an upper bound on its value. This is the calculation presented in Ref. [3], where the possible error for the bound is assessed by considering the NLO evolution associated with $\gamma_{N_f}(\alpha_s)$ and the size of $\Delta c_{partons}$.

Chapter 3

Nambu–Jona-Lasinio model

3.1 Concepts and Properties of the Nambu–Jona-Lasinio model

The dynamics of QCD is described by its Lagrangian and the applications of QCD to scattering processes at high momentum transfers has had considerable success. This is in no small part due to the property of QCD at short distances known as *asymptotic freedom*, which is the phenomenon, where the coupling strength between quarks and gluons reduces asymptotically as the momentum transfer increases. It is this feature of QCD that allows us to carry out perturbative calculations of scattering cross sections. However, at low momentum transfers (typically < 1 GeV^2), or equivalently large distances, such QCD calculations are not viable. This is due to the coupling strength being too large, which means that perturbative techniques that are valid at low strength can no longer be applied with the same certainty.

Several approaches have been considered to obtain results in the low energy region, though each must make approximations. Lattice gauge theory, which discretizes spacetime in to a number of points to produce a lattice, is one such approach which has received considerable resources [54]. Another method employed to model the low energy region is to construct a simpler Lagrangian density that retains some essential features of QCD, such as symmetries. This method allows the exploration of specific features of the strong interactions in the low energy

region.

The Nambu–Jona-Lasinio (NJL) model [55, 56] is one such model, with Lagrangian density constructed to contain symmetries of QCD. Chiral symmetry is one such symmetry that is necessary for understanding the properties of the lightest hadrons. The spontaneous breaking of chiral symmetry, which results in the dynamic generation of fermion masses, and the appearance of Goldstone bosons are two important features of the NJL model. One of the downsides of the NJL model is that the interactions between quarks are assumed to be point-like, which results in the NJL model being a nonrenormalizable field theory. This results in divergences appearing in the loop integrals. A suitable regularization scheme must be prescribed to deal with these. The regularization scheme chosen in this work is the Lepage-Brodsky invariant mass cutoff scheme [57]. Another downside of the NJL model is that due to the lack of gluons in the model, the confinement property of QCD is not described.

In this chapter we will discuss the Lagrangian used for the NJL model, the resultant quark mass gap equation, meson decay constant and the quark-meson coupling. The last two topics in particular are of importance for the later calculations of fragmentation functions from the NJL-jet model. A brief description of the Lepage-Brodsky regularization scheme is also presented.

3.1.1 Nambu–Jona-Lasinio Model Lagrangian

For the NJL model, we consider a Lagrangian density composed of two terms [58, 59]. The first is the free quark field Lagrangian, which describes quarks in isolation, while the second term is the chiral invariant interaction Lagrangian. This is expressed as

$$\mathcal{L}_{NJL} = \bar{\psi}(i\partial\!\!\!/ - m)\psi + G[(\bar{\psi}\psi)^2 + (\bar{\psi}i\gamma_5\tau\psi)^2] \tag{3.1}$$

In the three-flavor NJL model, the $SU(3)$-flavor symmetry is explicitly broken since the strange quark mass cannot be chosen equal to the mass of the the non-strange quarks. We note that the interaction Lagrangian here is for the four-quark interaction only, as we have chosen to restrict ourselves to interactions of this form. An additional six-quark interaction term can also be considered to

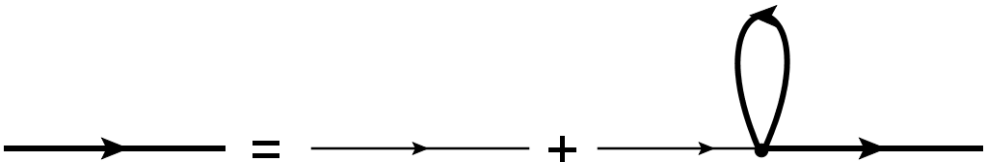

Figure 3.1: Diagrammatic representation of the mass gap equation in the NJL model. Bold lines represent the propagators for the dynamically generated massive constituent quarks and the thin lines are propagators for the current quarks.

explicitly break axial $U(1)$ symmetry, however we do not consider it here as it has its own consequences that we do not wish to study.

3.1.2 Mass Gap Equation

In the NJL model, the mass gap equation allows us to describe the interaction of a particle with the quark condensate. It has the form:

$$M = m_q - 2G\langle\bar{\psi}\psi\rangle, \tag{3.2}$$

where M is the dynamically generated quark mass, m_q is the current quark mass from the NJL Lagrangian, G is the coupling for the $\bar{q}q$ channel and $\langle\bar{\psi}\psi\rangle$ is the quark $\bar{q}q$ condensate. We show the diagrammatic representation of Eq. (3.2) in Fig. 3.1, where the bold lines represent the propagators of the dynamically generated massive constituent quarks and the thin lines are the propagators for the current quarks. The quark condensate is calculated as a quark self-energy $\Sigma = -2G\langle\bar{\psi}\psi\rangle$ and can thus be expressed in terms of the integral of the trace over color, isospin and Dirac indices for the Feynman propagator of a constituent quark in the form

$$\begin{aligned}
\langle\bar{\psi}\psi\rangle =& -i\int\frac{d^4q}{(2\pi)^4}TrS(q) \\
=& -i2N_c\int\frac{d^4q}{(2\pi)^4}Tr_D[S(q)] \\
=& -2N_c i\int\frac{d^4q}{(2\pi)^4}Tr_D\left[\frac{\not{q}+M}{q^2-M^2+i\epsilon}\right],
\end{aligned} \tag{3.3}$$

where N_c is the number of colors and the Dirac trace of the gamma matrices (see Appendix .2) can easily be solved using the properties shown in Appendix .3, resulting in

$$\begin{aligned}\langle\bar{\psi}\psi\rangle =& -2N_c i\int\frac{d^4q}{(2\pi)^4}\left[\frac{4M}{q^2-M^2+i\epsilon}\right]\\ =& -8MN_c iI_1(M^2),\end{aligned} \tag{3.4}$$

with

$$I_1(M^2)=\int\frac{d^4q}{(2\pi)^4}\frac{1}{q^2-M^2+i\epsilon}. \tag{3.5}$$

The integral in Eq. (3.5) is divergent as $q^2\to\infty$, and thus requires some form of regularization. By employing three-momentum cutoff regularization, which we discuss in Section 3.3.1 with the cutoff denoted as Λ_{3M}, and using integration by parts (some useful integral relations are included in Appendix .4), we obtain the following expression for the quark condensate:

$$\begin{aligned}\langle\bar{\psi}\psi\rangle =& -8MN_c i\int_{-\Lambda_{3M}}^{\Lambda_{3M}}\frac{d^3q}{(2\pi)^3}\left[\frac{i}{-2E_q}\right]\\ =& -4MN_c\int_{-\Lambda_{3M}}^{\Lambda_{3M}}\frac{dq}{(2\pi)^3}(4\pi)\mathbf{q}^2\left[\frac{1}{\sqrt{\mathbf{q}^2+M^2}}\right]\\ =& -\frac{2MN_c}{\pi^2}\left(\Lambda_{3M}\sqrt{\Lambda_{3M}^2+M^2}-M^2\text{arcsinh}\left(\frac{\Lambda_{3M}}{M}\right)\right),\end{aligned} \tag{3.6}$$

which leads to the mass gap equation of the form

$$M=m_q+12G\frac{M}{\pi^2}\left(\Lambda_{3M}\sqrt{\Lambda_{3M}^2+M^2}-M^2\text{arcsinh}\left(\frac{\Lambda_{3M}}{M}\right)\right). \tag{3.7}$$

We now consider Eq. (3.7) in the chiral limit, $m_q\to 0$, to investigate the constraint the mass gap equation places on values for the coupling G. Imposing

this limit, we obtain

$$\begin{aligned} M =& 12G\frac{M}{\pi^2}\left(\Lambda_{3M}\sqrt{\Lambda_{3M}^2+M^2}-M^2\text{arcsinh}\left(\frac{\Lambda_{3M}}{M}\right)\right) \\ \frac{\pi^2}{12G} =& \Lambda_{3M}\sqrt{\Lambda_{3M}^2+M^2}-M^2\text{arcsinh}\left(\frac{\Lambda_{3M}}{M}\right) \\ \frac{\pi^2}{12G\Lambda_{3M}^2} =& \sqrt{1+\frac{M^2}{\Lambda_{3M}^2}}-\frac{M^2}{\Lambda_{3M}^2}\text{arcsinh}\left(\frac{\Lambda_{3M}}{M}\right), \end{aligned} \tag{3.8}$$

where in the limit of $M \to 0$ the right hand side approaches one, resulting in a critical value of the coupling

$$G_{crit} = \frac{\pi^2}{12\Lambda_{3M}^2}. \tag{3.9}$$

For $G < G_{crit}$ in the chiral limit, the condensate equals zero as we require M to be positive. The right hand side of Eq. (3.8) decreases and eventually asymptotically approaches 0 as M becomes larger, and so $G \geq G_{crit}$, and thus G_{crit} is the value of the coupling strength above which the quark condensate becomes non-zero and chiral symmetry is dynamically broken.

3.2 Bethe-Salpeter Equation and the Bubble Graph

We now consider mesons within the NJL model. The mesons are bound states of quarks and antiquarks that are typically produced in a relativistic frame, and so in the NJL model we typically study them by solving the relativistic two-body bound state equation known as the Bethe-Salpeter equation (BSE) [60]. In the NJL model, the BSE is written as [61]

$$\mathcal{T}_{\alpha\beta,\gamma\delta}(k) = \mathcal{K}_{\alpha\beta,\gamma\delta} + \int \frac{d^4q}{(2\pi)^4}\mathcal{K}_{\alpha\beta,\lambda\epsilon}S_{\epsilon\epsilon'}(k-q)S_{\lambda\lambda'}(q)\mathcal{T}_{\epsilon'\lambda',\gamma\delta}(k), \tag{3.10}$$

where the indices ($\alpha,\ \beta,\ \gamma,\ \delta$, etc) denote the quark flavors, $\mathcal{T}$ is the two-body t-matrix, S is the fermion propagator and $\mathcal{K}$ is the relevant interaction kernel.

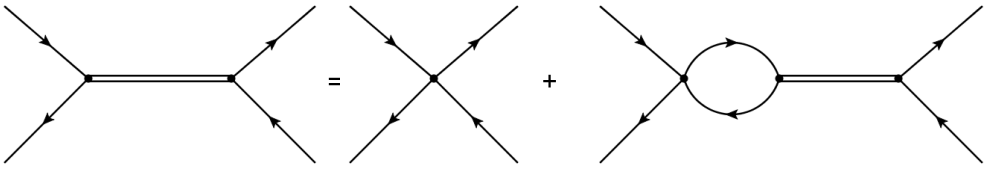

Figure 3.2: Diagrammatic representation of the Bethe-Salpeter equation shown in Eq. (3.10).

This equation is shown diagrammatically in Fig. 3.2. The relevant interaction kernel for the pseudoscalar mesons is of the form

$$\mathcal{K}_{\alpha\beta,\gamma\delta} = -2iG_m(\gamma_5\tau_i)_{\alpha\beta}(\gamma_5\tau_i)_{\gamma\delta}, \tag{3.11}$$

where τ_i are the generators of the isospin groups denoted with isospin indices i ($\tau_i = \sigma_i$ for SU(2), $\tau_i = \lambda_i$ for SU(3)). Eq. (3.10) can be rearranged to describe $\mathcal{T}$ in terms of $\mathcal{K}$ and S, which we show in Eq. (3.12) and Fig. 3.3,

$$\begin{aligned}\mathcal{T}_{\alpha\beta,\gamma\delta}(k) =& \frac{\mathcal{K}_{\alpha\beta,\gamma\delta}}{1 - \int \frac{d^4q}{(2\pi)^4} Tr\left[S_{\epsilon\epsilon'}(q-k)\mathcal{K}_{\alpha\beta,\lambda\epsilon}S_{\lambda\lambda'}(q)\right]} \\ =& (\gamma_5\tau_i)_{\alpha\beta}\tau_m(k)(\gamma_5\tau_i)_{\gamma\delta},\end{aligned} \tag{3.12}$$

where $\tau_m(k)$ is the reduced t-matrix given by

$$\tau_m(k) = \frac{-2iG_m}{1 + 2G_m\Pi_m(k^2)}, \tag{3.13}$$

and the quark-antiquark bubble graph is given by

$$\Pi_m(k^2) = i\int \frac{d^4q}{(2\pi)^4} Tr\left[(\gamma_5\tau_i)S_1(q)(\gamma_5\tau_{i'})S_2(q-k)\right], \tag{3.14}$$

with the subscripts on the propagators indicating quarks of different flavors which we call q and Q such that the meson can be identified as $m = q\bar{Q}$. The trace in Eq. (3.14) includes traces over Dirac, isospin and color indices and the labels on

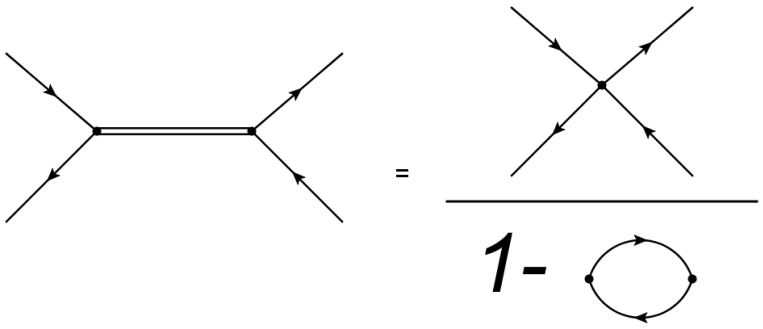

Figure 3.3: Diagrammatic representation of the rearranged Bethe-Salpeter equation shown in Eq. (3.12).

the propagators. Performing the trace we obtain

$$\Pi_m(k^2) = 2N_c i \int \frac{d^4q}{(2\pi)^4} Tr_D \left[\gamma_5 S_1(q)\gamma_5 S_2(q-k)\right], \tag{3.15}$$

where $N_c = 3$. Taking the trace using the properties of the gamma matrices listed in Appendix .3, and using the mass gap equation (3.2), we can rewrite Eq. (3.15) as

$$\Pi_m(k^2) = 12 i I_{12}(k^2)[k^2 - (M_1 - M_2)^2] - 4N_c i \int \frac{d^4q}{(2\pi)^4} \left[\frac{1}{q^2 - M_1^2} + \frac{1}{q^2 - M_2^2}\right] \tag{3.16}$$

where M_1 and M_2 are the masses of the quarks with propagators S_1 and S_2, respectively, and $I_{12}(k^2)$ is an integral of the form

$$I_{12}(k^2) = \int \frac{d^4q}{(2\pi)^4} \frac{1}{(q^2 - M_1^2 + i\epsilon)((q-k)^2 - M_2^2 + i\epsilon)}. \tag{3.17}$$

For the pion case, we note that since the up and down quarks are assumed to be equal in mass, M_1 and M_2 can simply be replaced by M. This allows us to right

the second term on the right hand side as

$$-4N_c i\int\frac{d^4q}{(2\pi)^4}\left[\frac{1}{q^2-M_1^2}+\frac{1}{q^2-M_2^2}\right]=-8N_c i\int\frac{d^4q}{(2\pi)^4}\left[\frac{2}{q^2-M^2}\right]$$
$$=\frac{\langle\bar{\psi}\psi\rangle}{M}, \tag{3.18}$$

where we replaced the integral with the quark condensate from Eq. (3.4). Using the mass gap equation (Eq. (3.2)), we obtain a much simpler form for $\Pi_\pi(k^2)$, written as

$$\Pi_\pi(k^2)=12k^2iI_{11}(k^2)-\frac{M-m_q}{2G_\pi M}. \tag{3.19}$$

The mass of the meson is obtained from the pole of the t-matrix, which can be expressed as

$$1+2G_m\Pi_m(k^2=m_m^2)=0, \tag{3.20}$$

where we will demonstrate the solution for the pion case due to its simplicity. This pole is then expressed as

$$1+2G_\pi\Pi_\pi(k^2=m_\pi^2)=0$$
$$1+2G_\pi\left(12m_\pi^2iI_{11}(m_\pi^2)-\frac{M-m_q}{2G_\pi M}\right)=0$$
$$-\frac{-m_q}{M}+24m_\pi^2iI_{11}(m_\pi^2)=0,$$

which rearranges into the expression for the mass of the pion as follows

$$m_\pi^2=-\frac{m_q}{M}\frac{1}{24iG_\pi I_{11}(m_\pi^2)}. \tag{3.21}$$

It is noted that, as a manifestation of chiral symmetry, the pion mass vanishes in the chiral limit $m_q\to 0$.

3.2.1 Quark-Meson Coupling

We now return to the diagram on the left hand side of Fig. 3.2 and its solution in Eq. (3.12), as it can be equivalently expressed in terms of the quark-meson coupling, g_{mqQ}. This coupling arises in several of the functions that we will be dis-

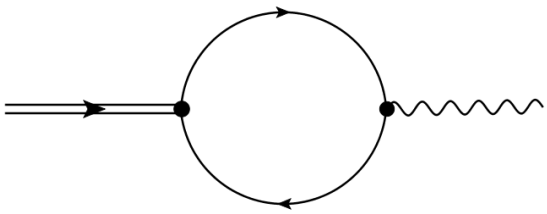

Figure 3.4: Feynman diagram for the decay of a meson

cussing the later sections, and thus we outline the way it is typically determined. In the pole approximation, we define the relationship between quark-meson coupling and the reduced t-matrix solution to the BSE as

$$\frac{ig_{mqQ}^2}{k^2 - m_{m^2}} \approx \frac{-2iG_m}{1 + 2G_m\Pi_m(k^2)}, \tag{3.22}$$

which is inverted and the derivative with respect to k^2 is taken to obtain

$$g_{mqQ}^{-2} = -\left(\frac{\partial\Pi_m(k^2)}{\partial k^2}\right)_{k^2=m_m^2}, \tag{3.23}$$

which for the pions can be expressed as

$$g_{\pi qQ}^{-2} = -12i\left(\frac{\partial(k^2 I_{11}(k^2))}{\partial k^2}\right)_{k^2=m_\pi^2}. \tag{3.24}$$

Before this expression can be determined, we require an appropriate regularization scheme. The regularization schemes employed will be discussed in Section 3.3. The quark-meson coupling is related to another important variable known as the meson decay constant, which we discuss now.

3.2.2 Meson Decay Constant

The meson decay constant, which we denote as f_m, is another observable quantity that arises in the determination of the constituent quark masses and is a measure of the strength of chiral symmetry breaking. It is defined by the matrix element of the diagram in Fig. 3.4 which we express as

$$
\begin{aligned}
if_m q_\mu \delta_{ab} &= \langle 0|\bar{\psi}\gamma_\mu\gamma_5\frac{1}{2}\tau_a\psi|m_b(q)\rangle \qquad (3.25)\\
&= \int \frac{d^4k}{(2\pi)^4} Tr\left[i\gamma_\mu\gamma_5\frac{\tau_a}{2}S_1(k)i\gamma_5 g_{mqQ}\tau_b S_2(k-q)\right]|_{q^2=m_m^2}\\
&f_m q_\mu \delta_{ab}\\
&= iN_c g_{mqQ}\delta_{ab}\int \frac{d^4k}{(2\pi)^4} Tr_D\left[\frac{\gamma_\mu\gamma_5(\gamma_\alpha k^\alpha + M_1)\gamma_5(\gamma_\nu(k^\nu - q^\nu)+M_2)}{(k^2-M_1^2+i\epsilon)((k-q)^2+M_2^2+i\epsilon)}\right]|_{q^2=m_m^2}, \qquad (3.26)
\end{aligned}
$$

where q_μ is the momentum of the meson m_b which has isospin τ_b and $\tau_a/2$ is the isospin associated with the axial vector current. Here, the isospin indices a and b run over the number of generators of the $SU(N_f)$ group (over 1 to 3 for $SU(2)$ and over 1 to 8 $SU(3)$).

Performing the trace over the Dirac indices, we obtain

$$
f_m q_\mu \delta_{ab} = iN_c g_{mqQ}\delta_{ab}\int \frac{d^4k}{(2\pi)^4}\left[\frac{4k_\mu(M_1-M_2)-4M_1 q_\mu}{(k^2-M_1^2+i\epsilon)((k-q)^2+M_2^2+i\epsilon)}\right]|_{q^2=m_m^2}. \qquad (3.27)
$$

It is easy to see that for the pion, the term involving k_μ disappears as a result of $M_1 = M_2 \equiv M$, leading to

$$
\begin{aligned}
&f_\pi q_\mu \delta_{ab}\\
&= -4Mq_\mu(iN_c g_{\pi qQ}\delta_{ab})\int \frac{d^4k}{(2\pi)^4}\left[\frac{1}{(k^2-M^2+i\epsilon)((k-q)^2+M^2+i\epsilon)}\right]|_{q^2=m_\pi^2}\\
f_\pi &= -4M(iN_c g_{\pi qQ})\int \frac{d^4k}{(2\pi)^4}\left[\frac{1}{(k^2-M^2+i\epsilon)((k-q)^2+M^2+i\epsilon)}\right]|_{q^2=m_\pi^2}\\
f_\pi &= -4M(iN_c g_{\pi qQ})I_{11}(m_\pi^2). \qquad (3.28)
\end{aligned}
$$

Combining the equations for the pion mass from Eq. (3.2) and the pion decay

constant from Eq. (3.28), we can write the following expression

$$\begin{aligned} f_\pi^2 m_\pi^2 =& (-4M(iN_c g_{\pi qQ}) I_{11}(m_\pi^2))^2 \left(-\frac{m_q}{M}\frac{1}{24iG_\pi I_{11}(m_\pi^2)}\right) \\ =& \frac{4^2 M^2 i^2 N_c^2 g_{\pi qQ}^2 I_{11}^2(m_\pi^2)}{24iG_\pi I_{11}(m_\pi^2)}\left(-\frac{m_q}{M}\right) \\ =& \frac{i12M^2 g_{\pi qQ}^2 I_{11}(m_\pi^2)}{2G_\pi}\left(-\frac{m_q}{M}\right), \end{aligned} \tag{3.29}$$

where

$$\begin{aligned} g_{\pi qQ}^2 &= \left[-12i\left(\frac{\partial(k^2 I_{11}(k^2))}{\partial k^2}\right)_{k^2=m_\pi^2}\right]^{-1} \\ &= \left[-12i\left(I(m_\pi^2) + m_\pi^2 \frac{\partial(I_{11}(m_\pi^2))}{\partial m_\pi^2}\right)\right]^{-1}. \end{aligned} \tag{3.30}$$

Inserting this into the previous expression, we obtain

$$\begin{aligned} f_\pi^2 m_\pi^2 =& \frac{i12M^2 I_{11}(m_\pi^2)}{2G_\pi}\left(-\frac{m_q}{M}\right)\left[\frac{1}{-12i\left(I_{11}(m_\pi^2) + m_\pi^2 \frac{\partial(I_{11}(m_\pi^2))}{\partial m_\pi^2}\right)}\right] \\ =& \frac{MI_{11}(m_\pi^2)}{2G_\pi}(m_q)\left[\frac{1}{\left(I_{11}(m_\pi^2) + m_\pi^2 \frac{\partial(I_{11}(m_\pi^2))}{\partial m_\pi^2}\right)}\right] \\ =& \frac{m_q M}{2G_\pi}\left[\frac{1}{1 + m_\pi^2 \frac{1}{I_{11}(m_\pi^2)}\frac{\partial(I_{11}(m_\pi^2))}{\partial m_\pi^2}}\right]. \end{aligned} \tag{3.31}$$

Inserting the mass gap equation (Eq. (3.2)) into Eq. (3.31), we can write this as

$$f_\pi^2 m_\pi^2 = \frac{m_q(m_q - 2G_\pi\langle\bar{\psi}\psi\rangle)}{2G_\pi}\left[\frac{1}{1 + m_\pi^2 \frac{1}{I_{11}(m_\pi^2)}\frac{\partial(I_{11}(m_\pi^2))}{\partial m_\pi^2}}\right], \tag{3.32}$$

which to first order in m_q, where $I_{11}(m_\pi^2)$ is regarded as a slowly varying function [62] so that fraction involving the integral is approximately one, is the the Gell-Mann-Oakes-Renner (GOR) relation [63]:

$$f_\pi^2 m_\pi^2 \approx -m_q \langle \bar{\psi}\psi \rangle. \tag{3.33}$$

The GOR relation describes the connection between the explicit (masses: m_π, m_q) and spontaneous (f_π, $\langle \bar{\psi}\psi \rangle$) breaking of chiral symmetry for pions and quarks.

3.3 Regularization

In the process of calculating Feynman diagrams, we repeatedly encounter integrals that are divergent as the momentum approaches infinity. We therefore require an appropriate regularization scheme to be able to obtain results with finite values. In the line of research in which previous calculations regarding PDFs and FFs have been calculated, there have been two particular schemes that have been employed, namely three-momentum cutoff regularization and Lepage-Brodsky (LB) invariant mass cutoff regularization. These two regularization schemes have been shown to be consistent with each other, as will be discussed later. We will first describe the three-momentum cutoff regularization scheme, which we will label with the subscript $3M$, and demonstrate its application to several of the divergent integrals we have encountered. This will be followed by a description of light-cone (LC) variables, which then leads on to the Lepage-Brodsky (LB) invariant mass cutoff regularization scheme.

3.3.1 Three-Momentum Cutoff Regularization

Feynman diagrams calculated in momentum space have an integration variable of the form $d^4q = dq_0 dq_1 dq_2 dq_3$ for a four-momentum q_μ. In the three-momentum cutoff regularization scheme, we first integrate out the time component of the momentum, q_0, which is typically achieved using the residue theorem. Integrals

of the form

$$\int \frac{d^4q}{(2\pi)^4}\frac{\mathcal{A}(q)}{q^2-M^2+i\epsilon} = \int \frac{d^3q}{(2\pi)^3}\int \frac{dq_0}{(2\pi)}\frac{\mathcal{A}(q)}{q_0^2-(\boldsymbol{q}^2+M^2)+i\epsilon}, \tag{3.34}$$

occur regularly throughout our calculations, for an arbitrary function $\mathcal{A}(q)$, such as the integral in the quark $\bar{q}q$ condensate of Eq. (3.4). We define the energy $E_q = \sqrt{\boldsymbol{q}^2+M^2}$ and note that the q_0 integral can expressed as

$$\int \frac{dq_0}{(2\pi)}\frac{\mathcal{A}(q_0,\boldsymbol{q})}{q_0^2-E_q^2+i\epsilon} = \int \frac{dq_0}{(2\pi)}\frac{\mathcal{A}(q_0,\boldsymbol{q})}{q_0-E_q+i\epsilon'}\frac{1}{q_0+E_q-i\epsilon'}, \tag{3.35}$$

where $\epsilon' = \epsilon/(2E_q)$. This shows that there are poles at $q_0 = E_q - i\epsilon'$ and $q_0 = -(E_q - i\epsilon')$. Since the integrand falls off quadratically as $|q_0| \to \infty$, we can choose a contour such that only the positive imaginary part of the complex plane contributes to the integral and the radius of the resultant semicircular contour is sufficient to include the necessary poles. This results in only the pole at $q_0 = -(E_q - i\epsilon')$ contributing the integral, which leads to Eq. (3.35) being expressed as

$$\begin{aligned}
&\int \frac{dq_0}{(2\pi)}\frac{\mathcal{A}(q_0,\boldsymbol{q})}{q_0-E_q+i\epsilon'}\frac{1}{q_0+E_q-i\epsilon'} \\
&= \frac{2\pi i}{2\pi} Res_{[q_0=-(E_q-i\epsilon')]}\left[\frac{\mathcal{A}(q_0,\boldsymbol{q})}{q_0-E_q+i\epsilon'}\right] \\
&= \frac{i}{-2E_q}\mathcal{A}(q_0=-(E_q-i\epsilon'),\boldsymbol{q}),
\end{aligned} \tag{3.36}$$

and therefore Eq. (3.34) becomes

$$\int \frac{d^4q}{(2\pi)^4}\frac{\mathcal{A}(q)}{q^2-M^2+i\epsilon} = \int \frac{d^3q}{(2\pi)^3}\frac{i}{-2E_q}\mathcal{A}(q_0=-(E_q-i\epsilon'),\boldsymbol{q}). \tag{3.37}$$

In a similar fashion, we encounter integrals involving two Feynman propagators, S_1 and S_2, for particles with masses M_1 and M_2, respectively. This results

in an integral of the form

$$\begin{aligned}
&\int \frac{d^4q}{(2\pi)^4}\frac{\mathcal{B}(q,k)}{q^2-M_1^2+i\epsilon}\frac{1}{(q-k)^2-M_2^2+i\epsilon} \\
&=\int \frac{d^3q}{(2\pi)^3}\int_0^1 dx\int \frac{dq_0}{(2\pi)}\frac{\mathcal{B}(q_0,\boldsymbol{q},k,x)}{(x((q-k)^2-M_2^2+i\epsilon)+(1-x)(q^2-M_1^2+i\epsilon))^2}
\end{aligned} \tag{3.38}$$

where $\mathcal{B}(q,k)$ is an arbitrary function and the Feynman parameterization has been used to combine the denominators:

$$\frac{1}{AB}=\int_0^1 dx\frac{1}{(xA+(1-x)B)^2}. \tag{3.39}$$

Expanding Eq. (3.38) and rewrite in terms of the variable $l=q-xk$, we obtain

$$\begin{aligned}
&\int \frac{d^3l}{(2\pi)^3}\int_0^1 dx\int \frac{dl_0}{(2\pi)}\frac{\mathcal{B}(l=q-xk,k)}{(l^2-((1-x)M_1^2+xM_2^2-k^2x(1-x))+i\epsilon)^2} \\
=&\int \frac{d^3l}{(2\pi)^3}\int_0^1 dx\int \frac{dl_0}{(2\pi)}\frac{\mathcal{B}(l=q-xk,k)}{(l^2-\Delta_{12}+i\epsilon)^2}
\end{aligned} \tag{3.40}$$

where

$$\Delta_{12}=(1-x)M_1^2+xM_2^2-k^2x(1-x). \tag{3.41}$$

The denominator can be expressed as

$$\begin{aligned}
&(l^2-(1-x)M_1^2+xM_2^2-k^2x(1-x)+i\epsilon)^2 \\
=&(l_0^2-(\boldsymbol{l}^2+\Delta_{12}+i\epsilon))^2 \\
=&\left(l_0-\sqrt{(\boldsymbol{l}^2+\Delta_{12}+i\epsilon)}\right)^2\left(l_0+\sqrt{(\boldsymbol{l}^2+\Delta_{12}+i\epsilon)}\right)^2,
\end{aligned} \tag{3.42}$$

from which we choose the pole at $l_0=\sqrt{(\boldsymbol{l}^2+\Delta_{12}+i\epsilon)}$, and obtain the residue

of the integral. This pole is of order 2 and so we obtain the residue as follows

$$\begin{aligned}
&\text{Res}\left(\frac{\mathcal{B}(l=q-xk,k)}{(l^2-\Delta_{12}+i\epsilon)^2}, l_0=\sqrt{(\boldsymbol{l}^2+\Delta_{12}+i\epsilon)}\right)\\
=&\frac{d}{dl_0}\left(\frac{\mathcal{B}(l=q-xk,k)}{\left(l_0+\sqrt{(\boldsymbol{l}^2+\Delta_{12}+i\epsilon)}\right)^2}\right)_{l_0=\sqrt{\boldsymbol{l}^2+\Delta_{12}+i\epsilon}}.
\end{aligned} \tag{3.43}$$

Inserting Eq. (3.43) in to Eq. (3.40), and relabelling $l \to q$, the integrals of this form can be calculated by setting the cutoff $|q|^2 < \Lambda_{3M}^2$.

For a simple example, we consider the bubble graph for the pion.

$$\begin{aligned}
\Pi_\pi(k^2) =&2N_c i\int\frac{d^4q}{(2\pi)^4}Tr_D\left[\gamma_5 S_1(q)\gamma_5 S_2(q-k)\right]\\
=&8N_c i\int\frac{d^4q}{(2\pi)^4}\frac{-q^2+q\cdot k+M_1M_2}{(q^2-M_1^2+i\epsilon)((q-k)^2+M_2^2+i\epsilon)},
\end{aligned} \tag{3.44}$$

which when we set $M_1 = M_2 = M$ and integrate over q_0 and the x variable we introduce when using Feynman parameterization, we obtain the same expression obtained in Ref. [64], written as

$$\Pi_\pi(k^2) =48\int_{|\boldsymbol{q}|<\Lambda_{3M}}\frac{d^3q}{(2\pi)^3}\frac{E_q}{k^2-4E_q^2+i\epsilon}. \tag{3.45}$$

Converting to spherical coordinates, $d^3q = dqd\phi d\theta q^2\sin(\phi)$, where the integrals over $d\phi\sin(\phi)$ and $d\theta$ produce a factor of 4π, we can write Eq. (3.45) as

$$\begin{aligned}
\Pi_\pi(k^2) =&48\int_{|\boldsymbol{q}|<\Lambda_{3M}}\frac{dq}{(2\pi)^3}4\pi q^2\frac{E_q}{k^2-4E_q^2+i\epsilon}\\
=&48\int_0^{\Lambda_{3M}^2}\frac{dq^2}{(2\pi)^3}4\pi\frac{q}{2}\frac{E_q}{k^2-4E_q^2+i\epsilon}
\end{aligned} \tag{3.46}$$

where $dqq^2 = dq^2q/2$. This equation can then be expressed by change of variables in terms of $\mu^2 = 4(\boldsymbol{q}^2+M^2)$. The resulting integration bounds are $\mu_{min}^2 = 4M^2$ and $\mu_{max}^2 = 4(\Lambda_{3M}^2+M^2) = \Lambda^2$, corresponding to $\boldsymbol{q}^2 = 0$ and $\boldsymbol{q}^2 = \Lambda_{3M}^2$,

respectively, and so Eq. (3.45) can be written as

$$\begin{aligned}\Pi_\pi(k^2) =& 48\int_{4M^2}^{\lambda^2}\frac{d\mu^2}{4(2\pi)^3}4\pi\frac{\sqrt{\frac{\mu^2}{4}-M^2}}{2}\frac{\mu}{k^2-\mu^2+i\epsilon}\\ =&\int_{\mu^2_{min}}^{\mu^2_{max}}\frac{d\mu^2}{(2\pi)^2}\frac{3\mu^2\sqrt{1-\frac{4M^2}{\mu^2}}}{k^2-\mu^2+i\epsilon}.\end{aligned} \tag{3.47}$$

This reproduces the result from Ref. [64]

$$\Pi_\pi(k^2) = \int_{\mu^2_{min}}^{\mu^2_{max}} d\mu^2 \frac{\rho(\mu^2)}{k^2-\mu^2+i\epsilon}, \tag{3.48}$$

where

$$\rho(\mu^2) = \frac{3\mu^2}{4\pi^2}\sqrt{1-\frac{4M^2}{\mu^2}}. \tag{3.49}$$

3.3.2 Light Cone Coordinates

Fragmentation functions and parton distribution functions are expressed in terms of light-cone (LC) variables, and this is of particular use for our description of the Lepage-Brodsky invariant mass cutoff scheme. For a four-vector V^μ $= (V^0, V^1, V^2, V^3)$ in spacetime coordinates, we define the change of variables to light-cone coordinates as:

$$V^\pm = \frac{V^0 \pm V^3}{\sqrt{2}} \tag{3.50}$$

$$\boldsymbol{V}^\perp = (V^1, V^2), \tag{3.51}$$

and write $V^\mu = (V^+, V^-, \boldsymbol{V}^\perp)$, where V^+ and V^- can act as 'time' coordinates, and $\boldsymbol{V}^\perp$ is the transverse spatial component. The dot product of two four-vectors V^μ and W_μ is expressed in LC coordinates as

$$\begin{aligned}V^\mu \cdot W_\mu &= V^+W_+ + V^-W_- - \boldsymbol{V}^\perp\cdot\boldsymbol{W}_\perp\\ &= V_-W_+ + V_+W_- - \boldsymbol{V}_\perp\cdot\boldsymbol{W}_\perp,\end{aligned} \tag{3.52}$$

where we used the property $V^{\pm} = V_{\mp}$.

Expressing Feynman propagators in terms of these coordinates results in

$$\begin{aligned} S(q) &= \frac{\not{q} + M}{q^2 - M^2 + i\epsilon} \\ &= \frac{\gamma^+ q_+ + \gamma^- q_- - \boldsymbol{\gamma}_\perp \cdot \mathbf{q}_\perp + M}{q^2 - M^2 + i\epsilon}, \end{aligned} \tag{3.53}$$

where the denominator can be expressed in light-cone coordinates as

$$\begin{aligned} \frac{1}{q^2 - M^2 + i\epsilon} =& \frac{1}{q^+ q_+ + q^- q_- - (\boldsymbol{q}_\perp^2 + M^2) + i\epsilon} \\ =& \frac{1}{2q_- q_+ - (\boldsymbol{q}_\perp^2 + M^2) + i\epsilon} \\ =& \frac{1}{2q_-} \left(\frac{\Theta(q_-)}{q_+ - e_q + i\epsilon} + \frac{\Theta(-q_-)}{q_+ - e_q - i\epsilon} \right), \end{aligned} \tag{3.54}$$

where Θ are Heaviside functions, and we denote

$$e_q = \frac{\mathbf{q}_\perp^2 + M^2}{2q_-}. \tag{3.55}$$

Inserting this into Eq. (3.15), and fixing $q_- = xk_-$, we can write the bubble graph [31] as

$$\begin{aligned} &\Pi_m(k^2) = 2N_c i \int \frac{d^4q}{(2\pi)^4} Tr_D \left[\gamma_5 S_1(q) \gamma_5 S_2(q-k)\right] \\ &= -2N_c \int dx \frac{\Theta(x)\Theta(1-x)}{x(1-x)} \int \frac{d^2q_\perp}{(2\pi)^3} \frac{\boldsymbol{q}_\perp^2 + ((1-x)M_1 + xM_2)^2}{\boldsymbol{q}_\perp^2 + (1-x)M_1^2 + xM_2^2 - x(1-x)k^2 - i\epsilon}, \end{aligned} \tag{3.56}$$

where $\boldsymbol{k}_\perp = 0$, and the appropriate poles are considered when employing the residue theorem.

3.3.3 Lepage-Brodsky Invariant Mass Cutoff Scheme

The bubble graph of Eq. (3.56) involves a $q\bar{Q}$ intermediate state with invariant mass squared, M_{12}^2 given by

$$M_{12}^2 = k^2 = (p_1 + p_2)^2, \tag{3.57}$$

where k is the total four-momentum for the state, with $p_1 = q$ and $p_2 = -(q-k)$ being the four-momentum for the quark q and antiquark $\bar{Q}$, respectively. In light cone coordinates, this can be expressed as

$$\begin{aligned} M_{12}^2 =& 2k_- k_+ - \boldsymbol{k}_\perp^2 \\ =& 2(q_- + (k-q)_-)(q_+ + (k-q)_+) - (\boldsymbol{q}_\perp + (\boldsymbol{k}-\boldsymbol{q})_\perp)^2 \\ =& 2(k_-)(e_q + e_{k-q}), \end{aligned} \tag{3.58}$$

where the total transverse momentum $\boldsymbol{k}_\perp = 0$, and the on-shell momentum for the components q_+ and $(k-q)_+$ are equal to e_q and e_{k-q} expressed by Eq. (3.55), with masses M_1 and M_2, respectively. Inserting the expressions for the plus components of momentum we obtain

$$\begin{aligned} M_{12}^2 =& 2(k_-)\left(\frac{\boldsymbol{q}_\perp^2 + M_1^2}{2q_-} + \frac{(\boldsymbol{k}-\boldsymbol{q})_\perp^2 + M_1^2}{2(k-q)_-}\right) \\ =& 2(k_-)\left(\frac{\boldsymbol{q}_\perp^2 + M_1^2}{2xk_-} + \frac{(-\boldsymbol{q})_\perp^2 + M_2^2}{2(1-x)k_-}\right). \end{aligned} \tag{3.59}$$

Canceling the factors of k_-, we obtain the invariant mass M_{12} of two quarks as

$$M_{12}^2 = \frac{\boldsymbol{q}_\perp^2 + M_1^2}{x} + \frac{\boldsymbol{q}_\perp^2 + M_2^2}{1-x}. \tag{3.60}$$

The maximum value of invariant mass that we set as a cutoff for the invariant mass in the Lepage-Brodsky regularization scheme is defined as

$$\Lambda_{12} = \sqrt{\Lambda_{3M}^2 + M_1^2} + \sqrt{\Lambda_{3M}^2 + M_2^2}, \tag{3.61}$$

where both particles have 3-momentum Λ_{3M}. Combining Eq. (3.60) and Eq. (3.61), and imposing the condition $M_{12}^2 \leq \Lambda_{12}^2$, we obtain the upper limit on $q_\perp^2$ of the form

$$\boldsymbol{q}_\perp^2 \leq \Lambda_{12}^2 x(1-x) - M_1^2(1-x) - xM_2^2. \tag{3.62}$$

In the previous subsection we finished by noting that for the pion case as in Ref. [64], after a change of variables to μ^2, the upper bound of the three-momentum cutoff version of Π_π could be expressed as $\mu_{max}^2 = \Lambda^2$. This Λ^2 is consistent with the invariant mass cutoff defined in Eq. (3.61), $\Lambda_{12}^2 = (2\sqrt{\Lambda_{3M}^2 + M^2})^2$ $= 4(\Lambda_{3M}^2 + M^2) \equiv \Lambda^2$. In fact, as suggested in Ref. [64], if we employ the change of variable

$$x = \frac{1}{2}\left(1 + \frac{q_3}{E_q}\right), \tag{3.63}$$

in Eq. (3.56) for the pion ($M_1 = M_2 = M$), we obtain Eq. (3.45), showing that the three-momentum cutoff and Lepage-Brodsky schemes are equivalent.

With the requirement that $p_\perp^2 \geq 0$, limitations are placed on the allowed values of x. The maximum allowed region of x is found at $p_\perp^2 = 0$, resulting in

$$\Lambda_{12}^2 x(1-x) - M_1^2(1-x) - xM_2^2 = 0. \tag{3.64}$$

Applying the quadratic equation, we obtain upper (x_{upp}) and lower (x_{low}) limits on x such that

$$x_{upp} = \frac{\Lambda_{12}^2 + M_1^2 - M_2^2 + \sqrt{(\Lambda_{12}^2 + M_1^2 - M_2^2)^2 - 4\Lambda_{12}^2 M_1^2}}{2\Lambda_{12}^2}, \tag{3.65}$$

$$x_{low} = \frac{\Lambda_{12}^2 + M_1^2 - M_2^2 - \sqrt{(\Lambda_{12}^2 + M_1^2 - M_2^2)^2 - 4\Lambda_{12}^2 M_1^2}}{2\Lambda_{12}^2}, \tag{3.66}$$

where $0 < x_{low} \leq x \leq x_{upp} < 1$. Outside of the range defined by x_{low} and x_{upp}, the integrals equate to zero.

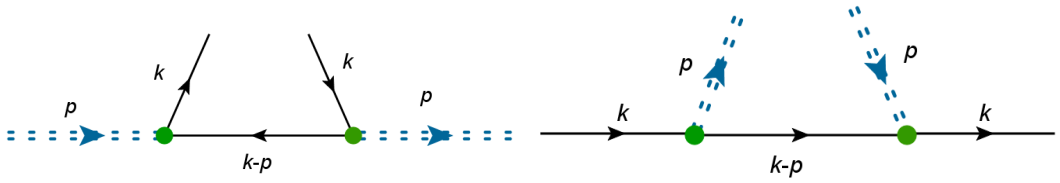

Figure 3.5: Cut diagrams for (a) valence quark distribution functions $f_q^m(x)$ and (b) elementary fragmentation functions $d_q^m(z)$.

3.4 Fragmentation Functions from the NJL-jet model

Quark distribution and fragmentation functions are process independent functions that appear in the convolutions of hard scattering cross sections and are therefore of interest to both the experimental and theoretical branches of particle physics. The valence quark distribution functions, denoted by $f_q^m(x)$, describe the probability of finding a quark q within a hadron h ($= m$ as we consider only mesons), where the quark has a momentum fraction x of the hadron's light-cone momentum, while the elementary fragmentation functions, denoted by $d_q^m(z)$, describe the probability that a fragmenting quark produces a hadron h ($= m$) with light-cone momentum fraction z of the fragmenting quark. The cut diagrams for the valence quark distribution functions and elementary fragmentation functions are shown diagrammatically in Figs. 3.5(a) and 3.5(b), respectively. The PDFs are expressed as

$$\begin{aligned} f_q^m(x) =& iN_c \frac{C_q^m}{2} g_{mqQ}^2 \int \frac{d^4k}{(2\pi)^4} Tr_D \left[S_1(k)\gamma^+ S_1(k)\gamma_5(\not{k} - \not{p} + M_2)\gamma_5 \right] \\ & \times \delta(k_- - p_- x) 2\pi\delta((p-k)^2 - M_2^2) \\ =& N_c \frac{C_q^m}{2} g_{mqQ}^2 \int \frac{d^2k_\perp}{(2\pi)^3} \frac{k_\perp^2 + ((1-x)M_1 + xM_2)^2}{(k_\perp^2 + (1-x)M_1^2 + xM_2^2 - x(1-x)m_m^2)^2}, \end{aligned} \tag{3.67}$$

and the FFs as

$$\begin{aligned} d_q^m(z) =& -\frac{C_q^m}{2} g_{mqQ}^2 \frac{z}{2} \int \frac{d^4k}{(2\pi)^4} Tr_D \left[S_1(k)\gamma^+ S_1(k)\gamma_5(\not{k} - \not{p} + M_2)\gamma_5 \right] \\ & \times \delta(k_- - p_-/z) 2\pi\delta((p-k)^2 - M_2^2) \\ =& \frac{C_q^m}{2} g_{mqQ}^2 z \int \frac{d^2p_\perp}{(2\pi)^3} \frac{p_\perp^2 + ((z-1)M_1 + M_2)^2}{(p_\perp^2 + z(z-1)M_1^2 + zM_2^2 + (1-z)m_m^2)^2}, \end{aligned} \tag{3.68}$$

where the flavor factors denoted by C_q^m are obtained from Ref. [31] and presented in Appendix .5. These functions are related by the Drell-Levy-Yan (DLY) relation [65–68], which describes them as the same function in different regions of the Bjorken x variable, with the elementary quark fragmentation functions being a continuation of the valence quark distribution functions in to the $x > 1$ region. The DLY relation is based on charge conjugation and crossing symmetry, and is expressed [30] as

$$d_q^m(z) = (-1)^{2(s_q+s_m)+1} \frac{z}{d_q} f_q^m \left(x = \frac{1}{z} \right) \tag{3.69}$$

$$= -\frac{z}{2N_c} f_q^m \left(x = \frac{1}{z} \right) \tag{3.70}$$

where s_q and s_m are the spins of q and m, respectively, and d_q is the spin-color degeneracy of q. This relation has been proved for these functions in Ref. [30].

The integrals in Eq. (3.67) and (3.68) are divergent and so the Lepage-Brodsky invariant mass regularization scheme, which we discussed in Section 3.3.3, is chosen to regularize the integrals. The focus of the work that we present in this thesis that relies on the NJL model relates to the fragmentation functions. Calculations involving the distribution functions from the NJL model have been carried out by others and can be found in Refs. [30, 31]. For the remainder of this section we will focus on the fragmentation functions.

The total probability of a quark splitting into a hadron of a given type plus a remnant quark is represented by the elementary quark fragmentation function, integrated over the light-cone momentum fraction z. In the construction of the NJL-jet model, only processes where a hadron is produced at each step are considered. Thus the renormalized elementary fragmentation functions, $\hat{d}_q^h(z)$, is

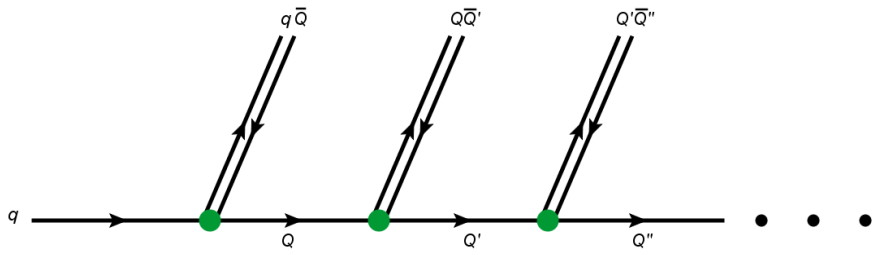

Figure 3.6: Cascade of hadrons produced in jet models.

constructed such that the total probability of emitting a hadron (summed over all possible hadron types h' that the quark q can emit in the elementary splitting process) is one:

$$\hat{d}_q^h(z) = \frac{d_q^h(z)}{\sum_{h'} \int_0^1 dz\, d_q^{h'}(z)}. \tag{3.71}$$

The elementary fragmentation functions only describe the probability for fragmentation to occur once. In the NJL-jet model we require the possibility that the fragmenting quark produces a cascade of hadrons as a result of multiple fragmentations within a jet. Field and Feynman [69] describe such a cascade of hadrons through fragmentation within their quark jet model, which is referred to as the Field-Feynman quark-jet model (FFQJM). The jet process producing a cascade within these models is shown diagrammatically in Fig. 3.6, where an incoming quark q fragments in to a remnant quark Q and a hadron of type $q\bar{Q}$, followed by further fragmentations of the remnant quark to other hadrons ($Q\bar{Q}'$, $Q'\bar{Q}''$, etc) and corresponding remnant quarks (Q', Q'', etc). The produced hadrons receive a light-cone momentum fraction η_i of the fragmenting quark's momentum and the remnant quarks receive light-cone momentum fractions $1 - \sum_i \eta_i$, where the subscript i corresponds to the emission step at which they are produced. For a detected hadron h, the total fragmentation function ($D_q^h(z)$) for the jet produced by a quark q can be written as the sum of the renormalized elementary fragmentation function and an integral term. The integral term describes the contribution to the total fragmentation function from the remnant quark fragmentations that occur when the detected hadron is not produced at the first emission step (first

green circle in Fig. 3.6). It is the convolution of the elementary fragmentation function for a remnant quark Q which is produced after the first hadron emission in the jet and is carrying a momentum fraction y of the original quark q, with the total fragmentation function for the quark Q to the hadron h carrying momentum fraction z. This results in a set of coupled integral equations for the total fragmentation function written as

$$D_q^h(z) = \hat{d}_q^h(z) + \int_z^1 dy\ \hat{d}_q^Q\left(\frac{z}{y}\right) D_Q^h(y), \tag{3.72}$$

which we discuss how to solve in Ref. [1].

The advantage of the NJL-jet model approach is that there is a single underlying effective quark model description at the microscopic level for both parton distribution functions and fragmentation functions, with no fitted parameters to fragmentation data. NJL-jet model calculations of pion fragmentation functions were performed in Ref. [30]. The NJL-jet model was extended to include the strange quark contributions and kaon fragmentation functions in Ref. [31]. Further extensions of the model involved the inclusion of vector meson, nucleon and antinucleon fragmentation channels [32], as well as the study of their transverse momentum dependence [33] and Collins fragmentation functions [70–72]. The dihadron fragmentation functions determined in Ref. [1], which are included as part of this thesis, were obtained from the single hadron fragmentation functions in Ref. [31], as the other extensions were being developed at the same time as this work was being carried out, and so the determination of the DFFs with these extensions is considered a future direction of this research.

Chapter 4

Portfolio of Publications

In this chapter of the thesis we include the three papers discussed in Chapter 1. All three papers were accepted to reputable journals within the field. Each paper is prefaced with a Statement of Authorship, signed by the authors, which identifies the contributions made by the author in the process of producing the paper, including the calculations. We document some minor errata to the papers in Appendix .6.

4.1 Calculating dihadron fragmentation functions in the Nambu–Jona-Lasinio–jet model

Statement of Authorship

Title of Paper	Calculating Dihadron Fragmentation Functions in the NJL-jet model
Publication Status	⦿ Published, ○ Accepted for Publication, ○ Submitted for Publication, ○ Publication style
Publication Details	Andrew Casey, Hrayr H. Matevosyan and Anthony W. Thomas Calculating Dihadron Fragmentation Functions in the NJL-jet model Physical Review D85 114049 (2012) Copyright 2012 by the American Physical Society.

Author Contributions

By signing the Statement of Authorship, each author certifies that their stated contribution to the publication is accurate and that permission is granted for the publication to be included in the candidate's thesis.

Name of Principal Author (Candidate)	Andrew Casey		
Contribution to the Paper	Formulation of research proposal. Carried out the literature review Performed primary calculation Wrote first draft of the paper Equal partner in the editing process that led to a final paper		
Signature		Date	12/8/13

Name of Co-Author	Hrayr H. Matevosyan		
Contribution to the Paper	Supervised the development of work Checked calculation Equal partner in the editing process that led to a final paper		
Signature		Date	12/08/13

Name of Co-Author	Anthony W. Thomas		
Contribution to the Paper	Supervised the development of work Checked calculation Equal partner in the editing process that led to a final paper		
Signature		Date	12/8/13

Name of Co-Author			
Contribution to the Paper			
Signature		Date	

PHYSICAL REVIEW D **85,** 114049 (2012)

Calculating dihadron fragmentation functions in the Nambu–Jona-Lasinio–jet model

Andrew Casey,[1,*] Hrayr H. Matevosyan,[1,*] and Anthony W. Thomas[1,*]

[1]*CSSM and ARC Centre of Excellence for Particle Physics at the Terascale, School of Chemistry and Physics, University of Adelaide, Adelaide SA 5005, Australia*

(Received 27 February 2012; published 27 June 2012)

The Nambu–Jona-Lasinio–jet model provides a framework for calculating fragmentation functions without the introduction of *ad hoc* parameters. We develop the Nambu–Jona-Lasinio–jet model to investigate dihadron fragmentation functions (DFFs) of the form $D_q^{h_1,h_2}(z_1, z_2)$. Here we studied DFFs for $q \to \{\pi^+\pi^-\}$, $\{\pi^+K^-\}$ and $\{K^+K^-\}$ with $q = u, d, s$. The driving terms, which represent the probability of one of the hadrons being emitted in the first emission step of the quark-jet hadronization picture, dominate the solutions of the DFFs where either z_1 or z_2 is large, and z_1 (z_2) is the light-cone momentum fraction of the emitted hadron, h_1 (h_2). The higher order terms, which represent the probability of neither of the hadrons being emitted in the first emission step of the quark-jet, become more significant as z_1 (z_2) is lowered. Finally, we present a sample result for QCD evolution of DFFs, that significantly modify the model solutions when evolved to typical experimental scale of 4 GeV^2.

DOI: 10.1103/PhysRevD.85.114049 PACS numbers: 13.87.Fh, 13.60.Le, 13.60.Hb, 12.39.Ki

I. INTRODUCTION

Deep inelastic scattering (DIS) has proven to be an invaluable source of information about the structure of the nucleon [1]. Initially it provided critical information on the relative distribution of momentum between valence and sea quarks and the gluons. As the experimental capabilities have grown so have our ambitions and over the past decade semi-inclusive deep-inelastic scattering (SIDIS) has helped (along with Drell-Yan) to expand our knowledge of quark flavor structure [2–10]. With several new experimental facilities with 100% duty factor under construction, SIDIS will become even more important. For example, we may finally be able to pin down the elusive $s - \bar{s}$ asymmetry [8,11–13]. Another area of great current excitement concerns the distribution of the spin of the proton [14–34]. There polarized SIDIS is potentially extremely valuable through the study of TMDs [35–44], which will complement work on GPDs [18,45–50].

For these studies to achieve their full potential it is vital that we develop the deepest understanding of the fragmentation functions [51], especially their flavor dependence, and ultimately their dependence on spin and transverse momentum. Fragmentation functions are an important theoretical tool in the investigation of scattering reactions, for example in the separation of the flavor dependence of parton distribution functions (PDFs). Experimental extractions of fragmentation functions from deep-inelastic scattering data [52,53] have increased theoretical activity in this area. Yet the phenomenological extraction of even favored fragmentation functions suffers from significant uncertainty while the situation for the unfavored is worse. This in turn affects the systematic errors associated with the extraction of the flavor dependence of parton distribution functions through SIDIS. These considerations have led us to develop and study the Nambu–Jona-Lasinio (NJL)-jet model [54–57]. This model builds on the field-Feynman quark-jet model (FFQJM) [58], by using an effective chiral quark model to provide a framework in which calculations of both quark distribution and fragmentation functions can be performed without introducing *ad hoc* parameters. Pion fragmentation functions in the NJL-jet model were calculated in Ref. [54]. The NJL-jet model was then extended to include strange quark contributions and kaon fragmentation functions were obtained [55]. Further extensions of the model are the inclusion of vector meson, nucleon and antinucleon fragmentation channels [56], and the inclusion of transverse momentum dependence [57].

Dihadron fragmentation functions (DFFs) represent the probability of producing two hadrons in the decay chain of a fragmenting quark. Some recent work in the area of DFFs include Refs. [59,60]. In Ref. [59], parameters for a spectator model are fitted to output from the PYTHIA event generator [61] tuned for HERMES [62] for dihadron fragmentation functions with a dependence on the sum of the light-cone momentum fractions of the two produced hadrons and their invariant mass squared. DFFs for large invariant mass are studied in Ref. [60]. The dihadron fragmentation functions' evolution equations are derived in Ref. [63] from factorization of the cross section for the production of two hadrons in e^+e^- annihilation in the $\overline{\text{MS}}$ factorization scheme. Evolution equations for nonsinglet quark DFFs are studied in Ref. [64], while the singlet quark and gluon DFF evolution equations are studied in Ref. [65]. In Refs. [64,65] the ratio of the dihadron and single hadron fragmentation functions are examined, as this ratio is useful when considering experimental measurements. The choice of initial conditions is studied in Ref. [66], primarily by considering the two-body correlation function.

*http://www.physics.adelaide.edu.au/cssm

Depending on the polarization of the fragmenting quark, special types of DFFs known as interference fragmentation functions (IFFs) can be constructed. The chiral-odd IFFs can be related to transversity [67–71]. Transversity is one area of current interest that requires knowledge of the fragmentation functions of quarks [29]. Out of the three leading-twist distribution functions that describe the quark structure of hadrons, it is the least well known, the other two being the unpolarized and helicity distributions. Recent work [72–74] suggests that DFFs may be useful in extracting transversity distributions by considering the SIDIS production of two hadrons with small invariant mass. Though transversity will not be the focus of this paper, it is presented as one possible motivation for further investigation into DFFs.

In this work we extend the latest version of the NJL-jet model, presented in Refs. [55,56], to investigate dihadron fragmentation functions. In Sec. II we present a summary of fragmentation functions in the NJL-jet model, as set out in the aforementioned papers, with a focus on those parts that are relevant to understanding the dihadron fragmentation functions. Section III outlines the extension of the NJL-jet model to be used in investigating DFFs, while results at the model scale for the DFFs are presented in Sec. IV. In Sec. V we briefly discuss the QCD evolution equations for DFFs and present sample evolution results for our model.

II. QUARK FRAGMENTATION FUNCTIONS

This section provides a quick overview of the calculation of the quark fragmentation functions in the NJL-jet model [54–56], focusing on the aspects important to obtaining dihadron fragmentation functions within the model. Here we employ the $SU(3)$ NJL effective quark model [75–79] using light-cone (LC) coordinates [55]. In the NJL model we include only the four-point quark interaction in the Lagrangian, with up, down, and strange quarks, and no additional free parameters. We employ Lepage-Brodsky (LB) "invariant mass" cutoff regularization for the loop integrals (see Ref. [55] for a detailed description as applied to the NJL-jet model).

The quark fragmentation function $D_q^h(z)$ is the probability for a quark of type q to emit a hadron of type h carrying fraction z of its light-cone momentum h (here meson $m = q\bar{Q}$). We denote the elementary quark fragmentation function, corresponding to the situation where the detected hadron is the only emitted hadron, by $d_q^h(z)$. The corresponding cut diagram for the elementary quark fragmentation function is shown in Fig. 1. The elementary fragmentation function depicted in Fig. 1 can be written as

$$d_q^m(z) = N_c \frac{C_q^m}{2} g_{mqQ}^2 \frac{z}{2} \int \frac{d^4k}{(2\pi)^4} Tr[S_1(k)\gamma_+ S_1(k)\gamma_5(k\!\!\!/ - p\!\!\!/ + M_2)\gamma_5] \times \delta(k_- - p_-/z) 2\pi\delta((p-k)^2 - M_2^2)$$
$$= \frac{C_q^m}{2} g_{mqQ}^2 z \int \frac{d^2p_\perp}{(2\pi)^3} \frac{p_\perp^2 + ((z-1)M_1 + M_2)^2}{(p_\perp^2 + z(z-1)M_1^2 + zM_2^2 + (1-z)m_m^2)^2}, \quad (1)$$

where C_q^m is the corresponding flavor factor and g_{mqQ} is the quark-meson coupling. The masses M_1, M_2 and m_m are the masses of the fragmenting quark, the remnant quark and the produced hadron (here the hadron is a meson), respectively.

If a sharp cutoff in the transverse momentum, $P_\perp^2$, is assumed, the integration in Eq. (1) can be evaluated analytically [Eq. (2)].

$$d_q^m(z) = \frac{C_q^m}{2} \frac{g_{mqQ}^2}{8\pi^2} z \left(\frac{A/B - 1}{B/P_\perp^2 + 1} + \ln(1 + P_\perp^2/B) \right), \quad (2)$$

where

$$A \equiv ((z-1)M_1 + M_2)^2, \quad (3)$$

$$B \equiv z(z-1)M_1^2 + zM_2^2 + (1-z)m_m^2. \quad (4)$$

The Lepage-Brodsky "invariant mass" cutoff regularization method (Refs. [54,80] describe this when applied to the NJL-jet model) is employed to regularize the loop integrals. The loop integrals are regularized by setting a cutoff on the invariant mass, M_{12}, such that

$$M_{12} \leq \Lambda_{12} \equiv \sqrt{\Lambda_3^2 + m_m^2} + \sqrt{\Lambda_3^2 + M_2^2}, \quad (5)$$

where Λ_{12} is the maximum invariant mass. Here the 3-momentum cutoff, denoted by Λ_3, is fixed by reproducing the value of the experimentally measured pion decay constant. In Lepage-Brodsky regularization, $P_\perp^2$ is given by

$$P_\perp^2 = z(1-z)(\sqrt{\Lambda_3^2 + m_m^2} + \sqrt{\Lambda_3^2 + M_2^2}) - (1-z)m_m^2 - zM_2^2. \quad (6)$$

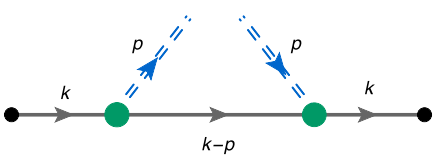

FIG. 1 (color online). Cut diagram for quark fragmentation function. Solid lines represent quarks and the double dashed lines a meson.

The value of the 3-momentum cutoff used in this work, $\Lambda_3 = 0.67\,\text{GeV}$, was obtained in Ref. [80] by choosing the constituent light quark mass $M = 0.3\,\text{GeV}$ and using pion decay $f_\pi = 0.093$. The corresponding constituent strange quark mass, $M_s = 0.537\,\text{GeV}$, was obtained by reproducing the pion and kaon masses, $m_\pi = 0.14\,\text{GeV}$ and $m_K = 0.495\,\text{GeV}$. The calculated values of the quark-meson couplings are $g_{\pi qQ} = 3.15$ and $g_{KqQ} = 3.3876$.

The elementary quark fragmentation function, integrated over the light-cone momentum fraction z, represents the total probability of a quark splitting into a hadron of a given type plus another quark. In construction of the NJL-jet model we are interested in processes where a hadron is produced at each step. Thus we construct the renormalized elementary fragmentation functions, $\hat{d}_q^m(z)$, such that the total probability of emitting a hadron (summed over all possible hadron types m' that the quark q can emit in the elementary splitting process) is one:

$$\hat{d}_q^{\,m}(z) = \frac{d_q^m(z)}{\sum_{m'} \int_0^1 d_q^{m'}(z)}. \tag{7}$$

In a quark-jet-model, the total fragmentation function, $D_q^m(z)$, is described by successive elementary splittings of a quark into hadrons. This process is shown diagrammatically in Fig. 2. The initial quark q fragments into a meson, $m = q\bar{Q}$, with light-cone momentum fraction z of the initial quark's momentum, and a quark, Q, with light-cone momentum fraction $1 - z$. The emitted quark Q fragments as well, and the process repeats, forming a cascade of hadrons. It is important to note that within the model the emitted hadrons do not interact with the other hadrons produced in the quark jet. An integral equation for the quark cascade process shown in Fig. 2 was derived in the quark-jet model of Ref. [58]. The integral equation for the total fragmentation function is

$$D_q^m(z) = \hat{d}_q^m(z) + \sum_Q \int_z^1 \frac{dy}{y} \hat{d}_q^Q\left(\frac{z}{y}\right) D_Q^m(y), \tag{8}$$

where $\hat{d}_q^Q(z) = \hat{d}_q^m(1-z)|_{m=q\bar{Q}}$.

The probabilistic interpretation of Eq. (8) can be clarified by multiplying both sides by a factor of dz. The term on the left-hand side is the probability for the quark q to emit meson m with light-cone momentum fraction z. On the right-hand side, the first term is the driving function, which represents the probability of creating a meson m carrying momentum fraction z to $z + dz$ from the first emission step and the second term represents the probability of creating the meson, m, further in the quark decay chain. The above equation is solved by uniformly discretizing z and y in the interval $[0, 1]$ and approximating the integrals as sums over these discrete values of z and y. Then $D_q^m(z)$ and $\hat{d}_q^m(z)$ can be expressed as vectors $\vec{D}_q^m$ and $\vec{f}$ of values at the discretization points of z, and the integrand of the second term, without $D_q^m(y)$, can be written as a matrix g over the values of the discretization points of z and y:

$$\vec{D}_q^{\,m} = \vec{f} + g \cdot \vec{D}_q^m (I - g) \cdot \vec{D}_q^m = \vec{f}\vec{D}_q^m = (I - g)^{-1}\vec{f}, \tag{9}$$

where I is the unit matrix.

Here it is important to use an appropriate number of discretization points to avoid large numerical errors when solving for $D_q^m(z)$. The number of points used was increased until there was sufficient convergence of the solutions of the fragmentation functions. The resulting solutions for the fragmentation functions of u, d and s quarks to π^+ and K^+ are presented in Ref. [56]. The fragmentation functions of u, d and s quarks to π^+ are also shown here in Fig. 3, as well as the driving function of the u to π^+, $\hat{d}_u^{\pi^+}$, which is labeled as Df:u (the notation Df:q will be adopted in Sec. IV A as well).

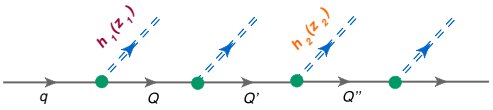

FIG. 2 (color online). Quark cascade

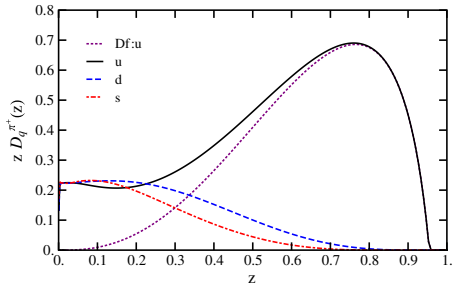

FIG. 3 (color online). Fragmentation functions of u (black solid line), d (blue dashed line) and s (red dot-dashed line) quarks to π^+ as a function of the light-cone momentum fraction z. Driving function of the u (purple dotted line) to π^+ is labeled as Df:u.

III. DIHADRON FRAGMENTATION FUNCTIONS

We now consider a semi-inclusive process in which two hadrons are detected in the final state. This requires a new fragmentation function, known as the dihadron fragmentation function, that describes the probability of this process. DFFs may be useful in the extraction of transversity distributions [72], which are the least well known of the three leading-twist distribution functions that describe the quark structure of hadrons, the other two being the unpolarized and helicity distribution functions. We now extend the NJL-jet model to describe the DFFs. Dihadron

fragmentation functions, $D_q^{h_1,h_2}(z_1, z_2)$, correspond to the probability of a quark q producing two hadrons, h_1 and h_2, that carry its light-cone momentum fractions z_1 and z_2, respectively. An illustration of how a quark cascade can produce two observed hadrons, h_1 and h_2, in the NJL-jet model is shown in Fig. 2.

The integral equation for the dihadron fragmentation function $D_q^{h_1,h_2}(z_1, z_2)$ has been constructed by Field and Feynman in the quark-jet model [Eqs. (2.43a)–(2.43d) of Ref. [58]], which is shown in Eq. (10). Here $\hat{d}_q^h(z)$ and $\hat{d}_q^Q(\eta)$ are the elementary splitting functions of the quark q to the corresponding hadron h and quark Q. On the left-hand side of Eq. (10) is the term representing the probability for the quark q to emit hadrons h_1 and h_2 with light-cone momentum fractions z_1 and z_2, respectively. The first term on the right-hand side of Eq. (10) corresponds to the probability of producing hadron h_1 from the quark q at the first step in the cascade, followed by hadron h_2 produced either directly afterwards or further down in the quark decay chain, while the second term is similar to the first one, except for $h_1 \leftrightarrow h_2$. The third term corresponds to the probability of having both h_1 and h_2 produced after the first hadron emission.

$$D_q^{h_1,h_2}(z_1, z_2) = \hat{d}_q^{h_1}(z_1)\frac{D_{q_1}^{h_2}(\frac{z_2}{1-z_1})}{1-z_1} + \hat{d}_q^{h_2}(z_2)\frac{D_{q_2}^{h_1}(\frac{z_1}{1-z_2})}{1-z_2} + \sum_Q \int_{z_1+z_2}^1 \frac{d\eta}{\eta^2}\hat{d}_q^Q(\eta) D_Q^{h_1,h_2}(\frac{z_1}{\eta}, \frac{z_2}{\eta}), \tag{10}$$

$$q \to h_1 + q_1; \quad q \to h_2 + q_2. \tag{11}$$

In the integral term we perform a change of integration variables to $\xi_1 = z_1/\eta$ and $\xi_2 = z_2/\eta$, so that the arguments of $D_Q^{h_1,h_2}(\xi_1, \xi_2)$ will correspond to ξ_1 and ξ_2 at grid point values when uniformly discretized:

$$\begin{aligned}\int_{z_1+z_2}^1 \frac{d\eta}{\eta^2}\hat{d}_q^Q(\eta) D_Q^{h_1,h_2}(\frac{z_1}{\eta}, \frac{z_2}{\eta}) &= \int_{z_1}^{\frac{z_1}{z_1+z_2}} d\xi_1 \int_{z_2}^{\frac{z_2}{z_1+z_2}} d\xi_2 \int_{z_1+z_2}^1 d\eta \frac{\delta(\xi_1 - z_1/\eta)}{\eta}\frac{\delta(\xi_2 - z_2/\eta)}{\eta}\hat{d}_q^Q(\eta) D_Q^{h_1,h_2}(\xi_1, \xi_2) \\ &= \int_{z_1}^{\frac{z_1}{z_1+z_2}} d\xi_1 \int_{z_2}^{\frac{z_2}{z_1+z_2}} d\xi_2 \int_{z_1+z_2}^1 d\eta\, \delta(z_1 - \xi_1\eta)\delta(z_2 - \xi_2\eta)\hat{d}_q^Q(\eta) D_Q^{h_1,h_2}(\xi_1, \xi_2) \\ &= \int_{z_1}^{\frac{z_1}{z_1+z_2}} d\xi_1 \int_{z_2}^{\frac{z_2}{z_1+z_2}} d\xi_2\, \delta(z_2\xi_1 - z_1\xi_2)\hat{d}_q^Q(z_1/\xi_1) D_Q^{h_1,h_2}(\xi_1, \xi_2)\end{aligned} \tag{12}$$

Then the equation for the dihadron fragmentation functions takes the following form:

$$D_q^{h_1,h_2}(z_1, z_2) = \hat{d}_q^{h_1}(z_1)\frac{D_{q_1}^{h_2}(\frac{z_2}{1-z_1})}{1-z_1} + \hat{d}_q^{h_2}(z_2)\frac{D_{q_2}^{h_1}(\frac{z_1}{1-z_2})}{1-z_2} + \sum_Q \int_{z_1}^{\frac{z_1}{z_1+z_2}} d\xi_1 \int_{z_2}^{\frac{z_2}{z_1+z_2}} d\xi_2\, \delta(z_2\xi_1 - z_1\xi_2)\hat{d}_q^Q(z_1/\xi_1) D_Q^{h_1,h_2}(\xi_1, \xi_2). \tag{13}$$

To solve the above equation for the dihadron fragmentation function $D_q^{h_1,h_2}(z_1, z_2)$, we discretize z_1, z_2, ξ_1, and ξ_2 uniformly in the interval $[0, 1]$ and approximate the integrals as sums over the discretized values of these variables. The fragmentation functions are written in matrix form, where the elements of the matrices are their values at the corresponding uniformly discrete values of the arguments. We used Mathematica to solve for both the single hadron and dihadron fragmentation functions. The number of discretization points used for the single hadron fragmentation functions was 500, while the number of the discretization points afforded for the dihadron fragmentation functions was 200. These values for the numbers of discretization points produced convergence of the solutions within typically 5%, while allowing for a reasonable computational time and computer memory size required by the problem. Several techniques were used to lower the memory use of the program, including the use of the sparse arrays in Mathematica. To calculate the third term of Eq. (13), the integrals over ξ_1 were converted to a sum over its uniformly discrete values. The delta function was used to eliminate the integration over ξ_2. The values of ξ_2 that are selected by the delta function may not match any of its uniformly discretized values. To account for this, the values of the DFFs at the selected ξ_2 were obtained using linear interpolation from neighboring discrete values.

The advantage of the approach presented here is that there is a single underlying effective quark model description at the microscopic level for both parton distribution functions and fragmentation functions, with no fitted parameters to fragmentation data. Moreover, recent developments of the model for the single quark fragmentations allow us to extend the model using Monte Carlo techniques to describe the production of hadronic resonances and the inclusion of transverse momenta [56,57]. In the future, this and other extensions of the model can also be incorporated for the DFFs.

IV. RESULTS

In this section we investigate various features of the DFFs obtained as solutions of Eq. (13). Section IV A investigates the contribution of the integral term versus that of the driving term to the solution of DFF. The impact of the inclusion of the strange quark on $D_u^{\pi^+\pi^-}$ and $D_u^{\pi^+\pi^-}$ is studied in Sec. IV B. In Sec. IV C, we consider $D_q^{\pi^+K^-}(z_1, z_2)$ and fix either z_1 or z_2, to study the dependence of this DFF on each of the variables.

A. Contribution of the integral term

In Eq. (13), the sum of the first two terms is considered to be the driving function of the dihadron fragmentation function, and they describe the probability of emitting one of the detected hadrons in the first emission step. The last term in Eq. (13) corresponds to the probability of emitting both detected hadrons after the emission of a hadron in the first step. We now consider the contribution of this last term to the solution for DFF by comparing them with the corresponding driving functions for three combinations of observed pions and kaons: $\pi^+\pi^-$, π^+K^- and K^+K^-.

The DFFs for the produced hadrons $\pi^+\pi^-$, π^+K^- and K^+K^- as functions of z_2 with $z_1 = 0.5$ are shown in Fig. 4. The plots in the figures show that the favored DFFs, where the initial quark can produce either of the detected hadrons from the initial quark, are almost equal to the driving function, with the integral term giving only a very small contribution. The unfavored DFFs, where neither of the hadrons can be directly produced by the initial quark, are generated entirely by the integral term.

In Figs. 4 and 5, the solution of the DFF for the up quark is shown by the orange circle points and the driving function is shown as a solid gray line. The green diamond points and dotted black line show the DFF and the driving function for the down quark, respectively. The DFF and the driving function for the strange quark are shown by the blue square points and the dot-dashed red line, respectively. In each of the figures, the number in the brackets in the corresponding legend indicate the scaling factor used in depicting the curve on the plot. This notation for the scaling factor is also used in Sec. IV B and Sec. IV C.

In Fig. 5, the results for the DFFs and driving functions for the $\pi^+\pi^-$, π^+K^- and K^+K^- are presented for the fixed value of $z_1 = 0.1$. Here the integral term contribution to the up quark DFFs become visible as the value of z_1 is lowered because the driving function's contribution to the DFF becomes less significant. The driving function's contribution for the down ($\rightarrow \pi^+\pi^-$) and strange quark ($\rightarrow \pi^+K^-$ and K^+K^-) DFFs are still very dominant, so there is no noticeable contribution from the integral term here. It is worth noting that the integral term contributions to both favored and unfavored DFFs are of the same magnitude, but the contributions to the favored DFFs are only noticeable when the driving function is not dominating the solution. We note also that the integral equations of $D_u^{\pi^+\pi^-}$ and $D_d^{\pi^+\pi^-}$ are symmetric in $z_1 \leftrightarrow z_2$, such that the integral equation of $q = u$ for fixed z_1 equals the integral

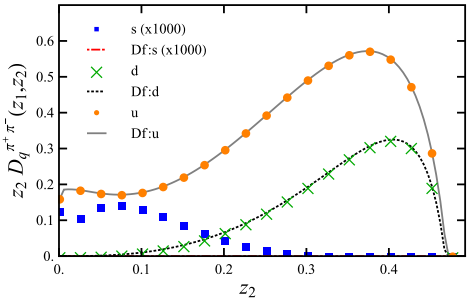

(a) $z_1 = 0.5$: $z_2\, D_q^{\pi^+\pi^-}$

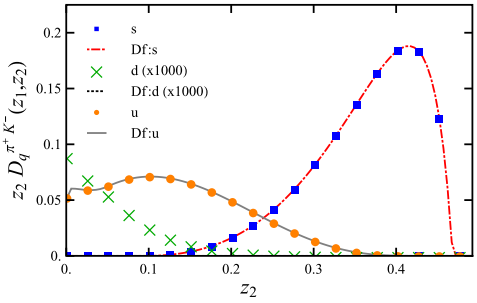

(b) $z_1 = 0.5$: $z_2\, D_q^{\pi^+K^-}$

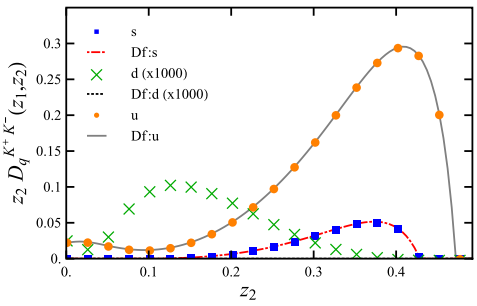

(c) $z_1 = 0.5$: $z_2\, D_q^{K^+K^-}$

FIG. 4 (color online). Dihadron fragmentation functions for $z_1 = 0.5$ for (a) $h_1 = \pi^+, h_2 = \pi^-$, (b) $h_1 = \pi^+, h_2 = K^-$ and (c) $h_1 = K^+, h_2 = K^-$. The DFFs and driving functions of the up, down and strange quarks are shown by the orange circle points and solid gray line, green diamond points and dotted black line, and the blue square points and the dot-dashed red line, respectively. Driving functions for fragmenting quark q are also labeled in the legend as Df:q. The number in the brackets in the legend indicates the scaling factor used in depicting the curve

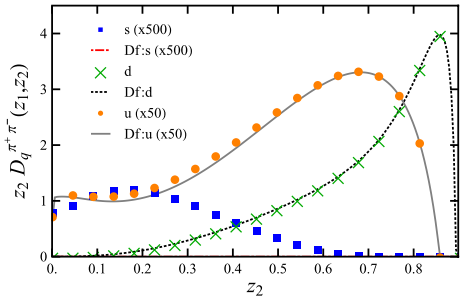

(a)$z_1 = 0.1$: $z_2\, D_q^{\pi^+\pi^-}$

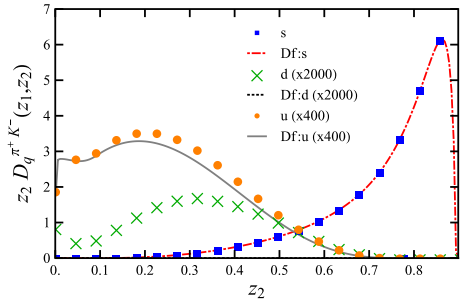

(b)$z_1 = 0.1$: $z_2\, D_q^{\pi^+K^-}$

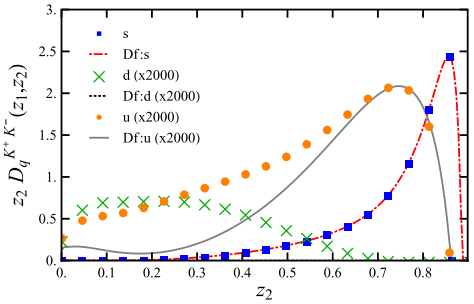

(c)$z_1 = 0.1$: $z_2\, D_q^{K^+K^-}$

FIG. 5 (color online). Dihadron fragmentation functions for $z_1 = 0.1$ for (a) $h_1 = \pi^+, h_2 = \pi^-$, (b) $h_1 = \pi^+, h_2 = K^-$ and (c) $h_1 = K^+, h_2 = K^-$. The DFFs and driving functions of the up, down and strange quarks are shown by the orange circle points and solid gray line, green diamond points and dotted black line, and the blue square points and the dot-dashed red line, respectively. Driving functions for fragmenting quark q are also labeled in the legend as Df:q. The number in the brackets in the legend indicates the scaling factor used in depicting the curve.

equation of $q = d$ for fixed z_2 ($D_u^{\pi^+\pi^-}(z_1, z_2) = D_d^{\pi^+\pi^-}(z_2, z_1)$). In Sec. IV C, we will use the same fixed values for z_1 and z_2 when examining $D_q^{\pi^+K^-}$, as this flavor symmetry is absent there.

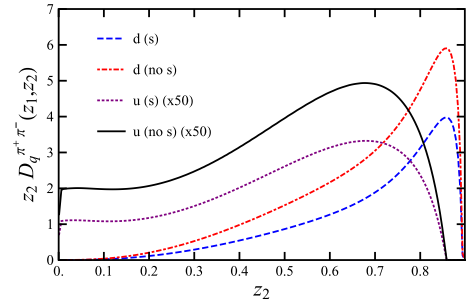

(a)$z_1 = 0.1$: $z_2\, D_q^{\pi^+\pi^-}$

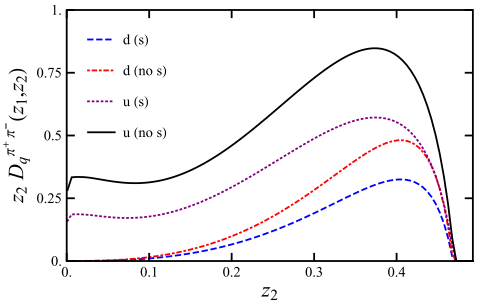

(b)$z_1 = 0.5$: $z_2\, D_q^{\pi^+\pi^-}$

FIG. 6 (color online). Comparison of strange quark contribution of $\pi^+\pi^-$ dihadron fragmentation functions for (a) $z_1 = 0.1$ and (b) $z_1 = 0.5$. The dashed blue line and the red dot-dashed line represent the results for up quark DFF with and without the strange quark [denoted by (s) and (no s) in the captions], respectively. Similarly, the purple dotted line and the black solid line represent the results for the down quark DFF with and without the strange quark, respectively. The number in the brackets in the legend indicates the scaling factor used in depicting the curve.

B. Impact of including the strange quark on the $D_q^{\pi^+\pi^-}$

We now study the impact of the inclusion of the strange quark on $D_u^{\pi^+\pi^-}$ and $D_d^{\pi^+\pi^-}$. In Eq. (13) the integral term contains a sum over Q that runs over the flavors of the quarks considered in the model, thus the inclusion of the strange quark couples the DFFs for the u and d quarks to those of the s quark. Also, the inclusion of the strange quark affects the single hadron fragmentations of the driving terms, as in their respective integral equations there is a sum over Q as well [Eq. (8)]. This potentially can have a large effect, as in Sec. IV A it was shown that the driving functions give most of the contribution to the favored DFFs.

The solution of $D_q^{\pi^+\pi^-}$ for z_1 fixed at 0.1 and 0.5 are shown in Fig. 6. Here, the dashed blue line and the red dot-dashed line represent the results for up quark DFF with and without the strange quark [denoted by (s) and

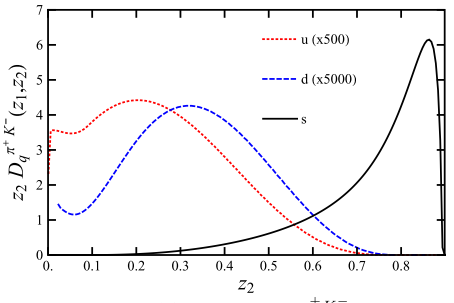

(a)$z_1 = 0.1$: $z_2\, D_q^{\pi^+K^-}$

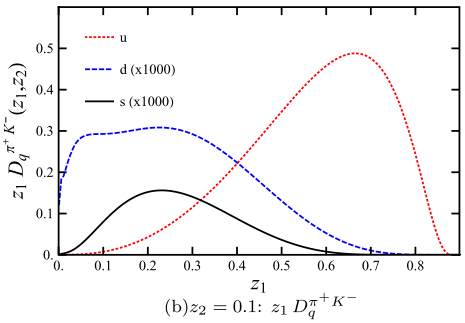

(b)$z_2 = 0.1$: $z_1\, D_q^{\pi^+K^-}$

FIG. 7 (color online). π^+K^- dihadron fragmentation functions for (a) $z_1 = 0.1$ and (b) $z_2 = 0.1$. The up, down and strange quark DFFs are represented by dotted red lines, dashed blue lines and solid black lines, respectively. The number in the brackets in the legend indicates the scaling factor used in depicting the curve.

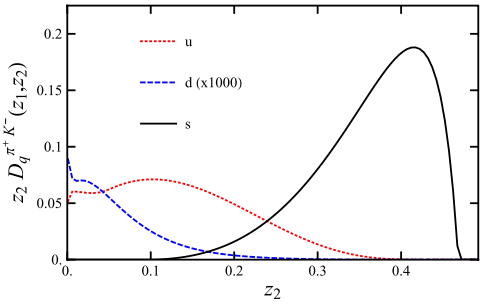

(a)$z_1 = 0.5$: $z_2\, D_q^{\pi^+K^-}$

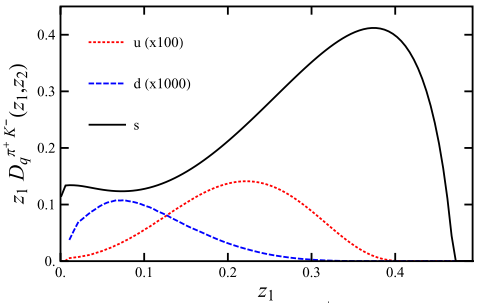

(b)$z_2 = 0.5$: $z_1\, D_q^{\pi^+K^-}$

FIG. 8 (color online). π^+K^- dihadron fragmentation functions for (a) $z_1 = 0.5$ and (b) $z_2 = 0.5$. The up, down and strange quark DFFs are represented by dotted red lines, dashed blue lines and solid black lines, respectively. The number in the brackets in the legend indicates the scaling factor used in depicting the curve.

(no s) in the captions], respectively. Similarly, the purple dotted line and the black solid line represent the results for the down quark DFF with and without the strange quark, respectively.

The shapes of the dihadron fragmentation functions remain the same for both the u and d quark DFFs, with the down quark DFF being the larger in magnitude compared to the up quark DFF for low z_1 and vice versa when z_1 is increased. The main change is the considerable reduction in the magnitude of DFFs when the strange quark is included, caused by the availability of the kaon emission channels. Thus the inclusion of the strange quark in our model proves to be very important in describing the light quark DFFs.

C. Study of $D_q^{\pi^+K^-}$

In this section, we examine the plots of $D_q^{\pi^+K^-}$, where either z_1 or z_2 is fixed. These particular DFFs were chosen since $q \to \pi^+K^-$ is a favored fragmentation channel to one of the hadrons both for a light and a strange quark q. This produces more interesting results to examine than if we had chosen $D_q^{\pi^+\pi^-}$, as those DFFs are symmetric in $q = u$ and $q = d$; thus the DFF for $q = u$ at fixed z_1 is the same as that for the DFF for $q = d$ at fixed z_2, etc. The results for fixed values of z_1 and z_2 are shown on the plots in Figs. 7 and 8. The up quark DFFs are represented by dotted red lines, while the down quark DFFs are represented by dashed blue lines and the strange quark DFFs are represented by solid black lines.

We first examine the DFFs for $z_1 = 0.1$ [Fig. 7(a)] and $z_2 = 0.1$ [Fig. 7(b)]. Since the hadron corresponding to the fixed light-cone momentum fraction only has a small amount of the fragmenting quark's momentum, most of the momentum is attributed to the favored fragmentation channel of the other hadron. For Figs. 7(a) and 7(b), this corresponds to the strange and up quark's fragmentations to the K^- and π^+, respectively. The down quark is unfavored for both hadrons and thus receives very little contribution to its DFF in both plots.

After increasing the fixed value of z_1 [Fig. 8(a)] and z_2 [Fig. 8(b)] to 0.5, the strange quark DFFs are the largest for both. The strange quark is the only initial quark that can produce both hadrons in the first two steps of the cascade, whereas both the up and down quarks require multiple

decays to produce both hadrons. The up quark's solutions are the second largest since it can produce the π^+ hadron in the first emission step, while the down quark's solutions are low for both plots, as it can't produce either of the hadrons in the first emission step.

V. EVOLUTION OF THE DFFS

The results for the dihadron fragmentation functions in the NJL-jet model presented in Sec. IV are all at the model scale of 0.2GeV^2. The model scale was obtained in Ref. [55] such that after NLO evolution the model-calculated u quark valence distribution function in the π^+ matched those experimentally measured in Refs. [81,82]. To compare our results to experiment or results from other models, we need to evolve the dihadron fragmentation functions to an appropriate momentum scale. In Ref. [63], the dihadron fragmentation functions' evolution equations are derived from factorization of the cross-section for the production of two hadrons in e^+e^- annihilation in the $\overline{\text{MS}}$ factorization scheme. Using JetCalculus, Ref. [83] deduces the evolution equations for DFFs with an explicit dependence on the invariant mass of the hadron pairs, M_h. The DFFs with a dependence on the invariant mass are addressed as extended dihadron fragmentation functions (extDFF). The extDFFs are important as they will relate to experimental results that include the dependence on invariant mass spectra.

The leading order (LO) evolution equation for DFF from Ref. [83] is presented in Eq. (14).

$$\frac{d}{dlnQ^2} D_i^{h_1h_2}(z_1, z_2, Q^2) = \frac{\alpha_s(Q^2)}{2\pi} \times \int_{z_1+z_2}^1 \frac{du}{u^2} D_j^{h_1h_2}\left(\frac{z_1}{u}, \frac{z_2}{u}, Q^2\right) P_{ji}(u) + \frac{\alpha_s(Q^2)}{2\pi} \times \int_{z_1}^{1-z_2} \frac{du}{u(1-u)} D_j^{h_1}\left(\frac{z_1}{u}, Q^2\right) D_k^{h_2}\left(\frac{z_2}{1-u}, Q^2\right) \hat{P}_{jk}^i(u), \tag{14}$$

where Q^2 is the momentum scale, $\alpha_s(Q^2)$ is the strong coupling at that momentum scale.

On the left-hand side of Eq. (14), the rate that the DFFs change with respect to $\ln Q^2$ is represented. The first term on the right-hand side represents the effect of the parton i emitting a parton j with light-cone momentum fraction u, with probability $P_{ji}(u)$ that it produces the two detected hadrons, h_1 and h_2, while the second term represents the effect of two partons, j and k, being emitted by i with light-cone momentum fractions u and $1-u$, respectively, with probability $\hat{P}_{jk}^i(u)$, and each of these partons producing one of the detected hadrons.

We developed a computer code to perform the QCD evolution of the dihadron fragmentation functions according to Eq. (14), where the DFFs were separated into non-singlet, singlet and gluon dihadron fragmentation functions. The code is based on the single hadron fragmentation function evolution program by the authors of Refs. [84–87]. The details on the evolution method employed, along with the full set of the results, will be presented in our upcoming paper [88]. As an example, here we present the results for LO evolution of $D_u^{\pi^+\pi^-}(z_1, z_2)$ from our model scale of 0.2GeV^2 to the typical experimental scale of 4GeV^2. The results for the evolved DFFs are presented in Figs. 9(a) and 9(b) corresponding to the solutions at $z_1 = 0.5$ and $z_2 = 0.5$, respectively. The dotted red line represents the solution at the model scale (0.2GeV^2) and the solid black line represents the solution at the final scale $Q^2 = 4\text{GeV}^2$. Both Figs. 9(a) and 9(b) show a shift in the peak of the model results towards the lower z region after the evolution, similar to the single hadron evolution.

VI. CONCLUSIONS AND OUTLOOKS

In this paper we have presented results for dihadron fragmentation functions calculated within the NJL-jet model. DFFs were obtained as numerical solutions of the corresponding integral equations derived using the quark-jet description of the hadronization process. In Sec. IV A, we showed that the integral term, that represents the effects of initial undetected hadron emission, has a very small effect on the DFFs, except when the driving function was zero or when z_1 was low. For driving functions equal to zero, the corresponding DFFs were generated entirely by the integral term and when z_1 was lowered to 0.1, the relative contribution of the driving function to the DFF was also lowered for most values of z_2. For the $u \to \pi^+\pi^-$ DFF, the peak value of $z_2 D_q^{h_1h_2}(z_1, z_2)$ at $z_1 = 0.5$ was almost ten times the peak value at $z_1 = 0.1$. Because of the lower value of the DFF at low z_1, the integral term contribution becomes a more significant part of the DFF, reducing the relative contribution of the driving function. This effect occurs when the fragmenting quark is the favored quark for the hadron that receives a small light-cone momentum fraction, but is unfavored for the hadron that has access to most of the light-cone momentum of the fragmenting quark. One example where this effect is particularly visible is in Fig. 5(c), where the $u \to K^+K^-$ DFF is mostly composed of the integral term at low z_2 and the driving function at higher z_2. In all three results with low z_1 (Fig. 5), the effect is seen for the up quark DFF, which is the favored quark for the hadrons $h_1 = \pi^+$ and $h_1 = K^+$, but is unfavored for hadrons $h_2 = \pi^-$ and $h_2 = K^-$.

In Sec. IV B we showed that the strange quark's inclusion has a significant impact on the DFFs. The main change

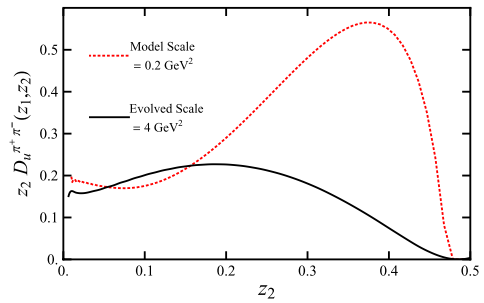

(a)$z_1 = 0.5$: $z_2\, D_u^{\pi^+\pi^-}$

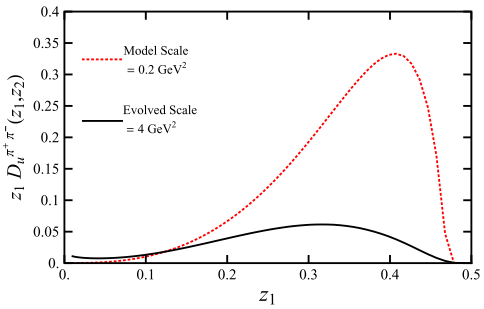

(b)$z_2 = 0.5$: $z_1\, D_u^{\pi^+\pi^-}$

FIG. 9 (color online). $u \to \pi^+\pi^-$ dihadron fragmentation functions are represented as the dotted red lines for the solutions at model scale ($Q_0^2 = 0.2\,\mathrm{GeV}^2$) and solid black lines for the solutions at the evolved scale ($Q^2 = 4\,\mathrm{GeV}^2$) for (a) $z_1 = 0.5$ and (b) $z_2 = 0.5$.

to the DFFs when the strange quark is included is a considerable reduction in magnitude, similar to the single hadron fragmentation functions [55], caused by the availability of the kaon emission channels. The comparison plots for the $\pi^+\pi^-$ dihadron fragmentation functions were shown in Fig. 6, where the results are similar for the $\pi^+\pi^+$ and $\pi^+\pi^0$ DFFs.

We examined $D_q^{\pi^+K^-}(z_1, z_2)$, where either z_1 or z_2 is fixed (Figs. 7 and 8), in Sec. IV C. The π^+K^- DFFs were chosen as they are favored both for a light quark and a strange quark. At low values of z_1 and z_2, the strange quark and up quark DFFs, respectively, are dominant. The strange quark DFF is dominant for low z_1 because the π^+ has a small fraction of the light-cone momentum of the initial quark, leaving most of the initial momentum available to the strange quark's favored fragmentation to K^-. Similarly, the up quark is dominant for low z_2 because the K^- has a small light-cone momentum fraction, allowing the π^+ to access most of the momentum for its favored fragmentation. Increasing the fixed value of either z_1 or z_2 to 0.5 in the π^+K^- DFF shows that the strange quark DFF is dominant. This can be easily interpreted within the model, as only the strange quark can produce both the K^- then the π^+ in the first two steps of the decay chain, whereas the up and down quarks both require at least three steps in the decay chain to produce both hadrons.

Finally, in Sec. V we discuss the QCD evolution of the dihadron fragmentation functions, which is essential in comparing our model calculations with experimental extractions, as well as Monte Carlo simulations or other analytical results. The evolution equations are presented and the method for the numerical solutions is briefly discussed. As an example, the results for $D_u^{\pi^+\pi^-}$ presented in Fig. 9, show the significant modification of the DFFs with evolution. The details for solving the evolution equations and the complete set of results for evolved DFFs will be presented in our upcoming paper [88]. A comparison between our results and others will also be presented in that work.

Future work to extend the NJL-jet model for DFFs include the inclusion of hadronic resonances and their decays, as well as the inclusion of the transverse momentum dependence. These have been accomplished in the single hadron fragmentations [56,57] using a Monte Carlo framework. These extensions for the DFFs are certainly possible, but lay beyond the scope of the current work and are left for the future.

ACKNOWLEDGMENTS

This work was supported by the Australian Research Council through Australian Laureate Fellowship FL0992247 (AWT) and the ARC Centre of Excellence for Particle Physics at the Terascale and by the University of Adelaide.

[1] A. W. Thomas and W. Weise, *The Structure of the Nucleon* (Wiley-VCH, Berlin, Germany, 2001).
[2] W. Melnitchouk, arXiv:hep-ph/9906488.
[3] M. Beckmann (HERMES Collaboration), arXiv:hep-ex/0210049.
[4] A. Airapetian *et al.* (HERMES Collaboration), Phys. Rev. Lett. **92**, 012005 (2004).
[5] V. Barone, T. Calarco, A. Drago, and M. Simani, Phys. Lett. B **571**, 50 (2003).
[6] A. Airapetian *et al.* (HERMES Collaboration), Phys. Rev. D **71**, 012003 (2005).

[7] A. Airapetian *et al.* (HERMES Collaboration), Phys. Rev. D **75**, 012007 (2007).
[8] I. C. Cloët, W. Bentz, and A. W. Thomas, Phys. Rev. Lett. **102**, 252301 (2009).
[9] M. Alekseev *et al.* (COMPASS Collaboration), Phys. Lett. B **693**, 227 (2010).
[10] F. Gross, G. Ramalho, and M. Pena, Phys. Rev. D **85**, 093006 (2012).
[11] A. I. Signal and A. W. Thomas, Phys. Lett. B **191**, 205 (1987).
[12] V. Barone, C. Pascaud, and F. Zomer, Eur. Phys. J. C **12**, 243 (2000).
[13] S. Davidson, S. Forte, P. Gambino, N. Rius, and A. Strumia, J. High Energy Phys. 02 (2002) 037.
[14] X.-D. Ji, Phys. Rev. Lett. **78**, 610 (1997).
[15] X.-D. Ji, Phys. Rev. D **55**, 7114 (1997).
[16] J. D. Bratt *et al.*. (LHPC Collaboration), Phys. Rev. D **82**, 094502 (2010).
[17] G. S. Bali *et al.* (QCDSF Collaboration), Phys. Rev. Lett. **108**, 222001 (2012).
[18] P. Hagler, J. Phys. Conf. Ser. **295**, 012009 (2011).
[19] A. W. Thomas, A. Casey, and H. H. Matevosyan, Int. J. Mod. Phys. A **25**, 4149 (2010).
[20] A. W. Thomas, Phys. Rev. Lett. **101**, 102003 (2008).
[21] F. Myhrer and A. W. Thomas, Phys. Lett. B **663**, 302 (2008).
[22] S. D. Bass and A. W. Thomas, Phys. Lett. B **684**, 216 (2010).
[23] S. D. Bass, A. Casey, and A. W. Thomas, Phys. Rev. C **83**, 038202 (2011).
[24] M. Wakamatsu, Eur. Phys. J. A **44**, 297 (2010).
[25] M. Wakamatsu, Phys. Rev. D **81**, 114010 (2010).
[26] M. Wakamatsu, Phys. Rev. D **83**, 014012 (2011).
[27] A. Adare *et al.* (PHENIX Collaboration), Phys. Rev. Lett. **103**, 012003 (2009).
[28] A. Bacchetta, D. Boer, M. Diehl, and P. J. Mulders, J. High Energy Phys. 08 (2008) 023.
[29] V. Barone, A. Drago, and P. G. Ratcliffe, Phys. Rep. **359**, 1 (2002).
[30] E. Leader, A. V. Sidorov, and D. B. Stamenov, arXiv:1012.5033.
[31] E. Leader, A. V. Sidorov, and D. B. Stamenov, Phys. Rev. D **82**, 114018 (2010).
[32] E. Leader, Phys. Rev. D **83**, 096012 (2011).
[33] E. Leader, A. V. Sidorov, and D. B. Stamenov, J. Phys. Conf. Ser. **295**, 012054 (2011).
[34] W. Vogelsang, Nucl. Phys. **A827**, 110c (2009).
[35] F. A. Ceccopieri, Czech. J. Phys. **56**, F175 (2006); arXiv:hep-ph/0610074v1.
[36] A. Bacchetta, M. Diehl, K. Goeke, A. Metz, P. J. Mulders, and M. Schlegel, J. High Energy Phys. 02 (2007) 093.
[37] L. P. Gamberg, A. Mukherjee, and P. J. Mulders, Phys. Rev. D **83**, 071503 (2011).
[38] L. Gamberg and M. Schlegel, AIP Conf. Proc. **1374**, 309 (2011).
[39] H. Wollny (COMPASS Collaboration), in *Exclusive Reactions at High Momentum Transfer IV*, edited by A. Radyushkin (World Scientific, Singapore, 2011), p. 303.
[40] M. Anselmino *et al.*, Eur. Phys. J. A **47**, 35 (2011).
[41] M. Anselmino, M. Boglione, U. D'Alesio, S. Melis, F. Murgia, E. R. Nocera, and A. Prokudin, Phys. Rev. D **83**, 114019 (2011).
[42] S. M. Aybat, A. Prokudin, and T. C. Rogers, arXiv:1112.4423.
[43] L. Gamberg, D. Boer, B. Musch, and A. Prokudin, AIP Conf. Proc. **1418**, 72 (2011).
[44] A. Bacchetta and M. Radici, Phys. Rev. Lett. **107**, 212001 (2011).
[45] K. Goeke, M. V. Polyakov, and M. Vanderhaeghen, Prog. Part. Nucl. Phys. **47**, 401 (2001).
[46] M. Burkardt, Int. J. Mod. Phys. A **18**, 173 (2003).
[47] M. Diehl, Phys. Rep. **388**, 41 (2003).
[48] X. Ji, Annu. Rev. Nucl. Part. Sci. **54**, 413 (2004).
[49] A. V. Belitsky and A. V. Radyushkin, Phys. Rep. **418**, 1 (2005).
[50] S. Boffi and B. Pasquini, Riv. Nuovo Cimento **30**, 387 (2007); arXiv:0711.2625v2.
[51] M. Radici, arXiv:1111.3383.
[52] M. Hirai, S. Kumano, T.-H. Nagai, and K. Sudoh, Phys. Rev. D **75**, 094009 (2007).
[53] D. de Florian, R. Sassot, and M. Stratmann, Phys. Rev. D **75**, 114010 (2007).
[54] T. Ito, W. Bentz, I. C. Cloët, A. W. Thomas, and K. Yazaki, Phys. Rev. D **80**, 074008 (2009).
[55] H. H. Matevosyan, A. W. Thomas, and W. Bentz, Phys. Rev. D **83**, 074003 (2011).
[56] H. H. Matevosyan, A. W. Thomas, and W. Bentz, Phys. Rev. D **83**, 114010 (2011).
[57] H. H. Matevosyan, W. Bentz, I. C. Cloët, and A. W. Thomas, Phys. Rev. D **85**, 014021 (2012).
[58] R. D. Field and R. P. Feynman, Nucl. Phys. **B136**, 1 (1978).
[59] A. Bacchetta and M. Radici, Phys. Rev. D **74**, 114007 (2006).
[60] J. Zhou and A. Metz, Phys. Rev. Lett. **106**, 172001 (2011).
[61] T. Sjostrand, P. Eden, C. Friberg, L. Lonnblad, G. Miu, S. Mrenna, and E. NorrbinComput. Phys. Commun. **135**, 238 (2001).
[62] P. Liebing, Ph.D. thesis, Universität Hamburg [DESY Report No. DESY-THESIS-2004-036, 2004 (unpublished)]; http://cdsweb.cern.ch/record/808379.
[63] D. de Florian and L. Vanni, Phys. Lett. B **578**, 139 (2004).
[64] A. Majumder and X.-N. Wang, Phys. Rev. D **70**, 014007 (2004).
[65] A. Majumder and X.-N. Wang, Phys. Rev. D **72**, 034007 (2005).
[66] L. Grigoryan, arXiv:0809.0281.
[67] S. Boffi, R. Jakob, M. Radici, and A. Bianconi, in *Perspectives in Hadronic Physics: Proceedings, 2nd International Conference, Trieste, Italy, May 10–14*, edited by S. Boffi, C. Ciofi degli Atti, and M. Giannini (World Scientific, Singapore, 2000), p. 467.
[68] M. Radici, arXiv:hep-ph/9906217.
[69] M. Radici, in *Gerasimov-Drell-Hearn Sum Rule and the Spin Structure of the Nucleon: Proceedings, 2nd International Symposium, GDH 2002, Genova, Italy, July 3–6, 2002*, edited by M. Anghinolfi, M. Battaglieri, and R. de Vita (World Scientific, Hackensack, NJ, 2003), p. 397.

[70] A. Bacchetta and M. Radici, Phys. Rev. D **70**, 094032 (2004).
[71] J. She, Y. Huang, V. Barone, and B.-Q. Ma, Phys. Rev. D **77**, 014035 (2008).
[72] A. Bacchetta, A. Courtoy, and M. Radici, Phys. Rev. Lett. **107**, 012001 (2011).
[73] A. Courtoy, A. Bacchetta, and M. Radici, arXiv:1106.5897.
[74] A. Courtoy, A. Bacchetta, M. Radici, and A. Bianconi, arXiv:1202.0323 [Phys. Rev. D **85**,114023 (2012).
[75] Y. Nambu and G. Jona-Lasinio, Phys. Rev. **122**, 345 (1961).
[76] Y. Nambu and G. Jona-Lasinio, Phys. Rev. **124**, 246 (1961).
[77] M. Kato, W. Bentz, K. Yazaki, and K. Tanaka, Nucl. Phys. **A551**, 541 (1993).
[78] S. Klimt, M. Lutz, U. Vogl, and W. Weise, Nucl. Phys. **A516**, 429 (1990).
[79] S. P. Klevansky, Rev. Mod. Phys. **64**, 649 (1992).
[80] W. Bentz, T. Hama, T. Matsuki, and K. Yazaki, Nucl. Phys. **A651**, 143 (1999).
[81] P. J. Sutton, A. D. Martin, R. G. Roberts, and W. J. Stirling, Phys. Rev. D **45**, 2349 (1992).
[82] K. Wijesooriya, P. E. Reimer, and R. J. Holt, Phys. Rev. C **72**, 065203 (2005).
[83] F. A. Ceccopieri, M. Radici, and A. Bacchetta, Phys. Lett. B **650**, 81 (2007).
[84] M. Miyama and S. Kumano, Comput. Phys. Commun. **94**, 185 (1996).
[85] M. Hirai, S. Kumano, and M. Miyama, arXiv:hep-ph/9610521.
[86] M. Hirai, S. Kumano, and M. Miyama, Comput. Phys. Commun. **108**, 38 (1998).
[87] M. Hirai and S. Kumano, Comput. Phys. Commun. **183**, 1002 (2012).
[88] A. Casey, I. C. Cloët, H. H. Matevosyan, and A. W. Thomas (unpublished).

4.2 Dihadron fragmentation functions from the NJL–jet model and their QCD evolution

Statement of Authorship

Title of Paper	Dihadron Fragmentation Functions from the NJL-jet model and their QCD Evolution
Publication Status	⦿ Published, ○ Accepted for Publication, ○ Submitted for Publication, ○ Publication style
Publication Details	Andrew Casey, Ian C. Cloet, Hrayr H. Matevosyan and Anthony W. Thomas Dihadron Fragmentation Functions from the NJL-jet model and their QCD Evolution Physical Review D86 114018 (2012) Copyright 2012 by the American Physical Society.

Author Contributions

By signing the Statement of Authorship, each author certifies that their stated contribution to the publication is accurate and that permission is granted for the publication to be included in the candidate's thesis.

Name of Principal Author (Candidate)	Andrew Casey		
Contribution to the Paper	Formulation of research proposal. Carried out the literature review Performed primary calculation Wrote first draft of the paper Equal partner in the editing process that led to a final paper		
Signature		Date	12/8/13

Name of Co-Author	Ian C. Cloet		
Contribution to the Paper	Supervised the development of work Checked calculation Equal partner in the editing process that led to a final paper		
Signature		Date	12/8/13

Name of Co-Author	Hrayr H. Matevosyan		
Contribution to the Paper	Supervised the development of work Checked calculation Equal partner in the editing process that led to a final paper		
Signature		Date	12/08/13

Name of Co-Author	Anthony W. Thomas		
Contribution to the Paper	Supervised the development of work Checked calculation Equal partner in the editing process that led to a final paper		
Signature		Date	12/8/13

PHYSICAL REVIEW D **86,** 114018 (2012)

Dihadron fragmentation functions from the NJL-jet model and their QCD evolution

Andrew Casey,* Ian C. Cloët,* Hrayr H. Matevosyan,* and Anthony W. Thomas*

CSSM and ARC Centre of Excellence for Particle Physics at the Terascale, School of Chemistry and Physics, University of Adelaide, Adelaide, South Australia 5005, Australia

(Received 24 July 2012; published 12 December 2012)

We present results for dihadron fragmentation functions from the Nambu–Jona-Lasinio-jet model evolved from the model scale to a typical experimental scale of 4 GeV^2. The numerical method used in this evolution is discussed in detail. The effect of evolution on the shapes of the dihadron fragmentation functions is discussed for a doubly favored process ($u \to \pi^+\pi^-$), as well as a singly favored ($u \to \pi^+ K^-$) process involving light quarks. Finally, we explore the production of K^+K^- pairs from an initial u, d or s quark.

DOI: 10.1103/PhysRevD.86.114018 PACS numbers: 13.87.Fh, 12.39.Ki, 13.60.Hb, 13.60.Le

I. INTRODUCTION

Experimental processes such as deep-inelastic scattering, semi-inclusive deep-inelastic scattering (SIDIS) and Drell-Yan have provided invaluable information about the structure of the nucleon [1–11]. With several new experimental facilities with 100% duty factor under construction, SIDIS will play an increasingly important role in the development of our theoretical and experimental understanding of the structure of the nucleon. The elusive s-$\bar{s}$ asymmetry [12–15] is one area of interest that may finally be pinned down through the results obtained at these new facilities. The distribution of the spin of the proton [16–36] is an area of current excitement where polarized SIDIS is potentially extremely valuable through the study of transverse momentum dependent parton distribution functions [37–47], which will complement work on generalized parton distributions [20,48–53].

To allow these studies to fulfill their potential, we must develop a deep understanding of the fragmentation functions [54], particularly their flavor, spin and transverse momentum dependence. Fragmentation functions appear in certain scattering reactions, for example, in SIDIS experiments [55,56] and in e^+e^- annihilation reactions [57–61]. Experiments are planned to use SIDIS to probe the flavor dependence of the parton distribution functions, for example, and therefore understanding fragmentation functions has become very important. Phenomenological extraction of fragmentation functions suffers from significant uncertainty, even for favored fragmentation functions, which effects the systematic errors associated with extracting the flavor dependence of parton distribution functions through SIDIS. The increasing interest in SIDIS experiments led to the development of the Nambu–Jona-Lasinio (NJL)-jet model [62–65], which builds on the Field-Feynman quark-jet model [66], by using an effective chiral quark model to provide a unified framework in which calculations of both quark distribution and fragmentation functions can be performed. NJL-jet model calculations of pion fragmentation functions were obtained in Ref. [62]. The NJL-jet model was extended to include strange quark contributions and kaon fragmentation functions were calculated in Ref. [63]. Further extensions of the model involved the inclusion of vector meson, nucleon and antinucleon fragmentation channels [64], as well as the study of their transverse momentum dependence [65] and Collins fragmentation functions [67–69].

The probability of a fragmenting quark to produce two hadrons is represented by dihadron fragmentation functions (DFFs). DFFs have been studied recently in Refs. [70,71] in order to understand their dependence on invariant mass of the two produced hadrons. The focus of Ref. [70] was to fit parameters for a spectator model to output from the PYTHIA event generator [72] tuned for HERMES experiments [73] for DFFs with a dependence on the sum of the light-cone momentum fractions of the two produced hadrons and their invariant mass squared. Reference [71] focused on studying DFFs for large invariant mass. DFFs with no invariant mass dependence were studied in the NJL-jet model in Ref. [74] at the model momentum scale of $Q_0^2 = 0.2\ \mathrm{GeV}^2$. In order to compare the results with experimental data, we need to evolve the DFFs up to a typical experimental scale. The evolution equations for the DFFs are derived in Ref. [58] from factorization of the cross section for the production of two hadrons in e^+e^- annihilation in the $\overline{\mathrm{MS}}$ factorization scheme. In Ref. [75], the nonsinglet quark evolution equations for DFFs were studied, while Ref. [76] focused on the QCD evolution equations for singlet quark and gluon DFFs. The ratio of the dihadron and single hadron fragmentation functions, which is useful when considering experimental measurements, was also examined in Refs. [75,76]. Initial conditions for DFFs for different pairs of hadrons and different values of z_1 and z_2 are investigated in Ref. [77], with a focus on the correlation function R_{cor} obtained in the Field-Feynman quark-jet model [66].

An area of current interest in which the dihadron fragmentation functions of quarks may be useful are transversity distributions [31]. Transversity distributions are one of the three leading-twist distribution functions that do not vanish when integrated over the transverse

*http://www.physics.adelaide.edu.au/cssm

momentum. They describe the quark structure of the nucleon (the other two being unpolarized and helicity quark distribution functions) and these functions enter into asymmetries with chiral-odd versions of a special type of DFF known as interference fragmentation functions [78–82]. Interference fragmentation functions are DFFs with a dependence on the polarization of the fragmenting quark. In Refs. [83–85], it was suggested that DFFs may be useful in extracting transversity distributions by considering the SIDIS production of two hadrons with small invariant mass. Transversity distribution functions are not a focus of this paper, but are presented as motivation for further investigation into DFFs.

This work focuses on performing QCD evolution of the DFFs from the NJL-jet model momentum scale of $Q_0^2 = 0.2$ GeV^2 to a typical experimental momentum scale of $Q^2 = 4$ GeV^2. In Sec. II we present a brief summary of fragmentation function equations from which the model scale solutions were obtained and used as input for the evolution equations of the DFFs. Section III describes the method for solving the evolution equations for single hadron fragmentation functions (SFFs), which are needed for the evolution of the DFFs. It also serves as a simple version of the method used to solve the DFF evolution equations, while the method for solving the evolution equations for the DFFs is described in Sec. IV. A comparison of the model scale and evolved scale DFFs is presented in Sec. V. Section VI shows how the evolution code works on data from Ref. [76] as well as comparing our solutions to that data. Our data is evolved to a range of values of Q^2 in this section to display how the up quark and gluon DFFs change for larger values of Q^2.

II. SINGLE HADRON AND DIHADRON FRAGMENTATION FUNCTIONS FROM THE NJL-JET MODEL

In Ref. [74], integral equations for the single hadron and dihadron fragmentation functions from the NJL-jet model are described, and the method employed to solve them at the model scale of $Q_0^2 = 0.2$ GeV^2 is presented. SFFs appear in the cross section for SIDIS experiments and thus play an important part in the theoretical understanding of these experiments. In the NJL-jet model the SFFs, $D_q^h(z)$, which correspond to the probability of producing a hadron h with light-cone momentum fraction z from a fragmenting quark q, are given by [62]

$$D_q^h(z) = \hat{d}_q^h(z) + \sum_Q \int_z^1 \frac{dy}{y} \hat{d}_q^Q\left(\frac{z}{y}\right) D_Q^h(y). \tag{1}$$

The first term on the right-hand side of Eq. (1) is the renormalized elementary quark fragmentation function, which corresponds to the process where the detected hadron is the only emitted hadron. We refer to this term as the driving function. The second term corresponds to the probability of emitting a hadron after the first emission step in the quark cascade and these terms have a sizable effect at low values of z, while vanishing for higher z values. To solve the second term we use $\hat{d}_q^Q(z) = \hat{d}_q^h(1-z)|_{h=q\bar{Q}}$ to write all functions in terms of their relation to the emitted hadron h.

Dihadron fragmentation functions are another important tool in the theoretical understanding of the structure of hadrons. In the NJL-jet model, the DFF are given by

$$\begin{aligned} D_q^{h_1,h_2}(z_1,z_2) = {} & \hat{d}_q^{h_1}(z_1)\frac{D_{q_1}^{h_2}(\frac{z_2}{1-z_1})}{1-z_1} + \hat{d}_q^{h_2}(z_2)\frac{D_{q_2}^{h_1}(\frac{z_1}{1-z_2})}{1-z_2} \\ & + \sum_Q \int_{z_1}^{\frac{z_1}{z_1+z_2}} d\xi_1 \int_{z_2}^{\frac{z_2}{z_1+z_2}} d\xi_2 \delta(z_2\xi_1 - z_1\xi_2) \\ & \times \hat{d}_q^Q(z_1/\xi_1) D_Q^{h_1,h_2}(\xi_1,\xi_2), \end{aligned} \tag{2}$$

where the first term corresponds to the probability of producing hadron h_1 from the quark q at the first emission step in the cascade, followed by hadron h_2 produced either directly afterwards or further down in the quark decay chain, while the second term is similar to the first one, except for $h_1 \leftrightarrow h_2$. These two terms constitute the driving function of the DFFs, similar to the first term in Eq. (1). The third term on the right-hand side of Eq. (2) corresponds to the probability of having both the detected hadrons

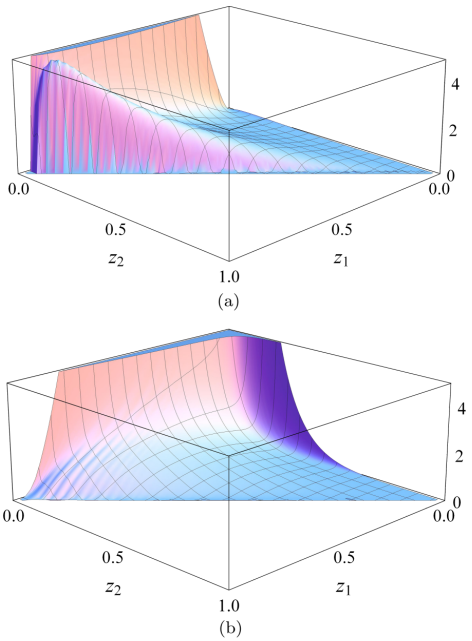

FIG. 1 (color online). $\pi^+\pi^-$ dihadron fragmentation function for the u quark at the (a) model scale ($Q_0^2 = 0.2$ GeV^2) and (b) the evolved scale ($Q^2 = 4$ GeV^2).

produced after the first hadron emission. DFFs correspond to the probability of producing two hadrons, h_1 and h_2, in the decay chain of a fragmenting quark q, with light-cone momentum fractions z_1 and z_2, respectively.

Results for the SFFs and DFFs from the NJL-jet model at the model scale of $Q_0^2 = 0.2$ GeV^2 are described in detail in Ref. [74]. In this paper, they are used as the input for the DFF evolution equations that will be discussed in Secs. III and IV. In Fig. 1(a), we present a 3-dimensional plot of $D_u^{\pi^+\pi^-}(z_1, z_2)$, at the model scale, while in Fig. 1(b) the result for the same DFF evolved to 4 GeV^2 is shown. These plots demonstrate the effect of evolution on the DFFs, particularly where the functions achieve their peaks with respect to z_1 and z_2.

III. EVOLUTION OF THE SFFS

To evolve the DFFs, we need to evolve the SFFs as well. This section will focus on the evolution of the SFFs, and will also serve as a simple introduction to the method used to solve the DFF evolution equations. This procedure for solving the SFF and DFF evolution equations can, of course, be used for models other than the NJL-jet model.

The single hadron fragmentation function evolution equations used in our calculations were based on those presented in Ref. [86]. The evolution equations are written in the form of nonsinglet quark, plus-type quark and gluon fragmentation function equations. The plus-type quark and gluon fragmentation functions are coupled and therefore need to be solved simultaneously, whereas the nonsinglet quark fragmentation functions are decoupled and can be solved separately. The nonsinglet $[D_{q_i^-}^h(z, Q^2)]$ and plus-type $[D_{q_i^+}^h(z, Q^2)]$ quark fragmentation functions are, respectively, constructed from the combinations of SFFs,

$$\begin{aligned} D_{q_i^-}^h(z, Q^2) &= D_{q_i}^h(z, Q^2) - D_{\bar{q}_i}^h(z, Q^2) \\ &= D_{q_i}^h(z, Q^2) - D_{q_i}^{\bar{h}}(z, Q^2), \end{aligned} \tag{3}$$

and

$$\begin{aligned} D_{q_i^+}^h(z, Q^2) &= D_{q_i}^h(z, Q^2) + D_{\bar{q}_i}^h(z, Q^2) \\ &= D_{q_i}^h(z, Q^2) + D_{q_i}^{\bar{h}}(z, Q^2), \end{aligned} \tag{4}$$

where q_i is the fragmenting quark. These combinations, rewritten using charge symmetry, allow for a simpler method of solving the evolution equations.

We define the variable t as

$$t \equiv -\frac{2}{\beta_0} \ln\left[\frac{\alpha_s(Q^2)}{\alpha_s(Q_0^2)}\right], \tag{5}$$

where

$$\alpha_s(Q^2) = 4\pi \Big/ \left(\beta_0 \ln \frac{Q^2}{\Lambda_{\rm QCD}^2}\right) \tag{6}$$

is the leading-order strong coupling constant, $\beta_0 = (33 - 2n_f)/3$ is the one-loop β function, n_f is the number of flavors and $\Lambda_{\rm QCD}$ is the QCD scale parameter.[1] We write the evolution equations with respect to t rather than $\ln Q^2$ to simplify the numerical calculation.

The QCD evolution equations for the SFFs allow us to determine the SFFs at momentum scales that vary from the scale at which they are originally defined. This is achieved by calculating the rate of change of the SFF with respect to the momentum scale. The nonsinglet, plus-type and gluon leading-order (LO) evolution equations are, respectively, given by

$$\frac{\partial}{\partial t} D_{q_i^-}^h(z, t) = \sum_j \int_z^1 \frac{dy}{y} P_{q_j q_i}(y) D_{q_j^-}^h\left(\frac{z}{y}, t\right), \tag{7}$$

$$\begin{aligned} \frac{\partial}{\partial t} D_{q_i^+}^h(z, t) = \int_z^1 \frac{dy}{y} \Bigg[&\sum_j P_{q_j q_i}(y) D_{q_j^+}^h\left(\frac{z}{y}, t\right) \\ &+ 2P_{gq}(y) D_g^h\left(\frac{z}{y}, t\right)\Bigg], \end{aligned} \tag{8}$$

$$\begin{aligned} \frac{\partial}{\partial t} D_g^h(z, t) = \int_z^1 \frac{dy}{y} \Bigg[&P_{qg}(y) \sum_j D_{q_j^+}^h\left(\frac{z}{y}, t\right) \\ &+ P_{gg}(y) D_g^h\left(\frac{z}{y}, t\right)\Bigg]. \end{aligned} \tag{9}$$

The left-hand sides of Eqs. (7)–(9) represent the rate of change of the corresponding SFFs with respect to t. The right-hand sides of these equations represent the effect that a parton j (either a quark of flavor q_j or a gluon g), that emits a hadron h with light-cone momentum fraction z/y, has on the evolution of the nonsinglet (q_i^-), plus-type (q_i^+) or gluon (g) SFFs, through the splitting functions $P_{ji}(y)$ (obtained from Ref. [86]), where i is the parton for the corresponding SFF on the left-hand side.

To solve Eqs. (7)–(9), we express the derivatives as finite differences using

$$\frac{\partial f(t)}{\partial t} \equiv \frac{f(t_{j+1}) - f(t_j)}{\Delta t}, \tag{10}$$

where $f(t)$ is the corresponding SFF. We divide the range of interest for t into N_t steps of size Δt.

The integrals on the right-hand side of the LO evolution equations are converted into sums over logarithmically discretized values of y (denoted by z_l). The corresponding equations for the nonsinglet, plus-type and gluon fragmentation functions are, respectively, rearranged to obtain the functions at the $(k+1)$th step in t such that

[1] In this work we take $n_f = 3$ and $\Lambda_{\rm QCD} = 0.25$.

$$D^h_{q_i^-}(z_m, t_{k+1}) = D^h_{q_i^-}(z_m, t_k) + \Delta t \sum_j \sum_{l=m}^{N_z} \frac{\Delta z_l}{z_l} P_{q_j q_i}(z_l) D^h_{q_j^-}\left(\frac{z_m}{z_l}, t_k\right), \tag{11}$$

$$D^h_{q_i^+}(z_m, t_{k+1}) = D^h_{q_i^+}(z_m, t_k) + \Delta t \sum_{l=m}^{N_z} \frac{\Delta z_l}{z_l}\left[\sum_j P_{q_j q_i}(z_l) D^h_{q_j^+}\left(\frac{z_m}{z_l}, t_k\right) + 2P_{gq}(z_l) D^h_g\left(\frac{z_m}{z_l}, t_k\right)\right], \tag{12}$$

$$D^h_g(z_m, t_{k+1}) = D^h_g(z_m, t_k) + \Delta t \sum_{l=m}^{N_z} \frac{\Delta z_l}{z_l}\left[P_{qg}(z_l)\sum_j D^h_{q_j^+}\left(\frac{z_m}{z_l}, t_k\right) + P_{gg}(z_l) D^h_g\left(\frac{z_m}{z_l}, t_k\right)\right]. \tag{13}$$

The first term on the right sides of Eqs. (11)–(13) are the fragmentation functions at the (k)th step in t. The second term on the right-hand side of each equation is the change in the fragmentation function from the (k)th step to the $(k+1)$th step in t. The SFF at Q_0^2 are inserted as the input at $k = 1$, with the evolution to the next step, $t_2 = t_1 + \Delta t$, calculated using the previous result. This process is repeated to obtain the SFF evolved to the chosen Q^2 at t_{N_t+1}.

IV. EVOLUTION OF THE DFFS

The DFF evolution equations are derived from factorization of the cross section for the production of two hadrons in e^+e^- annihilation in the $\overline{\text{MS}}$ factorization scheme in Ref. [58]. Using jet-calculus, Ref. [87] deduces the evolution equations for DFFs with an explicit dependence on the invariant mass of the hadron pairs, M_h, which are addressed as extended dihadron fragmentation functions. The latter are important as they relate to experimental results that include the dependence on invariant mass spectra. We concentrate on the DFF that have been integrated over the invariant mass. The LO evolution equation for DFFs, from Ref. [87], reads

$$\frac{d}{d\ln Q^2} D_i^{h_1 h_2}(z_1, z_2, Q^2) = \frac{\alpha_s(Q^2)}{2\pi} \int_{z_1+z_2}^1 \frac{du}{u^2} D_j^{h_1 h_2}\left(\frac{z_1}{u}, \frac{z_2}{u}, Q^2\right) P_{ji}(u) + \frac{\alpha_s(Q^2)}{2\pi} \int_{z_1}^{1-z_2} \frac{du}{u(1-u)} D_j^{h_1}\left(\frac{z_1}{u}, Q^2\right) \times D_k^{h_2}\left(\frac{z_2}{1-u}, Q^2\right) \hat{P}^i_{kj}(u), \tag{14}$$

where Q^2 is the momentum scale, $\alpha_s(Q^2)$ is the strong coupling constant at the corresponding momentum scale and a sum over the repeated indices is implied. The rate at which the DFFs change with respect to $\ln Q^2$ is represented on the left-hand side of Eq. (14). The first term on the right-hand side of the LO DFF evolution equation represents the effect that a parton j fragmenting into two hadrons, h_1 and h_2, has on the fragmentation of parton i into the two hadrons, through the splitting function $P_{ji}(u)$. The second term represents the effect of parton i splitting into two partons, j and k, that fragment separately to produce h_1 and h_2 with light-cone momentum fractions u and $1-u$, respectively, through the splitting function $\hat{P}^i_{kj}(u)$. For the QCD evolution of the DFFs, both $P_{ji}(u)$ and $\hat{P}^i_{kj}(u)$ were obtained from Ref. [87].

In Eq. (14), the parton i can be either a quark, antiquark or gluon. We choose to express the evolution equations for the quark and gluon DFFs, respectively, written in terms of t [Eq. (5)] as

$$\frac{d}{dt} D^{h_1 h_2}_{q_i}(z_1, z_2, t) = \int_{z_1+z_2}^1 \frac{du}{u^2} D^{h_1 h_2}_{q_j}\left(\frac{z_1}{u}, \frac{z_2}{u}, t\right) P_{q_j q_i}(u) + \int_{z_1}^{1-z_2} \frac{du}{u(1-u)} D^{h_1}_g\left(\frac{z_1}{u}, t\right) D^{h_2}_{q_k}\left(\frac{z_2}{1-u}, t\right) \hat{P}^{q_i}_{q_k g}(u) + \int_{z_1+z_2}^1 \frac{du}{u^2} D^{h_1 h_2}_g\left(\frac{z_1}{u}, \frac{z_2}{u}, t\right) P_{g q_i}(u) + \int_{z_1}^{1-z_2} \frac{du}{u(1-u)} D^{h_1}_{q_j}\left(\frac{z_1}{u}, t\right) D^{h_2}_g\left(\frac{z_2}{1-u}, t\right) \hat{P}^{q_i}_{g q_j}(u), \tag{15}$$

$$\frac{d}{dt} D^{h_1 h_2}_g(z_1, z_2, t) = \int_{z_1+z_2}^1 \frac{du}{u^2} D^{h_1 h_2}_{q_j}\left(\frac{z_1}{u}, \frac{z_2}{u}, t\right) P_{q_j g}(u) + \int_{z_1}^{1-z_2} \frac{du}{u(1-u)} D^{h_1}_{q_j}\left(\frac{z_1}{u}, t\right) D^{h_2}_{\bar{q}_j}\left(\frac{z_2}{1-u}, t\right) \hat{P}^g_{\bar{q}_j q_j}(u) + \int_{z_1+z_2}^1 \frac{du}{u^2} D^{h_1 h_2}_g\left(\frac{z_1}{u}, \frac{z_2}{u}, t\right) P_{gg}(u) + \int_{z_1}^{1-z_2} \frac{du}{u(1-u)} D^{h_1}_g\left(\frac{z_1}{u}, t\right) D^{h_2}_g\left(\frac{z_2}{1-u}, t\right) \hat{P}^g_{gg}(u). \tag{16}$$

To obtain nonsinglet $[D^{h_1 h_2}_{q_i^-}(z_1, z_2, t)]$ and plus-type $[D^{h_1 h_2}_{q_i^+}(z_1, z_2, t)]$ quark DFFs we use the combinations

$$D^{h_1 h_2}_{q_i^-}(z_1, z_2, t) = D^{h_1 h_2}_{q_i}(z_1, z_2, t) - D^{h_1 h_2}_{\bar{q}_i}(z_1, z_2, t) = D^{h_1 h_2}_{q_i}(z_1, z_2, t) - D^{\bar{h}_1 \bar{h}_2}_{q_i}(z_1, z_2, t), \tag{17}$$

and

$$D_{q_i^+}^{h_1h_2}(z_1,z_2,t) = D_{q_i}^{h_1h_2}(z_1,z_2,t) + D_{\bar{q}_i}^{h_1h_2}(z_1,z_2,t) = D_{q_i}^{h_1h_2}(z_1,z_2,t) + D_{\bar{q}_i}^{\bar{h}_1\bar{h}_2}(z_1,z_2,t), \tag{18}$$

respectively. The combination of terms on the second line of each equation has been rewritten using charge symmetry and this is the form that is employed to solve the LO DFF evolution equations.

Using Eqs. (17) and (18), we write the evolution equations in terms of the nonsinglet quark, plus-type quark and gluon DFFs as

$$\begin{aligned}\frac{d}{dt}D_{q_i}^{h_1h_2}(z_1,z_2,t) = &\sum_{j=u,d,s}\int_{z_1+z_2}^1\frac{du}{u^2}D_{q_j^-}^{h_1h_2}\left(\frac{z_1}{u},\frac{z_2}{u},t\right)P_{q_jq_i}(u) + \sum_{k=u,d,s}\int_{z_1}^{1-z_2}\frac{du}{u(1-u)}D_g^{h_1}\left(\frac{z_1}{u},t\right)D_{q_k^-}^{h_2}\left(\frac{z_2}{1-u},t\right)\hat{P}_{q_kg}^{q_i}(u)\\ &+\sum_{j=u,d,s}\int_{z_1}^{1-z_2}\frac{du}{u(1-u)}D_{q_j^-}^{h_1}\left(\frac{z_1}{u},t\right)D_g^{h_2}\left(\frac{z_2}{1-u},t\right)\hat{P}_{gq_j}^{q_i}(u),\end{aligned} \tag{19}$$

$$\begin{aligned}\frac{d}{dt}D_{q_i^+}^{h_1h_2}(z_1,z_2,t) = &\sum_{j=u,d,s}\int_{z_1+z_2}^1\frac{du}{u^2}D_{q_j^+}^{h_1h_2}\left(\frac{z_1}{u},\frac{z_2}{u},t\right)P_{q_jq_i}(u) + 2\int_{z_1+z_2}^1\frac{du}{u^2}D_g^{h_1h_2}\left(\frac{z_1}{u},\frac{z_2}{u},t\right)P_{gq_i}(u)\\ &+\sum_{k=u,d,s}\int_{z_1}^{1-z_2}\frac{du}{u(1-u)}D_g^{h_1}\left(\frac{z_1}{u},t\right)D_{q_k^+}^{h_2}\left(\frac{z_2}{1-u},t\right)\hat{P}_{q_kg}^{q_i}(u)\\ &+\sum_{j=u,d,s}\int_{z_1}^{1-z_2}\frac{du}{u(1-u)}D_{q_j^+}^{h_1}\left(\frac{z_1}{u},t\right)D_g^{h_2}\left(\frac{z_2}{1-u},t\right)\hat{P}_{gq_j}^{q_i}(u),\end{aligned} \tag{20}$$

$$\begin{aligned}\frac{d}{dt}D_g^{h_1h_2}(z_1,z_2,t) = &\sum_{j=u,d,s,\bar{u},\bar{d},\bar{s}}\int_{z_1+z_2}^1\frac{du}{u^2}D_{q_j}^{h_1h_2}\left(\frac{z_1}{u},\frac{z_2}{u},t\right)P_{q_jg}(u) + \int_{z_1+z_2}^1\frac{du}{u^2}D_g^{h_1h_2}\left(\frac{z_1}{u},\frac{z_2}{u},t\right)P_{gg}(u)\\ &+\sum_{j=u,d,s,\bar{u},\bar{d},\bar{s}}\int_{z_1}^{1-z_2}\frac{du}{u(1-u)}D_{q_j}^{h_1}\left(\frac{z_1}{u},t\right)D_{\bar{q}_j}^{h_2}\left(\frac{z_2}{1-u},t\right)\hat{P}_{\bar{q}_jq_j}^{g}(u)\\ &+\int_{z_1}^{1-z_2}\frac{du}{u(1-u)}D_g^{h_1}\left(\frac{z_1}{u},t\right)D_g^{h_2}\left(\frac{z_2}{1-u},t\right)\hat{P}_{gg}^{g}(u)\\ =&\sum_{j=u,d,s}\int_{z_1+z_2}^1\frac{du}{u^2}\left[D_{q_j^+}^{h_1h_2}\left(\frac{z_1}{u},\frac{z_2}{u},t\right)P_{q_jg}(u)\right] + \int_{z_1+z_2}^1\frac{du}{u^2}D_g^{h_1h_2}\left(\frac{z_1}{u},\frac{z_2}{u},t\right)P_{gg}(u)\\ &+\sum_{j=u,d,s,\bar{u},\bar{d},\bar{s}}\int_{z_1}^{1-z_2}\frac{du}{u(1-u)}D_{q_j}^{h_1}\left(\frac{z_1}{u},t\right)D_{\bar{q}_j}^{h_2}\left(\frac{z_2}{1-u},t\right)\hat{P}_{\bar{q}_jq_j}^{g}(u)\\ &+\int_{z_1}^{1-z_2}\frac{du}{u(1-u)}D_g^{h_1}\left(\frac{z_1}{u},t\right)D_g^{h_2}\left(\frac{z_2}{1-u},t\right)\hat{P}_{gg}^{g}(u).\end{aligned} \tag{21}$$

For clarity, we show the sums over the repeated indices and use Eq. (21) to display how the combinations are applied to simplify the equations. The nonsinglet quark evolution equation is decoupled from the plus-type quark and gluon DFFs and can be evolved separately from them. Using Eq. (10) and converting integrals into sums over logarithmically discretized values of u, expressions for the DFFs evolved to the $(k+1)$th step in t can be obtained, producing results analogous to Eqs. (11)–(13).

V. RESULTS

QCD evolution equations are derived in the regime where perturbative approximations are valid, that is where the scale $Q \gg \Lambda_{\rm QCD}$. The scale of the underlying model in these calculations ($Q_0^2 = 0.2$ GeV^2) is low, thus one needs to be cautious when applying the evolution equations. For that reason here we first present the results for model SFFs for $u \to \pi^+$ and $u \to K^+$ evolved to $Q^2 = 4$ GeV^2. We compare these results with empirical parametrizations of experimental data to ensure a reasonable description. Then we present the results comparing the model scale DFFs with those evolved to $Q^2 = 4$ GeV^2 for $u \to \pi^+\pi^-$, $u \to \pi^+K^-$ and $q \to K^+K^-$, where $q = u, d, s$. The first subsection explores the evolution of $D_u^{\pi^+\pi^-}$ by comparing the model and evolved DFFs at particular values of z_1 or z_2, while the second subsection focuses on favored and unfavored hadron emission in the evolution of $D_u^{\pi^+K^-}$. Finally, the last subsection demonstrates the evolution of $D_q^{K^+K^-}$ for $q = u$, d or s.

A. Q^2 evolution of $D_u^{\pi^+}$ and $D_u^{K^+}$

The results of the evolution of our model calculated SFFs for up quark to π^+ and K^+ to the scale $Q^2 = 4$ GeV^2 are shown in Fig. 2. In the plots the red solid line represents the NJL-jet model calculated fragmentation functions for (a) π^+ and (b) K^+ evolved at the leading order from the model scale of $Q_0^2 = 0.2$ GeV^2 to scale of $Q^2 = 4$ GeV^2. The grey dashed lines with the grey bands show the HKNS parametrizations with their uncertainties taken from Ref. [55] and the dash-dotted lines represent the DSS parametrizations of Ref. [56], both at the leading order. From these plots it appears that the NJL-jet model compares favorably to the empirical parametrizations within their uncertainties. Thus we can proceed with the evolution of our model DFFs.

B. Q^2 evolution of $D_u^{\pi^+\pi^-}$

We consider the DFF for an up quark fragmenting to π^+ and π^-. When the up quark fragments to π^+, for which it is the favored emission channel, it produces a down quark, which has the favored emission channel to π^-. Since both emissions are favored channels for the detected hadrons in this quark cascade, the DFF has sizable peaks in the higher z_2 and z_1 regions for $z_1 = 0.5$ [Fig. 3(a)] and $z_2 = 0.5$ [Fig. 3(b)], respectively. For $D_u^{\pi^+\pi^-}$, the second term of Eq. (2) is zero (because $\hat{d}_u^{\pi^-} = 0$) and the integral term is small, so this DFF is dominated by the first term of Eq. (2). The model scale plot for $D_u^{\pi^+\pi^-}$ fixed at $z_1 = 0.5$ [Fig. 3(a)] has the shape of a favored single hadron fragmentation function since fixing z_1 effectively makes the first term on the right-hand side of Eq. (2) a constant multiplied by the favored fragmentation $D_d^{\pi^-}$. For z_2 fixed at 0.5 [Fig. 3(b)] the model scale $D_u^{\pi^+\pi^-}$ is shaped by the elementary quark fragmentation function $\hat{d}_u^{\pi^+}$, resulting in a peak at higher z_1, while having a very small contribution at low values of z_1. After evolution of the DFF, there is a reduction in magnitude and a shift in the peak towards the low z_2 region for $z_1 = 0.5$ [Fig. 3(a)]. When z_2 is fixed at 0.5 [Fig. 3(b)], the magnitude of the DFF is reduced and the peak value shifts towards the low z_1 region. Both plots in Fig. 3 display a range of values at low z where the evolved DFF obtains a larger magnitude than the model scale DFF. At higher momentum scales, the low z_1 and z_2 regions of the DFFs grow in magnitude because they can access the gluon emission channel.

We present the results for z_1 and z_2 fixed to 0.2 in Figs. 4(a) and 4(b), respectively, to investigate the DFF at

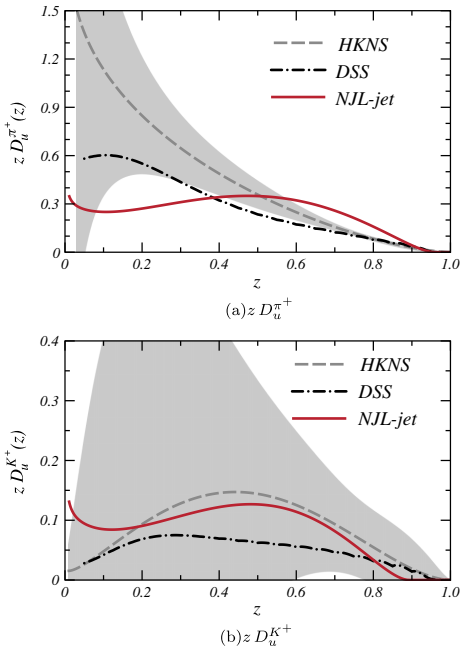

FIG. 2 (color online). NJL-jet fragmentation functions of u quark to (a) π^+ and (b) K^+ evolved at leading order to $Q^2 = 4$ GeV^2 (shown by solid red line) compared to HKNS [55] and DSS [56] parametrizations at the same scale (shown by a gray dashed line with a gray uncertain band and a black dash-dotted line respectively).

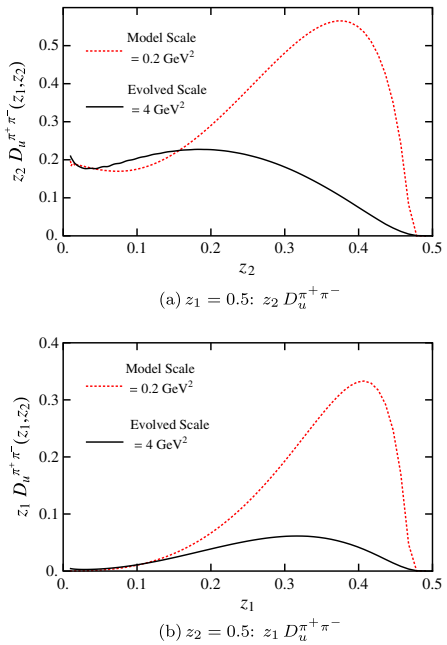

FIG. 3 (color online). $\pi^+\pi^-$ dihadron fragmentation functions for the u quark at the model scale ($Q_0^2 = 0.2$ GeV^2, shown by dotted red line) and the evolved scale ($Q^2 = 4$ GeV^2, shown by solid black line) for (a) $z_1 = 0.5$ and (b) $z_2 = 0.5$.

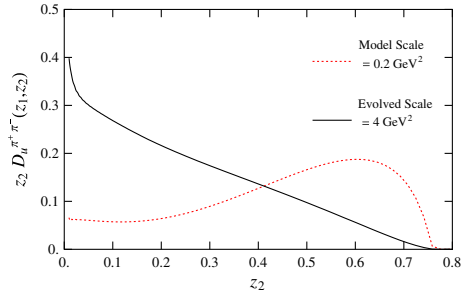

(a) $z_1 = 0.2$: $z_2\, D_u^{\pi^+\pi^-}$

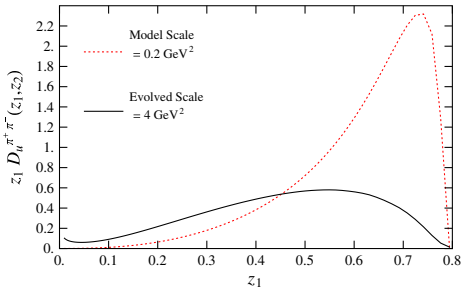

(b) $z_2 = 0.2$: $z_1\, D_u^{\pi^+\pi^-}$

FIG. 4 (color online). $\pi^+\pi^-$ dihadron fragmentation functions for the u quark at the model scale ($Q_0^2 = 0.2$ GeV^2, shown by dotted red line) and the evolved scale ($Q^2 = 4$ GeV^2, shown by solid black line) for (a) $z_1 = 0.2$ and (b) $z_2 = 0.2$.

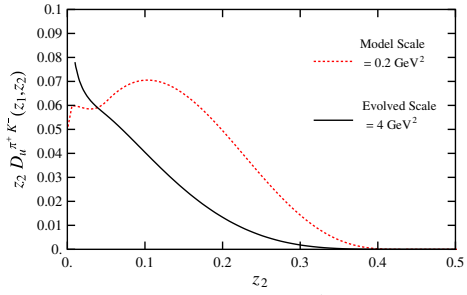

(a) $z_1 = 0.5$: $z_2\, D_u^{\pi^+K^-}$

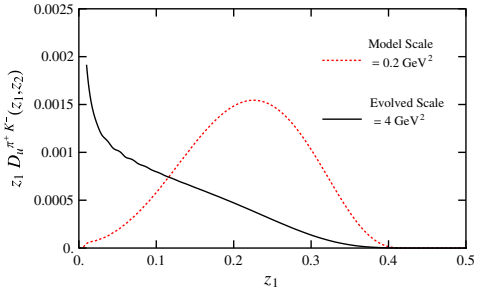

(b) $z_2 = 0.5$: $z_1\, D_u^{\pi^+K^-}$

FIG. 5 (color online). π^+K^- dihadron fragmentation functions for the u quark at the model scale ($Q_0^2 = 0.2$ GeV^2, shown by dotted red line) and the evolved scale ($Q^2 = 4$ GeV^2, shown by solid black line) for (a) $z_1 = 0.5$ and (b) $z_2 = 0.5$.

low fixed light-cone momentum fraction. The structure of the model scale $D_u^{\pi^+\pi^-}$ for $z_1 = 0.2$, shown in Fig. 4(a), is similar in shape to that of the model scale DFF at $z_1 = 0.5$, having the peak in the higher z_2, except it is spread out more and has a lower peak value. At $z_2 = 0.2$, the structure of the model scale DFF is again similar to the corresponding $z_2 = 0.5$ plot in Fig. 3(b), being small in the low z_1 region and having a large peak in the higher z_1 region, which is rather narrow. Evolution of the DFF results in a shift of the peak towards the lower z regions, with the magnitude of the evolved $D_u^{\pi^+\pi^-}$ becoming larger than the model scale $D_u^{\pi^+\pi^-}$ at midrange values of the allowed light-cone momentum fraction; rather than in the lower range of values that was observed for the z_1 and z_2 fixed to 0.5 results. The shape of the evolved $D_u^{\pi^+\pi^-}$ for $z_2 = 0.2$ in Fig. 4(b) appears very similar to that of the evolved $D_u^{\pi^+\pi^-}$ for $z_2 = 0.5$ in Fig. 3(b), whereas the shape for the evolved $D_u^{\pi^+\pi^-}$ for $z_1 = 0.2$ [Fig. 4(b)] is quite different to the corresponding result at $z_1 = 0.5$ in Fig. 3(a). Instead of the concave structure at $z_1 = 0.5$ shown in Fig. 3(a), at $z_1 = 0.2$ [Fig. 4(a)] the evolved DFF has a large contribution at low z_2 and steadily decreases as z_2 increases.

C. Q^2 evolution of $D_u^{\pi^+K^-}$

In Fig. 5 we present the results for $D_u^{\pi^+K^-}$, where the up quark is a favored channel for π^+ emission, but the remnant down quark is an unfavored channel for K^- emission. At the model scale, $D_u^{\pi^+K^-}$ shows no contribution in the large z_2 and z_1 regions for z_1 [Fig. 5(a)] and z_2 [Fig. 5(b)] fixed at 0.5, respectively. For $D_u^{\pi^+K^-}$ at the model scale the second term of Eq. (2) is zero (because $\hat{d}_u^{K^-} = 0$) and the integral term is small, so $D_u^{\pi^+K^-}$ is dominated by the first term of Eq. (2). In Fig. 5(a), the model scale DFF has the structure of the unfavored $D_d^{K^-}$, while also being suppressed in magnitude by $\hat{d}_u^{\pi^+}(z_1 = 0.5)$, which achieves its peak value in the high z_1 region while vanishing in the low z_1 region. For $z_2 = 0.5$ [Fig. 5(b)], the model scale DFF shows a very small magnitude for values of z_1 because of the combination of $\hat{d}_u^{\pi^+}$ multiplied by $D_d^{K^-}$. Elementary fragmentation functions for favored emission channels are very small in the low z region, and achieve large peak values in the high z region. This forces $D_u^{\pi^+K^-}(z_1, z_2)$ to have a very small magnitude in the low z_1 region as it is dependent on $\hat{d}_u^{\pi^+}(z_1)$. $D_d^{K^-}$ is an unfavored SFF and therefore is constructed by the integral term on the right-hand side of Eq. (1) because the first term

equals zero. Unfavored SFFs peak in the low z region and have very small magnitudes in the medium to high z region. Both of these effects combine to cause the resultant low peak in the middle of the allowed region of z_1.

When the DFF is evolved there is a shift towards the low z_2 region for z_1 fixed at 0.5 [Fig. 5(a)] and towards the low z_1 region for z_2 fixed at 0.5 [Fig. 5(b)]. We observe that the evolved DFF in Fig. 5 has a larger magnitude in the low z_1 and z_2 regions, while steadily decreasing as z_1 and z_2 increase. This is quite different to the results shown in Fig. 3, where there is either a large contribution for almost all the allowed range of values of z_2 [Fig. 3(a)] or a substantial peak still in the higher z_1 values with the magnitude of the DFF decreasing as z_1 is decreased. In both those cases, the DFF is largest away from the low values of z_2 and z_1. This effect could be caused by the down quark, which is produced in both fragmentations after the up quark fragments to π^+, being an unfavored emission channel for K^-, as opposed to the favored emission channel for π^-. The favored emission channel loses magnitude at higher z_1 as the momentum scale is increased, while the unfavored emission channels, which have no higher z_1 peak, increase at lower z_1 due to the greater access to the gluon emission channel.

D. Q^2 evolution of $D_q^{K^+K^-}$ for $q = u$, d or s

We now consider $D_q^{K^+K^-}$ for $q = u$ [Fig. 6(a)], d [Fig. 6(b)] or s [Fig. 6(c)]. The $q = u$ and $q = s$ DFFs both have large peaks in the high z_2 region at the model scale since both are favored fragmentation channels in the driving function of $D_q^{K^+K^-}$. The first term on the right-hand side of Eq. (2) produces most of the magnitude of the model scale $D_u^{K^+K^-}$ because the second term equates to zero and the integral term is small. $D_s^{K^+K^-}$ emerges from the second term on the right-hand side of Eq. (2) because the first term equates to zero and the integral term of the DFF is small. The first term on the right-hand side of Eq. (2) for $D_u^{K^+K^-}$ contains the elementary quark fragmentation function for the fragmentation from an up quark to K^+ as a function of z_1, multiplied by $D_s^{K^-}(z_2/(1-z_1))/(1-z_1)$. For z_1 fixed to 0.5, this term simplifies to a constant multiplied by $D_s^{K^-}(z_2/(1-z_1))$. However, for DFFs such as $D_s^{K^+K^-}$, which emerge from the second term on the right-hand side of Eq. (2), fixing z_1 to 0.5 restricts $\hat{d}_s^{K^-}(z_2)$ to values of z_2 less than 0.5. This suppresses the term considerably since the $z_2 > 0.5$ region of $\hat{d}_s^{K^-}(z_2)$ is where the function achieves its larger values. This is why the $u \to K^+K^-$ DFF is larger than the $s \to K^+K^-$ DFF when z_1 is fixed to 0.5.

After QCD evolution, the DFFs for fragmenting up [Fig. 6(a)] and strange [Fig. 6(c)] quarks at $z_1 = 0.5$ show the shift of the peak value to the lower z_2 region, with $D_u^{K^+K^-}$ having a structure similar to that seen for the evolved $D_u^{\pi^+\pi^-}$ at $z_1 = 0.5$ [Fig. 3(a)], while $D_s^{K^+K^-}$ has a structure similar to that of the evolved $D_u^{\pi^+\pi^-}$ at $z_2 = 0.5$ [Fig. 3(b)].

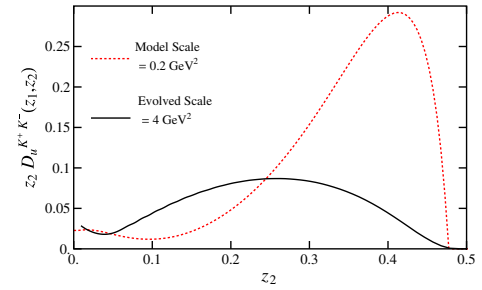

(a) $z_1 = 0.5$: $z_2\, D_u^{K^+K^-}$

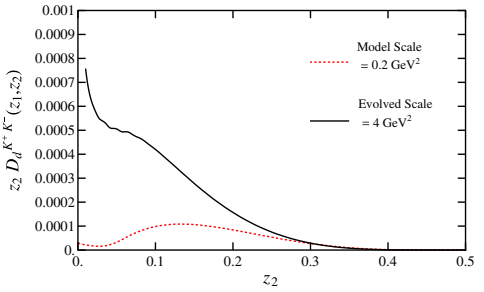

(b) $z_1 = 0.5$: $z_2\, D_d^{K^+K^-}$

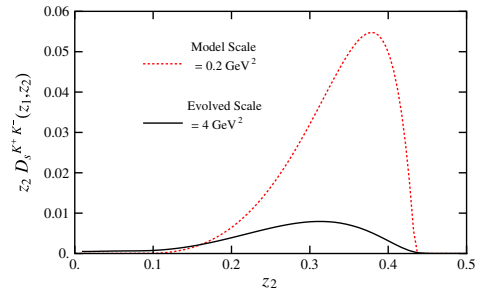

(c) $z_1 = 0.5$: $z_2\, D_s^{K^+K^-}$

FIG. 6 (color online). K^+K^- dihadron fragmentation functions for z_1 fixed to 0.5 at the model scale ($Q_0^2 = 0.2$ GeV^2, shown by dotted red line) and the evolved scale ($Q^2 = 4$ GeV^2, shown by solid black line) for a fragmenting (a) u quark, (b) d quark and (c) s quark.

For $D_d^{K^+K^-}$, the model scale plot is very small compared to $D_u^{K^+K^-}$ and $D_s^{K^+K^-}$, since it is unfavored for both detected hadrons. When the momentum scale is evolved up to 4 GeV^2, $D_d^{K^+K^-}$ increases in the low z_2 region for z_1 fixed to 0.5, because of the effects of gluon fragmentation.

VI. COMPARISON WITH OTHER WORK

With very little in the way of DFFs from experiments being available for comparison, we look to compare our

results with the work presented in Ref. [76]. We will first show that using our code and their parametrized DFFs as initial conditions, we do indeed obtain solutions comparable with those presented in Ref. [76] when evolved to $Q^2 = 109$ GeV^2. We also present our data evolved to a range of different scales for $D_u^{\pi^+\pi^-}$.

First, we briefly describe the procedures used in Ref. [76]. The evolution equations used there are those of Eqs. (15) and (16), with only minor rewriting of terms in the equations. For the gluon DFF evolution equations, the difference in the equations arises from alternate definitions of the functions. In Ref. [76], the DFF is taken to be identical for the up, down and strange quarks, and so the gluon evolution equation term involving these functions is written with the function multiplied by a factor of $2n_f$, whereas the DFFs in our approach differ and so we sum over each flavor. Similar reasoning is used for the other terms in the gluon evolution equation. To obtain the initial DFF at $Q^2 = 2$ GeV^2, the authors of Ref. [76] simulate three million dijet events, distributed equally over the number of flavors ($n_f = 3$), using JETSET. The resultant DFFs are parametrized by fitting to a functional form:

$$D(z_1, z_2) = N z_1^{\alpha_1} z_2^{\alpha_2} (z_1 + z_2)^{\alpha_3} (1 - z_1)^{\beta_1} (1 - z_2)^{\beta_2} \times (1 - z_1 - z_2)^{\beta_3}, \quad (22)$$

where N, α_1, α_2, α_3, β_1, β_2 and β_3 are the parameters fitted by minimizing the logarithm of χ^2. The fit describes the JETSET results better at larger values of z_1 and z_2, while not reproducing the results well for low values of z_1 and z_2. Values for the parameters are provided for the quark and gluon DFFs for momentum scales of $Q^2 = 2$ GeV^2 and $Q^2 = 109$ GeV^2. The SFFs used are obtained from the parametrization in Ref. [88]. The DFFs are QCD evolved from the initial scale of $Q^2 = 2$ GeV^2, and results are presented for several values of Q^2, including $Q^2 = 109$ GeV^2.

Using the initial parametrized DFFs at $Q^2 = 2$ GeV^2, in Fig. 7 we present the comparison of the parametrized $\pi^+\pi^-$ up quark and gluon DFFs obtained from JETSET at $Q^2 = 109$ GeV^2 (dotted red line) with the evolved solutions (blue circles) both taken from Ref. [76]. The solutions obtained using our code on the same initial parametrized DFFs (black crosses) and the solution to NJL-jet model DFFs evolved to the same momentum scale (solid orange line) are shown too.[2] We also consider solutions for the parametrized DFFs evolved using an altered version of our code that treats the QCD evolution of the SFFs with the same parametrized evolution as in Ref. [76] (purple dot-dashed line), rather than using the evolution equations. This serves the purpose of exhibiting how well our code reproduces the parametrized JETSET results.

[2]These comparisons are at best semiquantitative as we do not know the value of $\Lambda_{\rm QCD}$ used in Ref. [76].

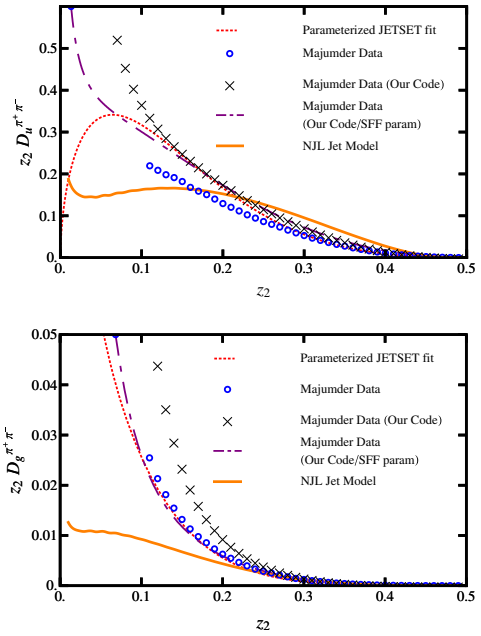

FIG. 7 (color online). $\pi^+\pi^-$ dihadron fragmentation functions for $z_1 = 0.5$ at $Q^2 = 109$ GeV^2 for a fragmenting (a) u quark and (b) gluon—see text for details.

The results for the NJL-jet model evolved to $Q^2 = 109$ GeV^2 are similar to the parametrized JETSET results of Ref. [76] for values of z_2 above 0.2 for both the up quark [Fig. 7(a)] and gluon [Fig. 7(b)] DFFs. Below $z_2 = 0.2$, our solutions are smaller. Such differences may be expected as the parametrization in Ref. [76] overestimates the JETSET results in the low z_1 and z_2 regions, and so the NJL-jet model results may well be closer to the actual JETSET output.

We also observe that for the up quark DFF [Fig. 7(a)], the solution for the parametrized JETSET input evolved using our code produces similar results to the parametrized solution of the JETSET results at $Q^2 = 109$ GeV^2 for values of z_2 greater than approximately 0.1. The gluon DFF [Fig. 7(b)] solutions differ only at values of z_2 lower than 0.25. In order to understand this difference we explored using the parametrized evolution of the SFFs [88] used by Ref. [76]. This produced an improved comparison between the parametrized JETSET solution and the DFFs obtained through our code. It is shown that by employing the parametrized SFF evolution we produce results that are similar to the parametrized JETSET solutions for both the up quark [Fig. 7(a)] and gluon [Fig. 7(b)] for values of z_2 above approximately 0.1.

In Fig. 8, we present the results for the NJL-jet model DFFs evolved to a range of Q^2 values: 5 GeV^2 (blue dotted

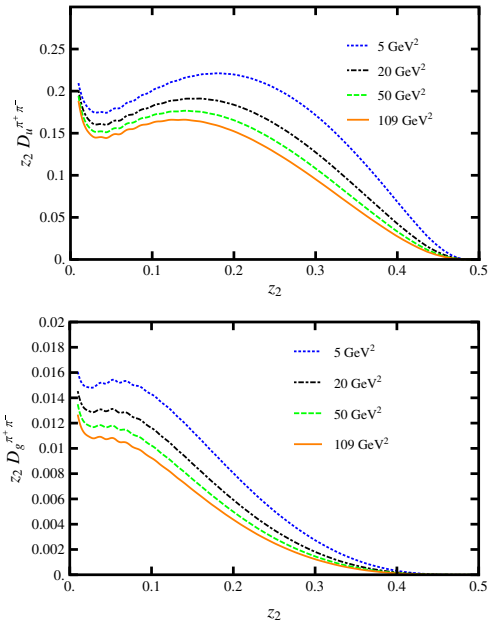

FIG. 8 (color online). $\pi^+\pi^-$ dihadron fragmentation functions for the NJL-jet model, for $z_1 = 0.5$ at $Q^2 = 5$ GeV^2, 20 GeV^2, 50 GeV^2, and 109 GeV^2 for a fragmenting (a) u quark and (b) gluon.

line), 20 GeV^2 (black dash-dotted line), 50 GeV^2 (green dashed line) and 109 GeV^2 (orange solid line). For $z_1 = 0.5$, the results show that as Q^2 increases, the DFFs appear to gradually reduce. The peak value is also observed to shift towards lower z_2 values.

VII. CONCLUSIONS AND OUTLOOKS

In this article, solutions are presented for dihadron fragmentation functions from the NJL-jet model evolved to a typical experimental scale of $Q^2 = 4$ GeV^2, from the model scale of $Q_0^2 = 0.2$ GeV^2. We first presented a brief summary of the integral equations used to obtain the model scale SFFs and DFFs in Sec. II. Sections III and IV describe the numerical method used to solve the evolution equations for SFFs and DFFs, respectively. The QCD evolution equations for the SFFs and the FORTRAN code used to solve them was based on the method described in Refs. [86,89–91]. The method used rearranges the evolution equations into nonsinglet quark and coupled plus-type quark and gluon equations, followed by discretizing the variables z and t and converting the integral terms into sums over the integration variable. The same method is employed to solve the QCD evolution equations for the DFFs with the variables z_1, z_2 and t being discretized.

Section V compares the model scale DFFs with the evolved DFFs for $\pi^+\pi^-$, π^+K^- and K^+K^-. In Sec. V B we investigated the evolution of $D_u^{\pi^+\pi^-}$ by comparing the model scale and evolved scale DFFs when either z_1 [Fig. 3(a)] or z_2 [Fig. 3(b)] is equal to 0.5. We also considered z_1 [Fig. 4(a)] or z_2 [Fig. 4(b)] equal to 0.2. For the fragmentation of the up quark to $\pi^+\pi^-$ we noted that the up quark was a favored emission channel for the π^+, while the down quark produced after the up quark fragments to a π^+ is a favored emission channel for the π^-. The evolved DFF showed a shift in the peak value towards the lower z regions, with each plot showing the evolved DFF obtaining a larger magnitude than the model scale DFF in the lower z region.

The focus of Sec. V C is on the evolution of $D_u^{\pi^+K^-}$. Similar to $D_u^{\pi^+\pi^-}$, the up quark is the favored emission channel for π^+, however the produced down quark is an unfavored emission channel for K^-. The magnitude of the model scale DFF was significantly smaller for $D_u^{\pi^+K^-}$ (Fig. 5) than for $D_u^{\pi^+\pi^-}$ (Fig. 3) at light-cone momentum fractions fixed to 0.5. After evolution, $D_u^{\pi^+K^-}$ displayed a similar shift in the peak value towards the low z region. For $z_1 = 0.5$ [Fig. 5(a)], the evolved DFF does not obtain a larger magnitude than the model scale DFF in the lower z_2 region, whereas for $z_2 = 0.5$ [Fig. 5(b)] the evolved DFF obtains a substantial increase over the model scale DFF in the lower z_1 region. This demonstrates the effect evolution has on favored and unfavored emission channels.

Finally, Sec. V D demonstrates the evolution of $D_q^{K^+K^-}$ for $q = u$, d or s. $D_q^{K^+K^-}$ has favored fragmentation channels for both the up quark and strange quark. This is observed in the results presented in Fig. 6 where both $D_u^{K^+K^-}$ and $D_s^{K^+K^-}$ have large peaks in the upper z_2 region. Both $D_u^{K^+K^-}$ and $D_s^{K^+K^-}$ display the shift of the peak value to the lower z region that has been shown in other favored emission channels at light-cone momentum fractions of 0.5. The down quark is an unfavored emission for both K^+ and K^-, and so $D_d^{K^+K^-}$ has a very small magnitude at the model scale. Evolving $D_d^{K^+K^-}$ shows a considerable increase in the lower z_2 region, though the magnitude is still much lower than that of $D_u^{K^+K^-}$ and $D_s^{K^+K^-}$ at $z_1 = 0.5$.

Evolution of the DFFs has the effect of reducing the magnitudes at higher z, resulting in peaks occurring earlier in the range of z values with a reduced magnitude. If the magnitude of the DFF was small at the model scale, a significant increase in the magnitude at the low z region is observed after evolution. The first of these two effects generally occurs for the favored emission channels, where the light-cone momentum fraction of the emitted hadron is not in the low z region. The second effect typically occurs when the fragmentation channel is unfavored or when the emitted hadron carries a small light-cone momentum fraction.

In Sec. VI, we evolve the parametrized JETSET data at 2 GeV^2 from Ref. [76] to 109 GeV^2 using our code to compare the solutions obtained with the parametrized JETSET data at the same scale for both the up quark and

gluon fragmenting to $\pi^+\pi^-$ (Fig. 7). We also presented solutions for the NJL-jet model up quark and gluon DFFs evolved to Q^2 values of 5 GeV^2, 20 GeV^2, 50 GeV^2 and 109 GeV^2 (Fig. 8). The solutions show that for $z_1 = 0.5$, the DFFs are reduced as Q^2 increases and the peak value shifts towards the lower z_2 region.

Extensions of the NJL-jet model for single hadron fragmentation functions such as the inclusion of hadronic resonances and their decays [64] and inclusion of the transverse momentum dependence [65] have been accomplished using a Monte Carlo framework. These extensions are possible for DFFs as well, but they are beyond the scope of this work and are left for the future.

ACKNOWLEDGMENTS

This work was supported by the Australian Research Council through Australian Laureate Fellowship FL0992247 (AWT), the ARC Centre of Excellence for Particle Physics at the Terascale and by the University of Adelaide.

[1] W. Melnitchouk, J. Speth, and A. W. Thomas, Phys. Rev. D **59**, 014033 (1998).
[2] A. W. Thomas, W. Melnitchouk, and F. M. Steffens, Phys. Rev. Lett. **85**, 2892 (2000).
[3] A. W. Thomas and W. Weise, *The Structure of the Nucleon* (Wiley-VCH, Berlin, 2001).
[4] M. Beckmann *et al.* (HERMES Collaboration), in *Testing QCD Through Spin Observables in Nuclear Targets*, edited by D. G. Crabb, D. B. Day, and J.-p. Chen (World Scientific Publishing Co., Singapore, 2003), pp. 292–298.
[5] A. Airapetian *et al.* (HERMES Collaboration), Phys. Rev. Lett. **92**, 012005 (2004).
[6] V. Barone, T. Calarco, A. Drago, and M. Simani, Phys. Lett. B **571**, 50 (2003).
[7] A. Airapetian *et al.* (HERMES Collaboration), Phys. Rev. D **71**, 012003 (2005).
[8] A. Airapetian *et al.* (HERMES Collaboration), Phys. Rev. D **75**, 012007 (2007).
[9] I. C. Cloët, W. Bentz, and A. W. Thomas, Phys. Rev. Lett. **102**, 252301 (2009).
[10] M. Alekseev *et al.* (COMPASS Collaboration), Phys. Lett. B **693**, 227 (2010).
[11] F. Gross, G. Ramalho, and M. Pena, Phys. Rev. D **85**, 093006 (2012).
[12] A. I. Signal and A. W. Thomas, Phys. Lett. B **191**, 205 (1987).
[13] V. Barone, C. Pascaud, and F. Zomer, Eur. Phys. J. C **12**, 243 (2000).
[14] S. Davidson, S. Forte, P. Gambino, N. Rius, and A. Strumia, J. High Energy Phys. 02 (2002) 037.
[15] W. Bentz, I. C. Cloët, J. T. Londergan, and A. W. Thomas, Phys. Lett. B **693**, 462 (2010).
[16] X.-D. Ji, Phys. Rev. Lett. **78**, 610 (1997).
[17] X.-D. Ji, Phys. Rev. D **55**, 7114 (1997).
[18] J. D. Bratt *et al.* (LHPC Collaboration), Phys. Rev. D **82**, 094502 (2010).
[19] G. S. Bali *et al.* (QCDSF Collaboration), Phys. Rev. Lett. **108**, 222001 (2012).
[20] P. Hagler, J. Phys. Conf. Ser. **295**, 012009 (2011).
[21] A. W. Thomas, A. Casey, and H. H. Matevosyan, Int. J. Mod. Phys. A **25**, 4149 (2010).
[22] A. W. Thomas, Phys. Rev. Lett. **101**, 102003 (2008).
[23] F. Myhrer and A. W. Thomas, Phys. Lett. B **663**, 302 (2008).
[24] S. D. Bass and A. W. Thomas, Phys. Lett. B **684**, 216 (2010).
[25] S. D. Bass, A. Casey, and A. W. Thomas, Phys. Rev. C **83**, 038202 (2011).
[26] M. Wakamatsu, Eur. Phys. J. A **44**, 297 (2010).
[27] M. Wakamatsu, Phys. Rev. D **81**, 114010 (2010).
[28] M. Wakamatsu, Phys. Rev. D **83**, 014012 (2011).
[29] A. Adare *et al.* (PHENIX Collaboration), Phys. Rev. Lett. **103**, 012003 (2009).
[30] A. Bacchetta, D. Boer, M. Diehl, and P. J. Mulders, J. High Energy Phys. 08 (2008) 023.
[31] V. Barone, A. Drago, and P. G. Ratcliffe, Phys. Rep. **359**, 1 (2002).
[32] E. Leader, A. V. Sidorov, and D. B. Stamenov, arXiv:1012.5033.
[33] E. Leader, A. V. Sidorov, and D. B. Stamenov, Phys. Rev. D **82**, 114018 (2010).
[34] E. Leader, Phys. Rev. D **83**, 096012 (2011).
[35] E. Leader, A. V. Sidorov, and D. B. Stamenov, J. Phys. Conf. Ser. **295**, 012054 (2011).
[36] W. Vogelsang, Nucl. Phys. **A827**, 110c (2009).
[37] F. A. Ceccopieri, Czech. J. Phys. **56**, F175 (2006).
[38] A. Bacchetta, M. Diehl, K. Goeke, A. Metz, P. J. Mulders, and M. Schlegel, J. High Energy Phys. 02 (2007) 093.
[39] I. C. Cloët, W. Bentz, and A. W. Thomas, Phys. Lett. B **659**, 214 (2008).
[40] L. P. Gamberg, A. Mukherjee, and P. J. Mulders, Phys. Rev. D **83**, 071503 (2011).
[41] L. Gamberg and M. Schlegel, AIP Conf. Proc. **1374**, 309 (2011).
[42] H. Wollny *et al.* (COMPASS Collaboration), in *Exclusive Reactions at High Momentum Transfer IV*, edited by A. Radyushkin (World Scientific, Singapore, 2011), pp. 303–311.
[43] M. Anselmino, H. Avakian, D. Boer, F. Bradamante, M. Burkardt *et al.*, Eur. Phys. J. A **47**, 35 (2011).
[44] M. Anselmino, M. Boglione, U. D'Alesio, S. Melis, F. Murgia, E. Nocera, and A. Prokudin, Phys. Rev. D **83**, 114019 (2011).
[45] S. M. Aybat, A. Prokudin, and T. C. Rogers, Phys. Rev. Lett. **108**, 242003 (2012).
[46] L. Gamberg, D. Boer, B. Musch, and A. Prokudin, AIP Conf. Proc. **1418**, 72 (2011).

[47] A. Bacchetta and M. Radici, Phys. Rev. Lett. **107**, 212001 (2011).
[48] K. Goeke, M. V. Polyakov, and M. Vanderhaeghen, Prog. Part. Nucl. Phys. **47**, 401 (2001).
[49] M. Burkardt, Int. J. Mod. Phys. A **18**, 173 (2003).
[50] M. Diehl, Phys. Rep. **388**, 41 (2003).
[51] X. Ji, Annu. Rev. Nucl. Part. Sci. **54**, 413 (2004).
[52] A. V. Belitsky and A. V. Radyushkin, Phys. Rep. **418**, 1 (2005).
[53] S. Boffi and B. Pasquini, Riv. Nuovo Cimento **30**, 387 (2007).
[54] M. Radici, Nuovo Cimento Soc. Ital. Fis. C **35**, 69 (2012).
[55] M. Hirai, S. Kumano, T.-H. Nagai, and K. Sudoh, Phys. Rev. D **75**, 094009 (2007).
[56] D. de Florian, R. Sassot, and M. Stratmann, Phys. Rev. D **75**, 114010 (2007).
[57] O. Biebel, P. Nason, and B. R. Webber, arXiv:hep-ph/0109282.
[58] D. de Florian and L. Vanni, Phys. Lett. B **578**, 139 (2004).
[59] M. Hirai, S. Kumano, T.-H. Nagai, and K. Sudoh, AIP Conf. Proc. **915**, 749 (2007).
[60] M. Hirai, S. Kumano, T.-H. Nagai, M. Oka, and K. Sudoh, arXiv:0709.2457.
[61] P. Francisconi, Nucl. Phys. B, Proc. Suppl. **207–208**, 129 (2010).
[62] T. Ito, W. Bentz, I. C. Cloët, A. W. Thomas, and K. Yazaki, Phys. Rev. D **80**, 074008 (2009).
[63] H. H. Matevosyan, A. W. Thomas, and W. Bentz, Phys. Rev. D **83**, 074003 (2011).
[64] H. H. Matevosyan, A. W. Thomas, and W. Bentz, Phys. Rev. D **83**, 114010 (2011).
[65] H. H. Matevosyan, W. Bentz, I. C. Cloët, and A. W. Thomas, Phys. Rev. D **85**, 014021 (2012).
[66] R. D. Field and R. P. Feynman, Nucl. Phys. **B136**, 1 (1978).
[67] H. H. Matevosyan, A. W. Thomas, and W. Bentz, Phys. Rev. D **86**, 034025 (2012).
[68] H. H. Matevosyan, A. W. Thomas, and W. Bentz, arXiv:1207.0812.
[69] H. H. Matevosyan, A. W. Thomas, and W. Bentz, arXiv:1207.1433.
[70] A. Bacchetta and M. Radici, Phys. Rev. D **74**, 114007 (2006).
[71] J. Zhou and A. Metz, Phys. Rev. Lett. **106**, 172001 (2011).
[72] T. Sjostrand, P. Eden, C. Friberg, L. Lonnblad, G. Miu, S. Mrenna, and E. Norrbin, Comput. Phys. Commun. **135**, 238 (2001).
[73] P. Liebing, Ph.D. thesis, Universität Hamburg [DESY Report No. DESY-THESIS-2004-036, 2004 (unpublished)]; http://cdsweb.cern.ch/record/808379.
[74] A. Casey, H. H. Matevosyan, and A. W. Thomas, Phys. Rev. D **85**, 114049 (2012).
[75] A. Majumder and X.-N. Wang, Phys. Rev. D **70**, 014007 (2004).
[76] A. Majumder and X.-N. Wang, Phys. Rev. D **72**, 034007 (2005).
[77] L. Grigoryan, arXiv:0809.0281.
[78] S. Boffi, R. Jakob, M. Radici, and A. Bianconi, in *Proceedings of the 2nd International Conference, Trieste, Italy*, edited by S. Boffi, C. C. degli Atti, and M. Giannini (World Scientific, Singapore, 2000), pp. 467–478.
[79] M. Radici, in *Physics with a High Luminosity Polarized Electron Ion Collider: Proceedings, Bloomington, Indiana, 1999*, edited by L. C. Bland, J. T. Londergan, and A. P. Szczepaniak (World Scientific, Singapore, 2000), pp. 113–122.
[80] M. Radici, in *Proceedings of the 2nd International Symposium, GDH 2002, Genova, Italy, 2002*, edited by M. A. Anghinolfi, M. Battaglieri, and R. de Vita (World Scientific, Hackensack, 2003), pp. 397–402.
[81] A. Bacchetta and M. Radici, Phys. Rev. D **70**, 094032 (2004).
[82] J. She, Y. Huang, V. Barone, and B.-Q. Ma, Phys. Rev. D **77**, 014035 (2008).
[83] A. Bacchetta, A. Courtoy, and M. Radici, Phys. Rev. Lett. **107**, 012001 (2011).
[84] A. Courtoy, A. Bacchetta, and M. Radici, in *Proceedings of the XIX International Workshop on Deep-Inelastic Scattering and Related Subjects (DIS 2011)*, (Newport News, VA, 2011), arXiv:1106.5897.
[85] A. Courtoy, A. Bacchetta, M. Radici, and A. Bianconi, Phys. Rev. D **85**, 114023 (2012).
[86] M. Hirai and S. Kumano, Comput. Phys. Commun. **183**, 1002 (2012).
[87] F. A. Ceccopieri, M. Radici, and A. Bacchetta, Phys. Lett. B **650**, 81 (2007).
[88] J. Binnewies, B. A. Kniehl, and G. Kramer, Phys. Rev. D **52**, 4947 (1995).
[89] M. Miyama and S. Kumano, Comput. Phys. Commun. **94**, 185 (1996).
[90] M. Hirai, S. Kumano, and M. Miyama, in *Proceedings of the 12th International Symposium, SPIN 96, Amsterdam, Netherlands, 1996*, edited by C. W. de Jager, T. J. Ketel, P. J. Mulders, J. E. J. Oberski, and M. Oskam-Tamboezer (World Scientific, Singapore, 1997), pp. 410–412.
[91] M. Hirai, S. Kumano, and M. Miyama, Comput. Phys. Commun. **108**, 38 (1998).

4.3 Gluon polarization in the proton

Statement of Authorship

Title of Paper	Gluon Polarization in the Proton
Publication Status	⦿ Published, ○ Accepted for Publication, ○ Submitted for Publication, ○ Publication style
Publication Details	Steven D. Bass, Andrew Casey and Anthony W. Thomas Gluon Polarization in the Proton Physical Review C83 038202 (2011) Copyright 2011 by the American Physical Society.

Author Contributions

By signing the Statement of Authorship, each author certifies that their stated contribution to the publication is accurate and that permission is granted for the publication to be included in the candidate's thesis.

Name of Principal Author (Candidate)	Andrew Casey		
Contribution to the Paper	Formulation of research proposal. Carried out the literature review Performed primary calculation Wrote first draft of the paper Equal partner in the editing process that led to a final paper		
Signature		Date	12/8/13

Name of Co-Author	Steven D. Bass		
Contribution to the Paper	Supervised the development of work Checked calculation Equal partner in the editing process that led to a final paper		
Signature		Date	12/8/13

Name of Co-Author	Anthony W. Thomas		
Contribution to the Paper	Supervised the development of work Checked calculation Equal partner in the editing process that led to a final paper		
Signature		Date	12/8/13

Name of Co-Author			
Contribution to the Paper			
Signature		Date	

PHYSICAL REVIEW C **83**, 038202 (2011)

Gluon polarization in the proton

Steven D. Bass
Institute for Theoretical Physics, Universität Innsbruck, Technikerstrasse 25, Innsbruck, A-6020 Austria

Andrew Casey and Anthony W. Thomas
CSSM, School of Chemistry and Physics, University of Adelaide, Adelaide SA 5005, Australia
(Received 14 January 2011; published 3 March 2011)

We combine heavy-quark renormalization group arguments with our understanding of the nucleon's wave function to deduce a bound on the gluon polarization Δg in the proton. The bound is consistent with the values extracted from spin experiments at COMPASS and RHIC.

DOI: 10.1103/PhysRevC.83.038202 PACS number(s): 13.60.Hb, 13.88.+e, 14.20.Dh

Polarized deep inelastic scattering (pDIS) experiments have revealed a small value for the nucleon's flavor-singlet axial-charge, $g_A^{(0)}|_{\rm pDIS} \sim 0.3$, suggesting that the quarks' intrinsic spin contributes little of the proton's spin. The challenge to understand the spin structure of the proton [1–6] has inspired a vast program of theoretical activity and new experiments. Why is the quark spin content $g_A^{(0)}|_{\rm pDIS}$ so small? How is the spin $\frac{1}{2}$ of the proton built up from the spin and orbital angular momentum of the quarks and gluons inside?

A major topic of investigation has been the role of polarized glue in the nucleon, both in terms of its contribution to the nucleon's spin and possible suppression of the nucleon's singlet axial charge through the QCD axial anomaly. Key experiments to measure gluon polarization are COMPASS at CERN and PHENIX and STAR at RHIC. In this paper we investigate gluon polarization via the charm-quark axial charge, matching the results of the heavy-quark renormalization group with what we know of the proton's wave function. We suggest a bound $|\Delta g(m_c^2)| \lesssim 0.3$, which is consistent with the results of the present experiments.

We start by recalling the g_1 spin sum rules, which are derived from the dispersion relation for polarized photon-nucleon scattering and, for deep inelastic scattering, the light-cone operator product expansion. At leading twist the first moment of the g_1 spin structure function measures a linear combination of the nucleon's scale-invariant axial charges $g_A^{(3)}$, $g_A^{(8)}$, and $g_A^{(0)}|_{\rm inv}$ plus a possible subtraction constant β_∞ in the dispersion relation [1]

$$\int_0^1 dx\; g_1(x,Q^2) = \left(\frac{1}{12}g_A^{(3)} + \frac{1}{36}g_A^{(8)}\right)c_{\rm NS}[\alpha_s(Q^2)] + \frac{1}{9}g_A^{(0)}|_{\rm inv}c_{\rm S}[\alpha_s(Q^2)] + \beta_\infty. \quad (1)$$

Here $c_{\rm NS}$ and $c_{\rm S}$ are the nonsinglet and singlet Wilson coefficients. In terms of the flavor dependent axial charges $2Ms_\mu\Delta q = \langle p,s|\bar{q}\gamma_\mu\gamma_5 q|p,s\rangle$ the isovector, octet, and singlet axial charges are $g_A^{(3)} = \Delta u - \Delta d$, $g_A^{(8)} = \Delta u + \Delta d - 2\Delta s$, and $g_A^{(0)}|_{\rm inv}/E(\alpha_s) \equiv g_A^{(0)}(Q^2) = \Delta u + \Delta d + \Delta s$. Here $E(\alpha_s) = \exp\int_0^{\alpha_s} d\tilde{\alpha}_s\,\gamma(\tilde{\alpha}_s)/\beta(\tilde{\alpha}_s)$ is a renormalization group factor which corrects for the (two-loop) nonzero anomalous dimension $\gamma(\alpha_s)$ of the singlet axial-vector current [7], $J_{\mu 5} = \bar{u}\gamma_\mu\gamma_5 u + \bar{d}\gamma_\mu\gamma_5 d + \bar{s}\gamma_\mu\gamma_5 s$, which is close to one and which goes to one in the limit $Q^2 \to \infty$; $\beta(\alpha_s) = -(11 - \frac{2}{3}f)(\alpha_s^2/2\pi) + \cdots$ is the QCD beta function and $\gamma(\alpha_s) = f(\alpha_s/\pi)^2 + \cdots$, where f is the number of active flavors. The singlet axial charge, $g_A^{(0)}|_{\rm inv}$, is independent of the renormalization scale μ and corresponds to $g_A^{(0)}(Q^2)$ evaluated in the limit $Q^2 \to \infty$. The flavor nonsinglet axial charges are renormalization group invariants.

The isovector axial charge is measured independently in neutron β decays ($g_A^{(3)} = 1.270 \pm 0.003$ [8]) and the octet axial charge is commonly taken to be the value extracted from hyperon β decays assuming a two-parameter SU(3) fit ($g_A^{(8)} = 0.58 \pm 0.03$ [9]). The uncertainty quoted for $g_A^{(8)}$ has been a matter of some debate [10,11]. There is considerable evidence that SU(3) symmetry may be badly broken and some have suggested that the error on $g_A^{(8)}$ should be as large as 25% [10]. Indeed, prompted by the work of Myhrer and Thomas [12], which showed that the effect of the one-gluon-exchange hyperfine interaction [13] and the pion cloud [14] of the nucleon was to reduce $g_A^{(0)}$ calculated in the cloudy bag model to near the experimental value, a reevaluation of these effects on $g_A^{(3)}$, $g_A^{(8)}$, and $g_A^{(0)}$ including kaon loops led to the value $g_A^{(8)} = 0.46 \pm 0.05$ [15]. Here the reduction from the SU(3) value came primarily from the pion cloud.

Assuming no twist-two subtraction constant, polarized deep inelastic scattering experiments have been interpreted in terms of a small value for the flavor-singlet axial charge: $g_A^{(0)}|_{{\rm pDIS},Q^2\to\infty} = 0.33 \pm 0.03\ ({\rm stat.}) \pm 0.05\ \ ({\rm syst.})$ [16] if one uses the SU(3) value for $g_A^{(8)}$. On the other hand, using the value $g_A^{(8)} = 0.46 \pm 0.05$ from SU(3) breaking, the corresponding experimental value of $g_A^{(0)}|_{\rm pDIS}$ would increase to $g_A^{(0)}|_{\rm pDIS} = 0.36 \pm 0.03 \pm 0.05$. In the naive parton model $g_A^{(0)}|_{\rm pDIS}$ is interpreted as the fraction of the proton's spin which is carried by the intrinsic spin of its quark and antiquark constituents.

Historically, the wish to understand the suppression of $g_A^{(0)}$ relative to $g_A^{(8)}$ led to considerable theoretical efforts to understand the flavor-singlet axial charge in QCD. QCD theoretical analysis leads to the formula [1,17–20]

$$g_A^{(0)} = \left(\sum_q \Delta q - 3\frac{\alpha_s}{2\pi}\Delta g\right)_{\rm partons} + \mathcal{C}_\infty. \quad (2)$$

Here $\Delta g_{\text{partons}}$ is the amount of spin carried by polarized gluons in the polarized proton ($\alpha_s \Delta g \sim$ constant as $Q^2 \to \infty$ [17,18]) and $\Delta q_{\text{partons}}$ measures the spin carried by quarks and antiquarks carrying "soft" transverse momentum $k_t^2 \sim P^2, m^2$ where P is a typical gluon virtuality and m is the light quark mass. The polarized gluon term is associated with events in polarized deep inelastic scattering where the hard photon strikes a quark or antiquark generated from photon-gluon fusion with $k_t^2 \sim Q^2$ [19,20]. It corresponds to the QCD axial anomaly in the flavor-singlet axial-vector current. $\mathcal{C}_\infty$ denotes a potential nonperturbative gluon topological contribution [1] associated with the possible subtraction constant in the dispersion relation for g_1 and possible spin contributions at Bjorken $x = 0$, that is outside the range of polarzed deep inelastic scattering experiments. The measured singlet axial charge is $g_A^{(0)}|_{\text{pDIS}} = g_A^{(0)} - C_\infty$.

In the parton model $\Delta q_{\text{partons}}$ is associated with the forward matrix of the partially conserved axial-vector current J_{+5}^{con} evaluated in the light-cone gauge $A_+ = 0$ and corresponds to the quark spin contribution extracted from experiments using the JET or AB factorization schemes [21]. For each flavor q, this term and the possible topological term $\mathcal{C}_\infty$ are renormalization group invariants [1]. All of the renormalization group scale dependence induced by the anomalous dimension, $\gamma(\alpha_s)$, is carried by the polarized glue term:

$$\left\{\frac{\alpha_s}{2\pi}\Delta g\right\}_{Q^2} = \left\{\frac{\alpha_s}{2\pi}\Delta g\right\}_{\infty} - \frac{1}{f}\{1/E(\alpha_s) - 1\}\, g_A^{(0)}\big|_{\text{inv}}, \tag{3}$$

where all quantities in this equation are understood to be defined in the f-flavor theory. Flavor nonsinglet combinations of the Δq are renormalization group invariant so that each flavor evolves at the same rate, including heavy-quark contributions ($q = c, b, t$). The growth in the gluon polarization $\Delta g \sim 1/\alpha_s$ at large Q^2 is compensated by growth with opposite signs in the gluon orbital angular momentum. The quark and gluon total angular momenta in the infinite scaling limit are given by [22] $J_q(\infty) = \frac{1}{2}\{3f/(16 + 3f)\}$ and $J_g(\infty) = \frac{1}{2}\{16/(16 + 3f)\}$. There is presently a vigorous program to disentangle the different contributions involving experiments in semi-inclusive polarized deep inelastic scattering and polarized proton-proton collisions [3,23].

Heavy-quark axial charges have been studied in the context of elastic neutrino-proton scattering [24,25] and heavy-quark contributions to g_1 at Q^2 values above the charm production threshold [26–29]. Charm production in polarized deep inelastic scattering is an important part of the COMPASS spin program at CERN [30].

Following Eq. (2) we can write the charm-quark axial-charge contribution as

$$\Delta c(Q^2) = \Delta c_{\text{partons}} - \left\{\frac{\alpha_s}{2\pi}\Delta g\right\}_{Q^2,\, f=4}, \tag{4}$$

where $\Delta c_{\text{partons}}$ corresponds to the forward matrix element of the plus component of the renormalization group invariant charm-quark axial current with just mass terms in the divergence (minus the QCD axial anomaly), viz. $(\bar{c}\gamma_\mu\gamma_5 c)_{\text{con}} = (\bar{c}\gamma_\mu\gamma_5 c) - k_\mu$ with k_μ the gluonic Chern-Simons current, and we neglect any topological contribution.[1] For scales $Q^2 \gg m_c^2$, $\Delta c_{\text{partons}}$ corresponds to the polarized charm contribution one would find in the JET or AB factorization schemes.

The heavy-quark contributions to the nonsinglet neutral current axial charge measured in elastic neutrino-proton scattering have been calculated to next-to-leading order (NLO) in Ref. [24]. For charm quarks, the relevant electroweak doublet contribution at leading order (LO) is

$$(\Delta c - \Delta s)_{\text{inv}}^{(f=4)} = -\frac{6}{27\pi}\alpha_s^{(3)}(m_c^2) g_A^{(0)}\big|_{\text{inv}}^{(f=3)} - \Delta s_{\text{inv}}^{(f=3)} + O(1/m_c^2). \tag{5}$$

For the LO contribution this is made up from

$$\Delta s_{\text{inv}}^{(f=4)} = \Delta s_{\text{inv}}^{(f=3)} + \left(\frac{6}{27\pi} - \frac{6}{25\pi}\right)\alpha_s^{(3)}(m_c^2) g_A^{(0)}\big|_{\text{inv}}^{(f=3)} + O(1/m_c^2), \tag{6}$$

$$\Delta c_{\text{inv}}^{(f=4)} = -\frac{6}{25\pi}\alpha_s^{(3)}(m_c^2)\, g_A^{(0)}\big|_{\text{inv}}^{(f=3)} + O(1/m_c^2).$$

Here $\Delta c_{\text{inv}} = \Delta c(Q^2)$ evaluated in the limit $Q^2 \to \infty$, where the charm-quark axial-charge contribution is $2Ms_\mu \Delta c = \langle p, s|\bar{c}\gamma_\mu\gamma_5 c|p, s\rangle$. The change in Δs_{inv} between the four- and three-flavor theories in Eqs. (6) comes from the different number of flavors in $E(\alpha_s)$ for the four- and three-flavor theories.

Equations (6) contain vital information about $\{(\alpha_s/2\pi)\,\Delta g\}_\infty$ in Eq. (4) if we know the renormalization group (RG) invariant quantity $\Delta c_{\text{partons}}$. Indeed, if the latter were zero and if we ignore the NLO evolution associated with the two-loop anomalous dimension $\gamma(\alpha_s)$, then Eqs. (6) would imply (at LO)

$$\Delta g^{(f=4)}(Q^2) = \frac{12}{25}\frac{\alpha_s^{(f=3)}(m_c^2)}{\alpha_s^{(f=4)}(Q^2)} g_A^{(0)}\big|_{\text{inv}}^{(f=3)}, \tag{7}$$

or $\Delta g \sim 0.23$ when $\alpha_s(Q^2) \sim 0.3$. The following discussion is aimed at assessing the possible size of $\Delta c_{\text{partons}}$ plus the NLO evolution associated with $\gamma(\alpha_s)$, and hence the error on this value.

Canonical (anomaly free) heavy-quark contributions to the proton wave function are, in general, suppressed by powers of $1/m_c^2$, so we expect $\Delta c_{\text{partons}} \sim O(1/m_c^2)$. The RG invariant quantity $\Delta c_{\text{partons}}$ takes the same value at all momentum scales. We may evaluate it using quark-hadron duality in a hadronic basis with meson cloud methods [32]. Experimental studies of the strange quark content of the nucleon over the past decade have given us considerable confidence that both the matrix elements of the vector and scalar charm-quark currents (which are anomaly free) in the proton are quite small [33,34]. This gives us confidence in estimating the polarized charm contribution through its suppression relative to the corresponding polarized strangeness -0.01 [15] by the factor

[1] Any topological contribution will be associated with some of the $\Delta c_{\text{partons}}$ being shifted to Bjorken $x = 0$. In general, topological contributions are suppressed by powers of $1/m_c^2$ for heavy-quark matrix elements [31].

$\sim (m_\Lambda - m_N + m_K)^2/4m_c^2 < 0.1$ so that $|\Delta c_{\rm partons}| < 0.001$. QCD four-flavor evolution and Eqs. (6) then enable an estimate of Δg at scales relevant to experiments at COMPASS and RHIC.

In perturbative QCD the LO contribution to heavy-quark production through polarized photon-gluon fusion yields

$$\int_0^1 dx\, g_1^{(\gamma^* g \to h\bar{h})} \sim 0, \quad Q^2 \gg m_h^2, \tag{8}$$

where m_h is the heavy-quark mass ($h = c, b, t$). The anomalous $-\alpha_s/2\pi$ term is canceled against the canonical term when $m_h^2 \gg P^2$ (the typical gluon virtuality in the proton) [19]. If the gluon polarization were large so that $-\frac{\alpha_s}{2\pi}\Delta g$ made a large contribution to the suppression of $g_A^{(0)}$, at this order one would also find a compensating large canonical polarized charm contribution in the proton. To understand this more deeply, we note that the result in Eq. (8) follows from the complete expression [20]

$$\int_0^1 dx\, g_1^{(\gamma^* g)} = -\frac{\alpha_s}{2\pi}\left[1 + \frac{2m^2}{P^2}\frac{1}{\sqrt{1+\frac{4m^2}{P^2}}}\ln\left(\frac{\sqrt{1+\frac{4m^2}{P^2}}-1}{\sqrt{1+\frac{4m^2}{P^2}}+1}\right)\right]. \tag{9}$$

Here m is the mass of the struck quark and P^2 is the gluon virtuality. We next focus on charm production. The first term in Eq. (9) is the QCD anomaly and the second, mass-dependent, canonical term gives $\Delta c_{\rm partons}^{\rm (gluon)}$ for a gluon "target" with virtuality P^2. Evaluating Eq. (9) for $m_c^2 \gg P^2$ gives the leading term $\int_0^1 dx\ g_1^{(\gamma^* g)} \sim -\frac{\alpha_s}{2\pi}\frac{5}{8}\frac{P^2}{m_c^2}$, hence the result in Eq. (8).

It is interesting to understand Eqs. (8) and (9) in terms of deriving the QCD axial anomaly via Pauli-Villars regularization (instead of the usual dimensional regularization derivation used in [19]). The anomaly corresponds to the heavy Pauli-Villars "quark," which will cancel against the heavy charm quark for a charm-quark mass much bigger than gluon virtualities in the problem (there are no other mass terms to set the scale). When the axial-vector amplitude is evaluated at the two-loop level there will be gluon loop momenta between m_c and the ultraviolet cut-off scale generating a small scale dependence so that the cancellation between canonical heavy-quark and anomalous polarized glue terms is not exact in full QCD. This scale dependence corresponds to the two-loop anomalous dimension $\gamma(\alpha_s)$ in $E(\alpha_s)$. The result in Eq. (8) was previously discussed in Refs. [10,27] in the context of the phenomenology that would follow if there were large gluon polarization in the proton. Nonperturbative evaluation of $\Delta c_{\rm partons}$ allows us to constrain the size of Δg given what we know about charm and strangeness in the nucleon's wave function.

There is a further issue that the derivation of Eqs. (6) involves matching conditions where the spin contributions are continuous between the three- and four-flavor theories at the threshold scale m_c modulo $O(1/m_c^2)$ corrections, which determine a theoretical error for the method. Using QCD evolution with the renormalization group factor $E(\alpha_s)$, the results in Eqs. (6) are equivalent to the leading twist term $\Delta c(m_c^2)$ vanishing at the threshold scale m_c modulo $O(1/m_c^2)$ corrections, viz. $\Delta c(m_c^2) = O(1/m_c^2)$ [10]. The leading $O(1/m_c^2)$ term is estimated using effective field theory in Refs. [10,25,27]. For polarized photon-gluon fusion, this is the $-(\alpha_s/2\pi)(5/8)(P^2/m_c^2)$ leading term in the heavy-quark limit of Eq. (9). The heavy charm quark is integrated out at threshold to give the matrix element of a gauge-invariant gluon operator with dimension 5 and the same quantum numbers as the axial-vector current, viz. $\Delta c(m_c^2) \sim O[\alpha_s(m_c^2)/4\pi](M^2/m_c^2)$ [27] or $\Delta c(m_c^2) \sim O[\alpha_s(m_c^2)\Lambda_{\rm QCD}^2/m_c^2] \sim 0.017$ [10].[2] Taking this as an estimate of the theoretical error gives $\Delta c(m_c^2) = 0 \pm 0.017$.

We next combine this number for $\Delta c(m_c^2)$ with our estimate of the canonical charm contribution $|\Delta c_{\rm partons}| < 0.001$ in quadrature to obtain a bound including theoretical error on the size of the polarized gluon contribution: $|-(\alpha_s/2\pi)\Delta g(m_c^2)| \lesssim 0.017$ or

$$|\Delta g(m_c^2)| \lesssim 0.3 \tag{10}$$

with $\alpha_s(m_c^2) = 0.4$. Values at other values of Q^2 are readily obtained with Eq. (3) or $\alpha_s \Delta g \sim$ constant for large values of Q^2.

It is interesting to extend this analysis to full six-flavor QCD. The values of $\Delta c_{\rm inv}^{(f=6)}$, $\Delta b_{\rm inv}^{(f=6)}$, and $\Delta t_{\rm inv}^{(f=6)}$ were derived in Ref. [24] to NLO in the heavy-quark expansion. Taking just the leading-order contribution plus the heavy-quark power correction according to the recipe [10,27] described above gives $\Delta c^{(f=5)}(m_b^2) = -0.006 \pm 0.017$ and $\Delta c^{(f=6)}(m_t^2) = -0.009 \pm 0.017$ for polarized charm. For the bottom and top quarks one obtains $\Delta b^{(f=5)}(m_b^2) = 0 \pm 0.001 \pm 0.017$, $\Delta b^{(f=6)}(m_t^2) = -0.003 \pm 0.001 \pm 0.017$, and $\Delta t(m_t^2) = 0 \pm 2 \times 10^{-7} \pm 0.017$. Here the first error comes from the $O(1/m_h^2)$ mass correction for the heaviest quark of c, b, and t. The second error comes from the other heavy-quarks with lesser mass as we evaluate these heavy-quark contributions in terms of the measured value of the light-quark quantity $g_A^{(0)}|_{\rm inv}^{(f=3)}$. These numbers overlap with a zero value for $(\alpha_s/2\pi)\,\Delta g$ in the relevant f-flavor theories. The QCD scale dependence of $(\alpha_s/2\pi)\,\Delta g$ starts with NLO evolution induced by Kodaira's two-loop anomalous dimension $\gamma(\alpha_s)$. The combination $(\alpha_s/2\pi)\,\Delta g$ is scale invariant at LO. This means that if we work just to LO and Δg vanishes at one scale, it will vanish at all scales (in LO approximation). The LO QCD evolution equation for gluon orbital angular momentum in the proton [22] then simplifies so that $L_g(\infty) = \frac{1}{2}\{16/(16+3f)\}$. In practice, the two-loop anomalous dimension generates slow evolution of $(\alpha_s/2\pi)\,\Delta g$. Dividing the finite value of this combination at large scales by the small value of α_s gives a finite value for the gluon polarization Δg, which can readily be the same order of magnitude as the gluon

[2] These $O(1/m_c^2)$ terms associated with the full Δc are manifest in polarized photon-gluon fusion through the heavy-quark limit of Eq. (9), $\int_0^1 dx\ g_1^{(\gamma^* g)} \sim -(\alpha_s/2\pi)(5/8)(P^2/m_c^2)$, and are to be distinguished from the model evaluation of $\Delta c_{\rm partons}$.

total angular momentum (or larger with cancellation against a correspondingly larger gluon orbital angular momentum contribution).

It is interesting that the value of Δg deduced from present experiments COMPASS at CERN and PHENIX and STAR at RHIC typically give $|\Delta g| < 0.4$ with $\alpha_s \sim 0.3$ corresponding to $|-3(\alpha_s/2\pi)\Delta g| < 0.06$ [3]. This experimental value is extracted from direct measurements of gluon polarization at COMPASS in the region around $x_{\text{gluon}} \sim 0.1$, NLO QCD motivated fits to inclusive g_1 data taken in the region $x > 0.006$, and RHIC spin data in the region $0.02 < x_{\text{gluon}} < 0.4$. The theoretical bound, Eq. (10), is consistent with this experimental result.

The research of S.D.B. is supported by the Austrian Science Fund, FWF, through Grant No. P20436, while A.W.T. is supported by the Australian Research Council and by the University of Adelaide.

[1] S. D. Bass, Rev. Mod. Phys. **77**, 1257 (2005).
[2] S. D. Bass, *The Spin Structure of the Proton* (World Scientific, Singapore, 2008).
[3] S. D. Bass, Mod. Phys. Lett. A **24**, 1087 (2009).
[4] A. W. Thomas, Prog. Part. Nucl. Phys. **61**, 219 (2008).
[5] A. W. Thomas, Phys. Rev. Lett. **101**, 102003 (2008).
[6] M. Anselmino, A. Efremov, and E. Leader, Phys. Rep. **261**, 1 (1995); H.-Y. Cheng, Int. J. Mod. Phys. A **11**, 5109 (1996); J. Ellis and M. Karliner, arXiv:hep-ph/9601280; G. Altarelli, R. D. Ball, S. Forte, and G. Ridolfi, Acta Phys. Pol. B **29**, 1145 (1998); G. M. Shore, arXiv:hep-ph/9812355; B. Lampe and E. Reya, Phys. Rep. **332**, 1 (2000); B. W. Filippone and X. Ji, Adv. Nucl. Phys. **26**, 1 (2001); S. J. Brodsky, Int. J. Mod. Phys. A **18**, 1531 (2003); S. E. Kuhn, J.-P. Chen, and E. Leader, Prog. Part. Nucl. Phys. **63**, 1 (2009).
[7] J. Kodaira, Nucl. Phys. B **165**, 129 (1980).
[8] C. Amsler *et al.* (Particle Data Group), Phys. Lett. B **667**, 1 (2008).
[9] F. E. Close and R. G. Roberts, Phys. Lett. B **316**, 165 (1993).
[10] R. L. Jaffe and A. Manohar, Nucl. Phys. B **337**, 509 (1990).
[11] P. G. Ratcliffe, Czech. J. Phys. **54**, B11 (2004).
[12] F. Myhrer and A. W. Thomas, Phys. Lett. B **663**, 302 (2008).
[13] F. Myhrer and A. W. Thomas, Phys. Rev. D **38**, 1633 (1988).
[14] A. W. Schreiber and A. W. Thomas, Phys. Lett. B **215**, 141 (1988).
[15] S. D. Bass and A. W. Thomas, Phys. Lett. B **684**, 216 (2010).
[16] V. Yu. Alexakhin *et al.* (COMPASS Collaboration), Phys. Lett. B **647**, 8 (2007).
[17] G. Altarelli and G. G. Ross, Phys. Lett. B **212**, 391 (1988).
[18] A. V. Efremov and O. Teryaev, JINR Report No. E2-88-287 (unpublished).
[19] R. D. Carlitz, J. C. Collins, and A. Mueller, Phys. Lett. B **214**, 229 (1988).
[20] S. D. Bass, B. L. Ioffe, N. N. Nikolaev, and A. W. Thomas, J. Mosc. Phys. Soc. **1**, 317 (1991).
[21] E. Leader, A. V. Sidorov, and D. B. Stamenov, Phys. Rev. D **58**, 114028 (1998); R. D. Ball, S. Forte, and G. Ridolfi, Phys. Lett. B **378**, 255 (1996).
[22] X. Ji, J. Tang, and P. Hoodbhoy, Phys. Rev. Lett. **76**, 740 (1996).
[23] G. K. Mallot, in *Proceedings of the 17th International Spin Physics Symposium (SPIN06), 2–7 Oct 2006, Kyoto, Japan*, edited by K. Imai, T. Murakami, K. Tanida, and N. Saito, AIP Conf. Proc. No. 915 (AIP, Melville, NY, 2007), p. 325.
[24] S. D. Bass, R. J. Crewther, F. M. Steffens, and A. W. Thomas, Phys. Rev. D **66**, 031901(R) (2002).
[25] D. B. Kaplan and A. V. Manohar, Nucl. Phys. B **310**, 527 (1988).
[26] G. Altarelli and B. Lampe, Z. Phys. C **47**, 315 (1990).
[27] A. V. Manohar, Phys. Lett. B **242**, 94 (1990).
[28] S. D. Bass and A. W. Thomas, Phys. Lett. B **293**, 457 (1992).
[29] S. D. Bass, S. J. Brodsky, and I. Schmidt, Phys. Rev. D **60**, 034010 (1999).
[30] M. Alekseev *et al.* (COMPASS Collaboration), Phys. Lett. B **676**, 31 (2009).
[31] E. V. Shuryak, Phys. Rep. **115**, 151 (1984).
[32] W. Melnitchouk and A. W. Thomas, Phys. Lett. B **414**, 134 (1997).
[33] R. D. Young and A. W. Thomas, Phys. Rev. D **81**, 014503 (2010).
[34] R. D. Young, J. Roche, R. D. Carlini, and A. W. Thomas, Phys. Rev. Lett. **97**, 102002 (2006).

Chapter 5

Concluding Remarks

5.1 Overview

In this thesis, several topics pertaining to the deep inelastic processes that probe the structure of hadrons have been considered. We begin with a literature review, which is separated into two chapters. In the first of these chapters we established the features of QCD that are relevant to our later discussions, including the QCD Lagrangian, asymptotic freedom and the running of the strong coupling constant. This was followed by a brief description of the QCD factorization theorem, as well as the DIS and SIDIS processes. We also discussed the parton model, and presented a simplified description of the DGLAP evolution equations for PDFs, SFFs and DFFs. The first chapter of background material was finished with a brief discussion of the proton spin crisis.

The second background chapter included a review of the NJL model, which is related to the calculations carried out in two of the papers we include here as part of the portfolio. We focus on discussing the mass gap equation, the bubble graph which arises in the solution to the Bethe-Salpeter equation, the quark-meson coupling and the meson decay coupling. The three-momentum cutoff and Lepage-Brodsky invariant mass cutoff regularization schemes are also discussed. This chapter is finished up with a discussion of the single hadron fragmentation functions within the NJL-jet model.

We now discuss the papers presented in the portfolio of publications, in terms of three aspects, with the first being a summary of the contributions each paper

provides and their significance to the field. This is followed by an account of the issues encountered throughout this research. Finally, ideas for future research directions are suggested.

5.2 Summary of Research and its Significance

This thesis has been presented as a portfolio of publications containing three peer-reviewed papers, with each paper contributing new knowledge to the field. In the paper labeled Ref. [3], we obtained a theoretical upper bound on the contribution of the gluon polarization to the spin of the proton, with an estimation of the error on this bound if next-to-leading order effects were considered. The value obtained for the upper bound was $|\Delta g(m_c^2)| \lesssim 0.3$ with $\alpha_s(m_c^2) = 0.4$, which is consistent with recent calculations from experimental data at COMPASS [48]. The proton spin crisis is still a topic of much discussion, with both experimental and theoretical considerations needed to determine the contributions to the proton's spin. We presented our theoretical calculation of the gluon polarization contribution to the spin of the proton as one piece of this very complicated puzzle, to aid the field in the building of a complete solution.

DFFs are interesting functions because they describe properties of the relationship between two hadrons produced in the same jet. Recently, DFFs have also been considered as an alternative way to study transversity distribution functions [29] because, much like the Collins fragmentation functions [25], they appear in SIDIS asymmetries with the transversity distribution functions. Two of the papers included in the portfolio relate to dihadron fragmentation functions from the NJL-jet model. In the first of the two papers, Ref. [1], we determine DFFs from the NJL-jet model for pion and kaon combinations, with results involving $\pi^+\pi^-$, π^+K^- and K^+K^- combinations discussed. It was shown that the inclusion of the strange quark in the $\pi^+\pi^-$ DFF had a significant effect, with a reduction in magnitude of approximately a third when compared to its corresponding function for the two-flavor case. This reduction effect is caused by the availability of the kaon emission channels when the strange quarks are included. By comparing the total DFF to its corresponding driving function we showed that the integral

term, which appears in the expression for the DFFs, contributes very little to the total DFF, except in the region where one of the light-cone momentum fractions was approximately 0.1 or smaller, or when the driving function was equal to zero. The first of these integral term effects was particularly visible for the up quark to K^+K^- combination.

The calculations of the DFFs from the NJL-jet model can only be meaningfully compared to other models, simulations or experimental results when we evolve them with respect to the momentum scale Q^2. DGLAP evolution equations for the DFFs had already been determined and so we used those included in Ref. [38]. Fortran code developed by the authors of Refs. [37, 73–75], which perform Q^2 evolution on the PDFs or FFs, was adapted to perform evolution on the DFFs, producing the results shown in Ref. [2], where we evolved the DFFs from the model momentum scale of $Q_0^2 = 0.2$ GeV^2 to a typical experimental scale of $Q^2 = 4$ GeV^2. This allowed us to examine some general features of the DFFs at an appropriate scale, and we also presented solutions for $z_2 D_u^{\pi^+\pi^-}$ and $z_2 D_g^{\pi^+\pi^-}$ from the NJL-jet model evolved to Q^2 values of 5 GeV^2, 20 GeV^2, 50 GeV^2 and 109 GeV^2 at $z_1 = 0.5$, which showed the functions, which are the DFFs multiplied by the LC momentum fraction z_2 to control the plot in the low z_2 region, are reduced as Q^2 increases and the peak value shifts, but the change is much less than that of $Q_0^2 = 0.2$ GeV^2 to $Q^2 = 4$ GeV^2.

This paper also compared the solutions for the NJL-jet model obtained DFFs to the DFFs of Majumder and Wang (Ref. [36]), at a momentum scale of 109 GeV^2. The results obtained for that comparison displayed agreement in the higher allowed z_2 region ($z_2 \leq (1 - z_1)$) for values above 0.2, while differing at the lower values. We suggested this difference may be attributed to the parameterization method employed in Ref. [36], in which data outputted from `JETSET` simulations are parameterized in such a way as to fit the data at the higher z_2 values well, while the lower region does not fit as well. To test our evolution code, we used their input functions for the DFFs in our code, with quite good agreement for about half of the range of allowed z_2 values. There was still quite a considerable difference in the low z_2 region, however, and so we investigated the evolution of the SFFs used in Ref. [36]. By replacing the code that we used for the SFFs evolution with the parameterized SFF evolution that was used in Ref. [36], which

we obtained from Ref. [76], and produced solutions that were a better fit to the parameterized JETSET results at 109 GeV^2. We have shown that the Q^2 evolution code for the DFFs produces solutions to a reasonable level of accuracy for most of the allowed z_2 region that we could compare our results to.

Through the two DFF focused papers, we have presented an NJL-jet model calculation of the DFFs, as well as produced solutions for the DFFs at typical experimental scales, allowing others in the field to compare their own models or experimentally obtained data to these results. There is currently very little data or model calculations for the DFFs, particularly the DFFs in the form which we used where the dependence is on just z_1 and z_2 rather than $z(= z_1 + z_2)$ and the invariant mass squared (M_h^2) of the two hadrons [27, 77], and so the results in these papers provide quite a valuable resource to the field, with others taking note of them already in Refs. [78] and [29].

5.3 Issues Encountered

The initial issues we encountered with the work presented in Ref. [3] was deciding on how we would calculate the value for Δg and what assumptions were necessary. Our initial attempt was focussed on employing DGLAP evolution equations to $\Delta\Sigma$ and Δg, at both LO and NLO, using a numerical method. However, we needed to be careful with the flavor properties, which led to discussion of the charm quark and its threshold. Further discussion on the heavy quark renormalization group equations led to a more developed understanding, resulting in the use of the expression for the charm quark contribution to the proton spin. The charm quark is much heavier than the up, down and strange quarks, and so producing one within the proton is much less probable, resulting in the charm quark contribution to the proton spin being, within error, consistent with zero. Using these properties, while noting possible values and errors, we obtained the result presented in the paper.

For both NJL-jet model DFF papers, time and data usage were significant factors in producing the results. For the model scale paper, we needed to vectorize the range of LC momentum fractions into a particular number of discretized

points, which defines the size of the matrix form of the DFF. Setting the number of points too large would result in durations for running the code that were too long, as well as requiring too much memory, which if it used up all the RAM, would result in paging, causing the duration to become even longer. If the number of points is set too small, the solutions for the DFFs didn't have enough data to converge to similar solutions. This issue was addressed in Ref. [79], where we compare solutions for the number of points set to 50, 100, 150 and 200 for the up quark to $\pi^+\pi^-$ ($z_2 D^{\pi^+\pi^-}$). For $z_1 = 0.5$ it was observed that the solutions had converged quite well for all four number of points, with less the variation being smaller at higher number of points, while for $z_1 = 0.1$ the solutions for 50 and 100 points were quite different, with the difference between 100 and 150 points being noticably less. By 200 points the solutions have converged quite well, with very little variation between the 200 point solution and the 150 point solutions, and so the error in the numerical process we used is greatly reduced if we use 200 points. To reduce the data usage of our code and speed up calculations, we implemented the DFF matrices as sparse arrays, which are a Mathematica array type that only store non-zero elements, and also made clever use of the properties of the integration kernel matrix.

Another issue we encountered for the model scale calculations was related to the integration variables, ξ_1 and ξ_2, and their bounds. For the ξ_2 variable, which appears as part of the DFF $D_q^{h_1 h_2}(\xi_1, \xi_2)$, the value was obtained through the implementation of the delta functions. Since we calculate the integration kernel with z_1 and z_2 fixed to particular points, and integrate (by converting to a sum over discrete points) over ξ_1, the ξ_2 points that we extract did not have to sit on the grid points defined by the discretization method. To deal with this, we employed linear interpolation between neighboring ξ_2 grid points, contributing fractions of the integral kernel to the points either side. We also needed to account for the integration over ξ_1, which had an upper bound of $\xi_{1_{upp}} = z_1/(z_1+z_2)$. This upper bound could lie between grid points, resulting in some of the integration kernel elements receiving the full regions contribution even though the integral cuts off inbetween the two grid points. This was dealt with by multiplying the last contributing element with the ratio $(\xi_{1_{upp}} - \xi_{1_{below}})/(\xi_{1_{above}} - \xi_{1_{below}})$, where $\xi_{1_{below}}$ and $\xi_{1_{above}}$ are the grid points that $\xi_{1_{upp}}$ lie between.

We note that the desription of the NJL-jet model DFFs are incomplete and therefore the solutions are subject to change. For a more complete description, we will need to include several of the extensions to the model discussed in the section that follows. The inclusion of these extensions will likely introduce their own issues that will need to be overcome. We cannot predict how troublesome these will be, but we can limit some of the mby making the developed code as efficient as possible, so that both time and data usage are not unnecessarily large.

For the Q^2 evolution of the DFFs, we encountered similar time and data usage obstacles. These were dealt with in much the same way, by choosing an appropriate discretization of the LC momentum fractions and discretizing the steps in the evolution. We also limited our output data to only the z_1 and z_2 combinations that summed to less than or equal to one, as the DFFs are defined to be zero for combinations greater than one.

Other problems were encountered when we decided to compare our results to those of Ref. [36], particularly when we decided to use our code to evolve their input functions. We first had to determine which particular functions to use as input. For the NJL-jet model, the strange quark to $\pi^+\pi^-$ fragmentations were set to be different than those of the up and down quark fragmentations, while in Ref. [36] they appeared to be set equal, which we ended up assuming. After performing the Q^2 evolution on the DFFs, we still observed some variation in the lower LC momentum fraction region between our results and the parameterized `JETSET` output at 109 GeV^2, as well as the evolution performed by Ref. [36], and so considered changing the implementation of the SFF Q^2 evolution. Since Ref. [36] used the parameterized evolution present in Ref. [76], we altered the code to perform the SFF evolution using that parameterization, producing results that matched closer to the parameterized `JETSET` results at 109 GeV^2 for a slightly larger range of LC momentum fraction.

5.4 Future Research

In Ref. [3] we considered only the contribution of the gluon polarization to the spin of the proton. Further research on this particular term may be higher or-

der (NLO or above) calculations of the terms used, particularly the anomalous dimension $\gamma_{N_f}(\alpha_s)$, or perhaps an alternative method to obtain the charm quark contributions may be suggested. The "proton spin" issue can be approached in several different ways [80–82]. Investigating other components that contribute to the proton's spin, such as the orbital angular momentum of the quarks [83] may also prove useful in formaing a better understanding of the proton spin and thus its deeper structure.

The NJL-jet model DFFs can be advanced in several possible directions. Though their contributions would be small, we could include more active quark flavors above the relevant Q^2 thresholds, which would in turn require changes to the way in which the evolution code handles the steps in Q^2 as $\alpha_s(Q^2)$ would need to be adjusted at each quark flavor threshold. Obtaining the NLO DGLAP evolution equations for the DFFs and performing that calculation is another possible direction with which to continue research, which would likely provide some correction to the DFFs at low LC momentum fractions. Recent progress in the DFFs from the NJL-jet model includes vector mesons [84], altering the results significantly, and so this is a very important avenue to continue with. Obtaining the DFFs with transverse momentum dependence not integrated out would also provide valuable insight into the hadron structure, with similar calculations already performed for SFFs. Implementation of Monte Carlo simulation methods to obtain the DFFs is another useful approach, particularly for the transverse momentum dependence calculations, and has already been done for the SFFs from the NJL-jet model [32].

Appendix

In this thesis we have used the following notations, with the matrix and trace properties being obtained from Ref. [13].

.1 Gell-Mann Matrices

We use the Gell-Mann matrices shown below as one of the representations of the generators of the $SU(3)$ matrices.

$$\lambda_1 = \begin{pmatrix} 0 & 1 & 0 \\ 1 & 0 & 0 \\ 0 & 0 & 0 \end{pmatrix}, \qquad \lambda_2 = \begin{pmatrix} 0 & -i & 0 \\ i & 0 & 0 \\ 0 & 0 & 0 \end{pmatrix}, \tag{1}$$

$$\lambda_3 = \begin{pmatrix} 1 & 0 & 0 \\ 0 & -1 & 0 \\ 0 & 0 & 0 \end{pmatrix}, \qquad \lambda_4 = \begin{pmatrix} 0 & 0 & 1 \\ 0 & 0 & 0 \\ 1 & 0 & 0 \end{pmatrix}, \tag{2}$$

$$\lambda_5 = \begin{pmatrix} 0 & 0 & -i \\ 0 & 0 & 0 \\ i & 0 & 0 \end{pmatrix}, \qquad \lambda_6 = \begin{pmatrix} 0 & 0 & 0 \\ 0 & 0 & 1 \\ 0 & 1 & 0 \end{pmatrix}, \tag{3}$$

$$\lambda_7 = \begin{pmatrix} 0 & 0 & 0 \\ 0 & 0 & -i \\ 0 & i & 0 \end{pmatrix}, \qquad \lambda_8 = \frac{1}{\sqrt{3}} \begin{pmatrix} 1 & 0 & 0 \\ 0 & 1 & 0 \\ 0 & 0 & -2 \end{pmatrix}. \tag{4}$$

.2 Dirac Gamma Matrices

Throughout this thesis we use the Dirac basis for representing the gamma matrices

$$\gamma^\mu = (\gamma^0, \gamma^1, \gamma^2, \gamma^3), \tag{5}$$

where

$$\gamma_0 = \begin{pmatrix} 1 & 0 & 0 & 0 \\ 0 & 1 & 0 & 0 \\ 0 & 0 & -1 & 0 \\ 0 & 0 & 0 & -1 \end{pmatrix}, \qquad \gamma^1 = \begin{pmatrix} 0 & 0 & 0 & 1 \\ 0 & 0 & 1 & 0 \\ 0 & -1 & 0 & 0 \\ -1 & 0 & 0 & 0 \end{pmatrix}, \tag{6}$$

$$\gamma^2 = \begin{pmatrix} 0 & 0 & 0 & -i \\ 0 & 0 & i & 0 \\ 0 & i & 0 & 0 \\ -i & 0 & 0 & 0 \end{pmatrix}, \qquad \gamma^3 = \begin{pmatrix} 0 & 0 & 1 & 0 \\ 0 & 0 & 0 & -1 \\ -1 & 0 & 0 & 0 \\ 0 & 1 & 0 & 0 \end{pmatrix}. \tag{7}$$

These matrices satisfy $\{\gamma^\mu, \gamma^\nu\} = 2g^{\mu\nu}$, where

$$g^{\mu\nu} = \begin{pmatrix} 1 & 0 & 0 & 0 \\ 0 & -1 & 0 & 0 \\ 0 & 0 & -1 & 0 \\ 0 & 0 & 0 & -1 \end{pmatrix} \tag{8}$$

is the metric tensor for the Minkowski space. A commonly used combination of these matrices is

$$\gamma^5 = i\gamma^0\gamma^1\gamma^2\gamma^3 = \begin{pmatrix} 0 & 0 & 1 & 0 \\ 0 & 0 & 0 & 1 \\ 1 & 0 & 0 & 0 \\ 0 & 1 & 0 & 0 \end{pmatrix}. \tag{9}$$

.3 Gamma Trace Properties

$$Tr[\gamma^\mu] = 0 \tag{10}$$

$$Tr[\gamma^\mu \gamma^\nu] = 4g^{\mu\nu} \tag{11}$$

$$Tr[\text{odd } \#'\text{s of } \gamma^\mu] = 0 \tag{12}$$

.4 Useful Integral Relations

Integration by parts can be written as

$$\int_a^b dx u(x)v'(x) = [u(x)v(x)]_a^b - \int_a^b dx u'(x)v(x). \tag{13}$$

We include here some integration formulae for $\text{arcsinh}(x)$ as they arose in the derivation of the mass gap equation.

$$\int_a^b \text{arcsinh}(cx)dx = \left[x\text{arcsinh}(cx) - \frac{\sqrt{c^2x^2+1}}{c}\right]_a^b \tag{14}$$

$$\int_a^b x\text{arcsinh}(cx)dx = \left[\frac{x^2\text{arcsinh}(cx)}{2} + \frac{x^2\text{arcsinh}(cx)}{4c^2} - \frac{x\sqrt{c^2x^2+1}}{4c}\right]_a^b \tag{15}$$

$$\int_a^b x^2\text{arcsinh}(cx)dx = \left[\frac{x^3\text{arcsinh}(cx)}{3} - \frac{(c^2x^2-2)\sqrt{c^2x^2+1}}{9c^3}\right]_a^b \tag{16}$$

Other useful properties of $\text{arcsinh}(x)$ are

$$\int_a^b \frac{dx}{\sqrt{c^2+x^2}} = \left[\text{arcsinh}\left(\frac{x}{c}\right)\right]_a^b \tag{17}$$

.5 Table of Flavor Factors for Distribution and Fragmentation Functions

Here is the table of flavor factors denoted by C_q^m which we obtained from Ref. [31].

C_q^m	π^0	π^+	π^-	K^0	$\bar{K}^0$	K^+	K^-
u	1	2	0	0	0	2	0
d	1	0	2	2	0	0	0
s	0	0	0	0	2	0	2
$\bar{u}$	1	0	2	0	0	0	2
$\bar{d}$	1	2	0	0	2	0	0
$\bar{s}$	0	0	0	2	0	2	0

.6 Errata

In the final published version of Ref. [1] there were a few minor errors present. In Eq. (9) of Ref. [1], there was supposed to be three separate lines, rather than one, written in the form:

$$\begin{aligned} \vec{D}_q^m &= \vec{f} + g \cdot \vec{D}_q^m \\ (I - g) \cdot \vec{D}_q^m &= \vec{f} \\ \vec{D}_q^m &= (I - g)^{-1} \vec{f}. \end{aligned} \tag{18}$$

The beginning paragraph of Section IV, in the third sentence, should be between written as:

> The impact of the inclusion of the strange quark on $D_u^{\pi^+\pi^-}$ and $D_d^{\pi^+\pi^-}$ is studied in Sec. *IV. A.*

Instead of:

> The impact of the inclusion of the strange quark on $D_u^{\pi^+\pi^-}$ and $D_u^{\pi^+\pi^-}$ is studied in Sec. *IV. A.*

In the third paragraph of Section *IV. A* and the description of Figs. 4 and 5, the points for the initial down quark DFF are said to be plotted with green diamonds, when they should have been described as green crosses.

References

[1] Andrew Casey, Hrayr H. Matevosyan, and Anthony W. Thomas. Calculating Dihadron Fragmentation Functions in the NJL-jet model. *Phys.Rev.*, D85:114049, 2012. vii, 18, 56, 93, 102

[2] Andrew Casey, Ian C. Cloet, Hrayr H. Matevosyan, and Anthony W. Thomas. Dihadron Fragmentation Functions from the NJL-jet model and their QCD Evolution. *Phys.Rev.*, D86:114018, 2012. viii, 21, 94

[3] Steven D. Bass, Andrew Casey, and Anthony W. Thomas. Gluon polarization in the proton. *Phys.Rev.*, C83:038202, 2011. viii, 33, 93, 95, 97

[4] Murray Gell-Mann. The Eightfold Way: A Theory of strong interaction symmetry. CTSL-20, TID-12608, 1961. 3

[5] Yuval Ne'eman. Derivation of strong interactions from a gauge invariance. *Nucl.Phys.*, 26:222–229, 1961.

[6] Murray Gell-Mann. Symmetries of baryons and mesons. *Phys.Rev.*, 125:1067–1084, 1962. 3

[7] Elliott D. Bloom, D.H. Coward, H.C. DeStaebler, J. Drees, Guthrie Miller, et al. High-Energy Inelastic e p Scattering at 6-Degrees and 10-Degrees. *Phys.Rev.Lett.*, 23:930–934, 1969. 4

[8] Richard P. Feynman. Very high-energy collisions of hadrons. *Phys.Rev.Lett.*, 23:1415–1417, 1969. 4, 18

[9] J.D. Bjorken and Emmanuel A. Paschos. Inelastic Electron Proton and gamma Proton Scattering, and the Structure of the Nucleon. *Phys.Rev.*, 185:1975–1982, 1969. 4

[10] Martin Breidenbach, Jerome I. Friedman, Henry W. Kendall, Elliott D. Bloom, D.H. Coward, et al. Observed Behavior of Highly Inelastic electron-Proton Scattering. *Phys.Rev.Lett.*, 23:935–939, 1969. 4, 20

[11] D.J. Gross and Frank Wilczek. Ultraviolet Behavior of Nonabelian Gauge Theories. *Phys.Rev.Lett.*, 30:1343–1346, 1973. 5

[12] H. David Politzer. Reliable Perturbative Results for Strong Interactions? *Phys.Rev.Lett.*, 30:1346–1349, 1973. 5

[13] Anthony William Thomas and Wolfram Weise. *The Structure of the Nucleon*. Wiley-VCH, Berlin, Germany, 2001. 5, 10, 14, 18, 99

[14] Yuri L. Dokshitzer. Calculation of the Structure Functions for Deep Inelastic Scattering and e+ e- Annihilation by Perturbation Theory in Quantum Chromodynamics. *Sov.Phys.JETP*, 46:641–653, 1977. 11, 20

[15] V.N. Gribov and L.N. Lipatov. Deep inelastic e p scattering in perturbation theory. *Sov.J.Nucl.Phys.*, 15:438–450, 1972. 20

[16] Guido Altarelli and G. Parisi. Asymptotic Freedom in Parton Language. *Nucl.Phys.*, B126:298, 1977. 11, 20, 21

[17] John C. Collins, Davison E. Soper, and George F. Sterman. Factorization of Hard Processes in QCD. *Adv.Ser.Direct.High Energy Phys.*, 5:1–91, 1988. 11, 22

[18] Raymond Brock et al. Handbook of perturbative QCD: Version 1.0. *Rev.Mod.Phys.*, 67:157–248, 1995. 11, 17, 22

[19] W.K. Tung. *"Perturbative QCD and the parton structure of the nucleon" in "Shifman, M. (ed.): At the frontier of particle physics"*. World Scientific, Singapore, New York, 2001. 11

[20] M. Anselmino, M. Boglione, U. D'Alesio, A. Kotzinian, F. Murgia, et al. The Role of Cahn and sivers effects in deep inelastic scattering. *Phys.Rev.*, D71:074006, 2005. 15

[21] A. De Roeck and R.S. Thorne. Structure Functions. *Prog.Part.Nucl.Phys.*, 66:727–781, 2011. 16, 22

[22] M.G. Alekseev et al. Quark helicity distributions from longitudinal spin asymmetries in muon-proton and muon-deuteron scattering. *Phys.Lett.*, B693:227–235, 2010. 16

[23] Alexei Prokudin. Transversity Parton Distribution. arXiv:1304.0469 [hep-ph], 2013. 17

[24] M. Anselmino, M. Boglione, U. D'Alesio, A. Kotzinian, F. Murgia, et al. Transversity and Collins functions from SIDIS and e+ e- data. *Phys.Rev.*, D75:054032, 2007. 17, 18

[25] M. Anselmino, M. Boglione, U. D'Alesio, A. Kotzinian, F. Murgia, et al. Update on transversity and Collins functions from SIDIS and e+ e- data. *Nucl.Phys.Proc.Suppl.*, 191:98–107, 2009. 93

[26] M. Anselmino, M. Boglione, U. D'Alesio, S. Melis, F. Murgia, et al. Simultaneous extraction of transversity and Collins functions from new SIDIS and e+e- data. *Phys.Rev.*, D87:094019, 2013. 17, 18

[27] Alessandro Bacchetta and Marco Radici. Modeling dihadron fragmentation functions. *Phys.Rev.*, D74:114007, 2006. 18, 95

[28] Alessandro Bacchetta, Aurore Courtoy, and Marco Radici. First glances at the transversity parton distribution through dihadron fragmentation functions. *Phys.Rev.Lett.*, 107:012001, 2011. 18

[29] Alessandro Bacchetta, A. Courtoy, and Marco Radici. First extraction of valence transversities in a collinear framework. *JHEP*, 1303:119, 2013. 18, 93, 95

[30] T. Ito, W. Bentz, I. C. Cloët, A. W. Thomas, and K. Yazaki. The NJL-jet model for quark fragmentation functions. *Phys.Rev.*, D80:074008, 2009. 18, 54, 56

[31] Hrayr H. Matevosyan, Anthony W. Thomas, and Wolfgang Bentz. Calculating Kaon Fragmentation Functions from NJL-Jet Model. *Phys.Rev.*, D83:074003, 2011. 50, 54, 56, 102

[32] Hrayr H. Matevosyan, Anthony W. Thomas, and Wolfgang Bentz. Monte Carlo Simulations of Hadronic Fragmentation Functions using NJL-Jet Model. *Phys.Rev.*, D83:114010, 2011. 56, 98

[33] Hrayr H. Matevosyan, Wolfgang Bentz, Ian C. Cloët, and Anthony W. Thomas. Transverse Momentum Dependent Fragmentation and Quark Distribution Functions from the NJL-jet Model. *Phys.Rev.*, D85:014021, 2012. 18, 56

[34] George F. Sterman. Partons, factorization and resummation, TASI 95. 1995. 19

[35] J.D. Bjorken. Asymptotic Sum Rules at Infinite Momentum. *Phys.Rev.*, 179:1547–1553, 1969. 20

[36] A. Majumder and Xin-Nian Wang. Evolution of the parton dihadron fragmentation functions. *Phys.Rev.*, D72:034007, 2005. 21, 94, 97

[37] M. Hirai and S. Kumano. Numerical solution of Q^2 evolution equations for fragmentation functions. *Comput.Phys.Commun.*, 183:1002–1013, 2012. 24, 94

[38] Federico A. Ceccopieri, Marco Radici, and Alessandro Bacchetta. Evolution equations for extended dihadron fragmentation functions. *Phys.Lett.*, B650:81–89, 2007. 25, 27, 94

[39] J. Ashman et al. A Measurement of the Spin Asymmetry and Determination of the Structure Function g(1) in Deep Inelastic Muon-Proton Scattering. *Phys.Lett.*, B206:364, 1988. 30

[40] Anthony W. Thomas. Spin and orbital angular momentum of the proton. *Int.J.Mod.Phys.*, E18:1116–1134, 2009. 31

[41] A.V. Efremov and O.V. Teryaev. Spin Structure of the Nucleon and Triangle Anomaly. *Nucl.Phys.*, 1988. 31

[42] Guido Altarelli and Graham G. Ross. The Anomalous Gluon Contribution to Polarized Leptoproduction. *Phys.Lett.*, B212:391, 1988.

[43] Robert D. Carlitz, John C. Collins, and Alfred H. Mueller. The Role of the Axial Anomaly in Measuring Spin Dependent Parton Distributions. *Phys.Lett.*, B214:229, 1988.

[44] Elliot Leader and Mauro Anselmino. A Crisis in the Parton Model: Where, Oh Where is the Proton's Spin? *Z.Phys.*, C41:239, 1988.

[45] Geoffrey T. Bodwin and Jian-Wei Qiu. The Gluonic Contribution to G(1) and Its Relationship to the Spin Dependent Parton Distributions. *Phys.Rev.*, D41:2755, 1990.

[46] Steven D. Bass, Boris L. Ioffe, Nikolai N. Nikolaev, and Anthony William Thomas. On the infrared contribution to the photon - gluon scattering and the proton spin content. *J.Moscow.Phys.Soc.*, 1:317–333, 1991. 31

[47] E.S. Ageev et al. Measurement of the spin structure of the deuteron in the DIS region. *Phys.Lett.*, B612:154–164, 2005. 31

[48] V. Yu. Alexakhin et al. The Deuteron Spin-dependent Structure Function g1(d) and its First Moment. *Phys.Lett.*, B647:8–17, 2007. 93

[49] A. Airapetian et al. Precise determination of the spin structure function g(1) of the proton, deuteron and neutron. *Phys.Rev.*, D75:012007, 2007. 31

[50] F. Myhrer and A. W. Thomas. A possible resolution of the proton spin problem. *Phys.Lett.*, B663:302–305, 2008. 31

[51] A. Adare et al. The Polarized gluon contribution to the proton spin from the double helicity asymmetry in inclusive pi0 production in polarized p + p collisions at s**(1/2) = 200-GeV. *Phys.Rev.Lett.*, 103:012003, 2009. 31

[52] A.W. Thomas. The Spin of the Proton. *Prog.Part.Nucl.Phys.*, 61:219–228, 2008. 31

[53] Jiro Kodaira. QCD Higher Order Effects in Polarized Electroproduction: Flavor Singlet Coefficient Functions. *Nucl.Phys.*, B165:129, 1980. 32

[54] Stephan Durr. Recent Progress in Lattice QCD. PSNUM-31, arXiv:1301.1914 [hep-lat], 2013. 34

[55] Yoichiro Nambu and G. Jona-Lasinio. Dynamical model of elementary particles based on an analogy with superconductivity. I. *Phys. Rev.*, 122:345–358, 1961. 35

[56] Yoichiro Nambu and G. Jona-Lasinio. Dynamical model of elementary particles based on an analogy with superconductivity. II. *Phys. Rev.*, 124:246–254, 1961. 35

[57] Stanley J. Brodsky and G. Peter Lepage. Exclusive Processes in Quantum Chromodynamics. SLAC-PUB-2762, C81-03-25.1-10, 1981. 35

[58] S. Klimt, M. Lutz, U. Vogl, and W. Weise. Generalized SU(3) Nambu–Jona-Lasinio Model. Part. 1. Mesonic Modes. *Nucl. Phys.*, A516:429–468, 1990. 35

[59] U. Vogl, Matthias F.M. Lutz, S. Klimt, and W. Weise. Generalized SU(3) Nambu–Jona-Lasinio Model. Part 2. From Current to Constituent Quarks. *Nucl.Phys.*, A516:469–495, 1990. 35

[60] E.E. Salpeter and H.A. Bethe. A Relativistic equation for bound state problems. *Phys.Rev.*, 84:1232–1242, 1951. 38

[61] N. Ishii, W. Bentz, and K. Yazaki. Baryons in the NJL model as solutions of the relativistic Faddeev equation. *Nucl.Phys.*, A587:617–656, 1995. 38

[62] S.P. Klevansky. The Nambu-Jona-Lasinio model of quantum chromodynamics. *Rev.Mod.Phys.*, 64:649–708, 1992. 45

[63] Murray Gell-Mann, R.J. Oakes, and B. Renner. Behavior of current divergences under SU(3) x SU(3). *Phys.Rev.*, 175:2195–2199, 1968. 45

[64] W. Bentz, T. Hama, T. Matsuki, and K. Yazaki. NJL model on the light cone and pion structure function. *Nucl.Phys.*, A651:143–173, 1999. 48, 49, 52

[65] S. D. Drell, Donald J. Levy, and Tung-Mow Yan. A Theory of Deep Inelastic Lepton-Nucleon Scattering and Lepton Pair Annihilation Processes. 1. *Phys.Rev.*, 187:2159–2171, 1969. 54

[66] S. D. Drell, Donald J. Levy, and Tung-Mow Yan. A Theory of Deep Inelastic Lepton Nucleon Scattering and Lepton Pair Annihilation Processes. 2. Deep Inelastic electron Scattering. *Phys.Rev.*, D1:1035–1068, 1970.

[67] S. D. Drell, Donald J. Levy, and Tung-Mow Yan. A Theory of Deep Inelastic Lepton-Nucleon Scattering and Lepton Pair Annihilation Processes. 3. Deep Inelastic electron-Positron Annihilation. *Phys.Rev.*, D1:1617–1639, 1970.

[68] J. Blumlein, V. Ravindran, and W. L. van Neerven. On the Drell-Levy-Yan relation to O(alpha(s)**2). *Nucl.Phys.*, B586:349–381, 2000. 54

[69] R. D. Field and R. P. Feynman. A Parametrization of the Properties of Quark Jets. *Nucl.Phys.*, B136:1, 1978. 55

[70] Hrayr H. Matevosyan, Anthony W. Thomas, and Wolfgang Bentz. Collins Fragmentation Function within NJL-jet Model. *Phys.Rev.*, D86:034025, 2012. 56

[71] Hrayr H. Matevosyan, Anthony W. Thomas, and Wolfgang Bentz. Effects of Quark Spin Flip on the Collins Fragmentation Function in a Toy Model. *J.Phys.Conf.Ser.*, 403:012042, 2012.

[72] Hrayr H. Matevosyan, Anthony W. Thomas, and Wolfgang Bentz. Higher Order Collins Modulations in Transversely Polarized Quark Fragmentation. arXiv:1207.1433 [hep-ph], 2012. 56

[73] M. Miyama and S. Kumano. Numerical solution of Q**2 evolution equations in a brute force method. *Comput.Phys.Commun.*, 94:185–215, 1996. 94

[74] M. Hirai, S. Kumano, and M. Miyama. Numerical solution of NLO Q**2 evolution equations for spin dependent structure functions. In C. W. de Jager, T. J. Ketel, P. J. Mulders, J. E. J. Oberski, and M. Oskam-Tamboezer, editors, *High-energy spin physics. Proceedings, 12th International Symposium, SPIN 96, Amsterdam, Netherlands, September 10-14, 1996.*, pages 410–412, 1996.

[75] M. Hirai, S. Kumano, and M. Miyama. Numerical solution of Q**2 evolution equations for polarized structure functions. *Comput.Phys.Commun.*, 108:38, 1998. 94

[76] J. Binnewies, Bernd A. Kniehl, and G. Kramer. Pion and kaon production in e+ e- and e p collisions at next-to-leading order. *Phys.Rev.*, D52:4947–4960, 1995. 95, 97

[77] Jian Zhou and Andreas Metz. Dihadron fragmentation functions for large invariant mass. *Phys.Rev.Lett.*, 106:172001, 2011. 95

[78] Wouter J. Waalewijn. Calculating the Charge of a Jet. *Phys.Rev.*, D86:094030, 2012. 95

[79] A. Casey, A.W. Thomas, and H.H. Matevosyan. Dihadron Fragmentation Functions in the NJL-jet model. *AIP Conf.Proc.*, 1418:143–146, 2011. 96

[80] Xiang-Dong Ji. Gauge invariant decomposition of nucleon spin and its spin - off. *Phys.Rev.Lett.*, 78:610–613, 1997. 98

[81] M. Wakamatsu. The Role of orbital angular momentum in the proton spin. *Eur.Phys.J.*, A44:297–303, 2010.

[82] Christine A. Aidala, Steven D. Bass, Delia Hasch, and Gerhard K. Mallot. The Spin Structure of the Nucleon. *Rev.Mod.Phys.*, 85:655–691, 2013. 98

[83] A. W. Thomas, A Casey, and H. H. Matevosyan. What we know and don't know about the origin of the spin of the proton. *Int.J.Mod.Phys.*, A25:4149–4162, 2010. 98

[84] Hrayr H. Matevosyan, Anthony W. Thomas, and Wolfgang Bentz. The Effect of Vector Meson Decays on Dihadron Fragmentation Functions. arXiv:1307.8125 [hep-ph], in proceedings of INPC 2013, Firenze, Italy, June 2-7, 2013. 98